On the cornerstone of our body

Functional and clinical anatomy of the hindfoot

Kleipool, R.P.

Publication date
2022

Document Version
Final published version

On the cornerstone of our body: Functional and clinical anatomy of the hindfoot

Roeland P. Kleipool

On the cornerstone of our body

Functional and clinical anatomy of the hindfoot

Roeland P. Kleipool

Amsterdam Movement Sciences

VU VRIJE UNIVERSITEIT AMSTERDAM

Amsterdam UMC University Medical Centers

Amsterdam Movement Sciences conducts scientific research to optimize physical performance in health and disease based on a fundamental understanding of human movement in order to contribute to the fulfillment of a meaningful life.

On the cornerstone of our body

Functional and clinical anatomy of the hindfoot

Roeland P. Kleipool

The sculpture depicted on the cover and in the thesis was created by C.Th.F. Kleipool and photographed and modelled by R.P. Kleipool.

On the cornerstone of our body
Functional and clinical anatomy of the hindfoot
Roeland P. Kleipool | Academic Thesis | University of Amsterdam | The Netherlands

ISBN 978-94-6423-582-1

Cover design and lay-out: R.P. Kleipool

Printed by: ProefschriftMaken || www.proefschriftmaken.nl

The research in this thesis was embedded in Amsterdam Movement Sciences Research Institute, at the department of Medical Biology, Amsterdam UMC, location AMC, University of Amsterdam, Netherlands.

Financial support for the publication of this thesis was kindly provided by:
- AmsterdamUMC, location AMC, Department of Medical Biology
- Amsterdam Movement Sciences (AMS)

On the cornerstone of our body
Functional and clinical anatomy of the hindfoot

ACADEMISCH PROEFSCHRIFT

ter verkrijging van de graad van doctor
aan de Universiteit van Amsterdam
op gezag van de Rector Magnificus
prof. dr. ir. K.I.J. Maex
ten overstaan van een door het College voor Promoties ingestelde commissie,
in het openbaar te verdedigen in de Agnietenkapel
op woensdag 19 januari 2022, te 10.00 uur

door Roeland Paulus Kleipool
geboren te Alphen aan den Rijn

Promotiecommissie

Promotores:	Prof. dr. R.J. Oostra	AMC-UvA
	Dr. ir. L. Blankevoort	AMC-UvA
Overige leden:	Prof. dr. M. Maas	AMC-UvA
	Prof. dr. D. Eygendaal	AMC-UvA
	Dr. ir. G.J. Streekstra	AMC-UvA
	Prof. dr. G.J. Kleinrensink	Erasmus Universiteit Rotterdam
	Prof. dr. ir. J. Harlaar	Technische Universiteit Delft
	Prof. dr. R.L.A.W. Bleys	Universiteit van Utrecht

Faculteit der Geneeskunde

Voor Joppe en Olle

Table of contents

Chapter 1

General introduction

'get off on the right foot'
Cambridge dictionary: to make a successful start

The body plan of the human body is a blueprint that directs prenatal development to generate similarities in development of form and function in all individuals (1). This blueprint is not strict as with a plan for a building or machine. It allows to a certain extend variations; a range of possible alteration for any characteristic. Congenital variations arise from the individual's unique genome and intra-uterine conditions. Post-natal development with the individual's unique behaviours and the influences from the environment further shapes these variations, resulting in that all individuals look alike, but are also very different.

The term anatomical variation is often used interchangeably with 'normal variation' or 'normal anatomical variation'. This stems from the assumption that most variation between individuals has no effect on health. The term normal can be used as a statistical measure of usually observed structures, which is typical. Anomaly in this description is something outside the usual variation from the norm, an inconsistency, irregularity or abnormality. The difficulty here is the determination of the norm and the range. Normal can also be described as non-symptomatic. This implies that even a variation that is rare and does not impair the health of that individual can be considered normal.

The reports of anatomical variations are numerous in journals that go back to as early as the 15th century. In 2011 Bergman claimed to have cataloged approximately 95 percent of all gross anatomical variations recorded in 884 journals (2). Before the introduction of noninvasive medical imaging most anatomical variants were discovered through cadaveric dissection, or incidentally during surgery. Non-invasively identified variations or anomalies of gross anatomy were limited to externally visible entities such as polydactyly, that is the presence of more than five digits on a hand or foot. This is an example of a rare variation (incidence between 5 to 19 per 10,000 live births (3)) that does not necessarily impair health. The introduction of medical imaging brought about new ways to examine the anatomy and also demonstrated that the spectrum of human variations was larger than thought before (4). The (clinical) significance of these

variations has been discussed in historical works, such as by Cunningham (5) in 1898 and is still a topic in current anatomic research.

Quantitative variations such as supernumerary or missing digits, lobes, arteries, veins, muscles, tendons, ligaments, and bones, form only a part of all inter-individual variations. Shape and size variations also add to the spectrum of inter-individual variations. Shape is intricately coupled to function and as such, shape variations can reflect functional variations. Shape variations can also have a role in dysfunction and pathogenesis. This is especially true for the musculoskeletal system, wherein not only inter-individual variation exists, but also intra-individually between the left and right sides (6). How shape, size, or quantity of structures are related to function or dysfunction, or what role the variation has in the pathogenesis is not always clear at first sight. Further research is most often necessary to demonstrate a relationship and to understand its role. For example, the existence of an os trigonum, a supernumerary ossicle in the hindfoot, has first been described by Rosenmüller in 1804 (7), but a relationship with posterior ankle pain was not reported until about one and half century later (8). This example demonstrates that whether a variation can be related to pathology or considered a risk factor can be subjected to progressive insight. Therefore, the prefix 'normal' in 'normal variations' better be avoided (9).

Noninvasive imaging has the advantage to study the variation in living and active individuals and as such can identify not only the variation, but also expose its role in the (dys-)functioning of that individual. This relationship is far more difficult or even impossible to assess in variations identified post-mortem. New technologies, such as provided by advances in medical imaging and computational power, have the potential to unveil new information that demonstrate (hidden) relationships between specific variations and pathology or risk factors (e.g. (10)). These relationships can even be found within what is presently considered the normal range of inter-individual variations and not only in the range of what is considered abnormal.

The focus of this thesis is on the hindfoot, the posterior part of the foot. It is the most caudal part in the mechanical chain of the lower extremity for transfer of loads from the ground to the hip; a true *cornerstone* (11). It has an important role in walking, running, jumping and all kinds of other activities (12–15). The hindfoot is a good example of a situation in which apparently the same overall function is achieved with variations in sizes and shapes. For many morphological characteristics it is unknown what the range of variations is and how these variations relate to the functioning of the hindfoot or potentially have a role in pathogenesis. This thesis aims to contribute to closing this gap in current literature.

Hindfoot injuries like after an inversion trauma of the ankle, are frequent and form a high socio-economic burden for the society (16,17). It can be very beneficial to have information on which specific shape variations have positive or negative influence on the functioning of the hindfoot. For example, are there specific shape variations of the hindfoot that make an individual prone for an inversion trauma, or the development of osteoarthritis after a trauma? This information will help to adequately develop strategies to help the patient or to develop a customized prevention program. This appeals well to the ongoing tendency for patient-specific treatment and prevention programs (18–20), and will hopefully reduce the socio-economic burden.

Although it is beyond the scope of this introduction to extensively describe the (functional) anatomy, imaging techniques, quantitative analyses, and common pathology and injuries of the hindfoot, an elaboration of certain, for this thesis relevant, aspects of these topics is presented here as a prelude to the research questions.

Anatomy of bones and joints of the hindfoot

The two bones of the hindfoot are the talus and the calcaneus. The hindfoot comprises several synovial joints between these two bones and adjacent bones. These joints must bear forces of up to five times the body weight (21), and at the same time they must also accommodate movements (12–15). The talocrural, the talocalcaneal, and the talocalcaneonavicular joints together are also referred to as the 'ankle joint complex' (22). However, for this term multiple definitions are used in the literature (15,23,24). In this thesis the term is used as the combination of the talocrural, talocalcaneal, and talocalcaneonavicular joints. The talocalcaneal and talocalcaneonavicular joints have separate synovial cavities, but they do not have independent motion, comparable to a door with two hinges (25). Therefore, the anatomical distinction between the two joints is irrelevant from a kinematical perspective .

The talus is intercalated, which means that no tendons are attached to it. The talus articulates proximally with the tibia and fibula, and distally with the calcaneus and navicular bone. The talus is covered with articular cartilage for about 60% (26). The superior surface (the trochlea of talus) and medial surface articulate with the distal inferior surface of the tibia and the lateral surface of the medial malleolus, respectively. The lateral surface of the talus articulates with the medial surface of the lateral malleolus (fibula). These surfaces are part of the ankle joint, or talocrural joint.

Inferior to the talus is the calcaneus. Different names are used for the articulation between the talus and calcaneus. In the Terminologica Anatomica (English version) (27) two relevant articulations are named the subtalar or talocalcaneal joint, and the talocalcaneonavicular joint. In the latter the navicular bone, that is located anteriorly to

the talar head, is part of this combined joint. In this description the subtalar joint is restricted to the articulation between the concave posterior calcaneal facet on the posterior part of the inferior surface of the talus, and the convex posterior facet on the superior surface of the calcaneus. The other more anteriorly located articulations between the talus and calcaneus are considered to be part of the talocalcaneonavicular joint. Other literature define the talocalcaneal joint as all posteriorly and anteriorly located articulations between the talus and the calcaneus (28), also referred to as the subtalar or talocalcaneal joints (plural) (29). In this thesis the last definition is used.

In the Terminologica Anatomica (27) the posterior, middle, and anterior facets of both the talus and calcaneus of the talocalcaneal joints are separately named. Most classical anatomy textbooks follow this description (30,31). However, there are variations in the number and fusion pattern of these joint facets. Ethnic differences have been reported in the distribution of morphological variants (32,33). In one variant all three facets on the calcaneus are connected to make one irregular articular surface (34). This variation is not frequently found (<2%) and absent in the native European population (34,35). In the majority, the posterior facet of the calcaneus is separated by the calcaneal sulcus from the facet that arches the *sustentaculum tali* (talar shelf). This sulcus together with the talar sulcus, located at the inferior surface of the talus, forms the tarsal sinus. In some literature the sinus tarsi is split in a lateral and a medial part. The medial part is then named the tarsal canal and this part is small and narrow, with the lateral part being dubbed the tarsal sinus, which is funnel shaped (30,36,37). Only one study presents data on the dimensions of this space, and only in one static position in children (38). The question that is dealt with in a chapter of this thesis is what the dimensions are in adults and how the dimensions change between different foot positions, as this is not described in the current literature. The two hindfoot bones articulate with each other and the dimensions of this space are likely to change with motion between these bones. The way in which the dimensions change can potentially explain impingement of soft tissue, or undue tensioning of structures such as ligaments, and help to maneuver in this tight space with surgical instruments or scopes, or determine the choice of the appropriate size of tarsal sinus implants.

In reconstructive surgery after fracture, the contralateral non-injured side is often used as a reference for the ipsilateral injured side. The basis for this approach is the assumption of a high degree of bilateral symmetry. It is known that there is indeed, to a certain extent, bilateral osseous symmetry and that this symmetry is higher for the lower extremity than for the upper extremity (6). The degree of this symmetry is however not explored to the full extend for every characteristic, and the literature on the bilateral symmetry of the hindfoot is sparse (39–41). Part of this thesis provides additional data to reduce the gap in current literature concerning this issue.

The ligaments of the ankle joint complex provide passive stability to the joints. Rupture of these ligaments results in instability, or at least in a greater range of motion (42). Other sources that passively contribute to the stability of the joints are the contour of the articulating surfaces, the retinacular system, and the crossing of tendons and the tendon tunnels attached to the bones. Muscle action and the ground reaction force contribute to dynamic stability (43). The ligaments can span one joint or multiple joints. The ligaments of the talocrural joint are generally divided in the lateral and medial collaterals, and those of the distal tibiofibular joint. The former provide stability for this syndesmosis that forms the ankle mortise (44).

Role of hindfoot in alignment of the lower extremity

From a biomechanical perspective, the lower extremity can be considered a mechanical chain from the ground to the hip. The hindfoot is located at the most caudal point in the chain. The alignment of the whole limb is a construct of all joints and bones. Normal alignment is necessary for a normal load distribution over the joints and thereby preventing wear of the cartilaginous surfaces, and preserve normal physiological ligament tension. The hip-knee-ankle angle is an important measure for evaluating the overall limb alignment in a coronal plane (45,46). A drawback of this widely used method is that the caudal reference point for this angle determination is the center of the tibiotalar joint. Thus, the more caudal part of the chain is not included. Several studies demonstrate the importance of including the hindfoot in the analysis of lower extremity alignment (47–50). A compensatory alignment of the hindfoot is demonstrated for knee malalignment. For example, individuals with valgus knee deformity often have hindfoot varus, and vice versa (51). At present day, the role of hindfoot alignment in for example corrective surgery for knee deformity is gaining interest (e.g. (11,52)). However, many current methods to determine hindfoot alignment rely on 2D measurements (e.g. (28,53–55)). The 3D orientation of the articulating surfaces of the hindfoot is scarcely described in current literature. Part of this thesis addresses this issue. The influence of hindfoot alignment has further been related to surgical outcome in calcaneal fractures (56), to chronic ankle instability (54), and to Patient-Reported Outcome Measures (PROMs) and Performance Measures, and prosthesis-component survival of ankle (57,58) and/or knee arthroplasty (51,59).

Medical imaging of the hindfoot

In daily clinical practice the hindfoot is most often imaged in a static position and by plain radiographs, for example to diagnose fractures. It can also be used to assess staging of osteoarthritis (60,61), whole lower-limb alignment (62), or as introduced above,

specifically hindfoot alignment (63). Different positions and orientations of the hindfoot relative to the X-ray beam are needed to image specific parts. The difficulty here is to position the foot correctly and to plan the appropriate positions and orientations. This illustrates that the three-dimensional (3D) morphology is hard to grasp from two-dimensional (2D) images. With the use of Computer Tomography (CT) or Magnetic Resonance Imaging (MRI) is it possible to reconstruct multiple differently orientated 2D planes. The positioning of the hindfoot in the scanning device is of less importance. Generally, CT is used to image bony structures, and MRI is used to image soft tissue structures. MRI is of limited value in orthopedic applications because the cortical bone is difficult to depict. CT is currently the preferred imaging modality that is used for diagnoses of (complex) fractures and deformations, for surgical planning (e.g. (64)), for input for 3D printing (e.g. (65)), and for assessment of bone mineral density (e.g. (66)).

In the last decade the use of a weight-bearing condition with CT has demonstrated to be of added value (67). Particularly, pathology such as joint space narrowing, impingement, or malalignment can be missed or underestimated in non-weight bearing conditions (67). For true weight-bearing conditions a special CT scanner is required with a horizontally tilted gantry. Since many institutes lack such a specialized and dedicated device, custom-made loading devices were built to create a simulated weight-bearing condition using the standard supine CT table (68–71). Disadvantages of such simulated-loading devices include the lack of muscle forces when the load is applied passively, and the fact that loading is only at a percentage of full body weight (67).

3D quantitative analyses

With advances in 3D-imaging technology it became possible to create virtual 3D surface models of anatomical structures. Such models can be acquired by manual, semi-automatic, or automatic segmentation of the structure of interest in the 3D images (72). Segmentation is the technique of dividing or partitioning an image into parts, called segments. The 3D image is made of voxels, which are the 3D equivalents of the pixels of a digital 2D image. During the segmentation voxels are added or removed from the region of interest. The selected voxels on the surface can be modelled as a surface polygon mesh. Here, the 3D points, or vertices, are connected with each other by edges and the faces usually consist of triangles or quadrilaterals. These 3D models help in visualization of the structures and is therefore a valuable tool in the diagnostic process. Furthermore, it also allows 3D quantitative measurements for determining bone geometry (e.g. (73)), which is also used extensively in this thesis.

Common pathologies and injuries of the hindfoot

One of the most frequent injuries that present at the emergency unit are ankle sprains (74). Both inversion and eversion sprains occur, but inversion sprains are more common (75). Sprains occur both during sporting activities and in daily ambulation. The ligaments that span the ankle joint complex allow a certain range of motion (ROM), but excessive ROM can stretch the ligaments beyond their maximal limits and the ligaments will tear. Some individuals have multiple recurrent ankle sprains after a first sprain and develop chronic ankle instability (CAI) (76). The causes for development of CAI are multifactorial (77). Many risk factors have been studied. These can be morphological characteristics such as the alignment of the hindfoot (78), or neuromuscular control characteristics (79). To protect the joints from recurrent sprains, a brace or tape can be used to mechanically support the ankle. Both are effective protective means. Each also have disadvantages. Taping can cause skin irritation, has to be applied by a professional, and is only effective for a short period of time. Bracing causes discomfort because of a poor design or poor fit, and limits ROM other than only inversion. These factors make the use of taping and/or bracing unappealing. A newly introduced ankle brace, named Exo-L® (EXO-L BV, Delft, The Netherlands) is designed to overcome part of these disadvantages. Since this brace is unconventional in its design a first functional evaluation in-vivo using a highly accurate and objective method is included in this thesis.

Osteoarthritis can result from both an one-time sprain or from chronic ankle instability (80). Osteoarthritis can also result from abnormal loading conditions such as in malalignment of the hindfoot or elsewhere in the mechanical chain of the lower extremity (81). Articular joint congruency and stability are other factors for development of osteoarthritis (81). The stability can decrease after a ligamentous rupture. Congruency is a way to express the geometric relation of the shapes of opposing articulating surfaces. A high congruency means that the two opposing surfaces have the same contours and follow each other's shapes. This also means that the joint reaction force is transmitted over a large area of the surfaces, thereby reducing the contact stresses. Considering the multiple variations in the talocalcaneal joints, the question addressed in this thesis is whether particular morphological characteristics can be related to the presence of osteoarthritis.

Aim and outline of this thesis

In general, this thesis introduces and applies several 3D modelling and imaging techniques to address several issues regarding the morphology and functioning of the hindfoot and its intra- and inter-individual variations. The focus of this thesis is the assessment of morphological characteristics that are related to clinical symptoms or are

related to injuries. This information can help to optimize the prevention and treatment of problems of the hindfoot and adjacent regions.

In **Part 1, Chapters 2 to 4,** the focus is on the mechanics of the hindfoot. In **Chapter 2** a narrative review is described that gives answers that are reported in the literature to the following research questions: How high are the joint forces in the talocrural joint and what are the determining factors for the magnitude of the forces? Secondly, what is the normal ROM of the talocrural and talocalcaneal joints during walking and running, and how do these ROMs relate to the maximal ROMs? Finally, what is the role of the articulating surfaces and the ligaments in the intricate interaction between shape and function? **Chapter 3** investigates the dimensions of the tarsal sinus and canal within the limits of maximal ranges of motion between different foot positions. This provides information on the (quasi-)dynamic changes in the tarsal canal and sinus dimensions between different foot positions and helps to understand normal subtalar functioning and sinus tarsi pathologies such as impingement or undue stretch of tissue. In **Chapter 4** a further analysis is performed on the maximal ROM of the ankle and subtalar joint. Here, ROMs of patients with chronic ankle instability are measured with and without the Exo-L ankle brace.

In **Part 2**, **Chapters 5 to 7**, the focus is on the variation of the inter- and/or intra-individual morphology of the hindfoot. In **Chapter 5** the 3D morphology and orientation of the posterior calcaneal facet is addressed. This facet is difficult to comprehend in 2D and to image in plain radiographs. CT imaging provides better information, but usually the 3D potential is reduced to 2D, and with this comes an additional difficulty that the orientation of the facet varies in different planes. In order to simplify and to describe the 3D shape and orientation of the facet, it is modelled in geometrical shapes (by a plane and a cylinder). With the cylinder model the difference of the orientation in multiple coronal planes is explained and quantified. **Chapter 6** elaborates on the geometrical approach of the posterior calcaneal subtalar facet and analyses the superior and inferior talar facets in the kinematic chain from the ground to the tibia. These analyses are performed to explore bony morphological characteristics in the search for factors that are related to CAI. The orientations and interrelationships between the facets are compared between healthy feet and the feet of the patients with chronic ankle instability from chapter 4. In **Chapter 7** the hypothesis is tested that hindfoot stability is partly provided by the morphology of the articulating facets of the talocalcaneal joints. This is performed by quantitative and qualitative observations of the variations of the number of and the connections between these facets, and relating these findings to the presence of osteoarthritic changes. Furthermore, the hypothesis of a high degree of bilateral symmetry of these facets is tested.

In **Chapter 8** the results and conclusions of the preceding chapters are discussed and recommendations are giving for future research. In **Chapter 9** the results are summarized in English and Dutch respectively.

References

1. Wolpert L, Tickle C AA. No Title. 5th ed. Oxford: Oxford University Press; 2015.
2. Bergman RA. Thoughts on human variations. Clin Anat. 2011 Nov;24(8):938–40.
3. Malik S. Polydactyly: phenotypes, genetics and classification. Clin Genet. 2014 Mar;85(3):203–12.
4. A K. Lexikon der Grenzen des Normalen und der Anfäge des Pathologischen im Röntgenbilde. 1st ed. Hamburg: Lucas Gräfe & Sillem; 1910.
5. Cunningham DJ. The Significance of Anatomical Variations. J Anat Physiol. 1898 Oct;33(Pt 1):1–9.
6. Latimer HB, Lowrance EW. Bilateral asymmetry in weight and in length of human bones. Anat Rec. 1965 Jun;152(2):217–24.
7. Rosenmüller J. De mon nullis musculorum corpus humani varietatibus. 8th ed. Leipzig; 1804.
8. McDOUGALL A. The os trigonum. J Bone Joint Surg Br. 1955 May;37-B(2):257–65.
9. Moore K. The meaning of "normal." Clin Anat. 1989;2(4):235–9.
10. Tumer N, Vuurberg G, Blankevoort L, Kerkhoffs GMMJ, Tuijthof GJM, Zadpoor AA. Typical Shape Differences in the Subtalar Joint Bones Between Subjects with Chronic Ankle Instability and Controls. J Orthop Res. 2019 Sep;37(9):1892–902.
11. Burssens ABM, Buedts K, Barg A, Vluggen E, Demey P, Saltzman CL, et al. Is Lower-limb Alignment Associated with Hindfoot Deformity in the Coronal Plane? A Weightbearing CT Analysis. Clin Orthop Relat Res. 2020 Jan;478(1):154–68.
12. Benink RJ. The constraint-mechanism of the human tarsus. A roentgenological experimental study. Acta Orthop Scand Suppl. 1985;215:1–135.
13. Maceira E, Monteagudo M. Subtalar anatomy and mechanics. Foot Ankle Clin. 2015 Jun;20(2):195–221.
14. Sangeorzan A, Sangeorzan B. Subtalar Joint Biomechanics: From Normal to Pathologic. Foot Ankle Clin. 2018 Sep;23(3):341–52.
15. Brockett CL, Chapman GJ. Biomechanics of the ankle. Orthop Trauma. 2016 Jun;30(3):232–8.
16. De Boer AS, Schepers T, Panneman MJM, Van Beeck EF, Van Lieshout EMM. Health care consumption and costs due to foot and ankle injuries in the Netherlands, 1986-2010. BMC Musculoskelet Disord. 2014 Apr;15:128.
17. Belatti DA, Phisitkul P. Economic burden of foot and ankle surgery in the US Medicare population. Foot ankle Int. 2014 Apr;35(4):334–40.
18. León-Muñoz VJ, Martínez-Martínez F, López-López M, Santonja-Medina F. Patient-specific instrumentation in total knee arthroplasty. Expert Rev Med Devices. 2019 Jul;16(7):555–67.
19. Haglin JM, Eltorai AEM, Gil JA, Marcaccio SE, Botero-Hincapie J, Daniels AH. Patient-Specific Orthopaedic Implants. Orthop Surg. 2016 Nov;8(4):417–24.
20. Academy of Medical Sciences. Stratified, personalised or P4 medicine: a new direction for placing the patient at the centre of healthcare and health education. In: FORUM. London; 2015. p. 1–37.
21. Stauffer RN, Chao EY, Brewster RC. Force and motion analysis of the normal, diseased, and prosthetic ankle joint. Clin Orthop Relat Res. 1977;(127):189–96.

22. van den Bogert AJ, Smith GD, Nigg BM. In vivo determination of the anatomical axes of the ankle joint complex: an optimization approach. J Biomech. 1994 Dec;27(12):1477–88.
23. Allinger TL, Engsberg JR. A method to determine the range of motion of the ankle joint complex, in vivo. J Biomech. 1993 Jan;26(1):69–76.
24. Rosenbaum D, Becker HP, Wilke HJ, Claes LE. Tenodeses destroy the kinematic coupling of the ankle joint complex. A three-dimensional in vitro analysis of joint movement. J Bone Joint Surg Br. 1998 Jan;80(1):162–8.
25. Jastifer JR, Gustafson PA. The subtalar joint: biomechanics and functional representations in the literature. Foot (Edinb). 2014 Dec;24(4):203–9.
26. Kelly PJ, Sullivan CR. Blood supply of the talus. Clin Orthop Relat Res. 1963;30:37–44.
27. Federative Committee on Anatomical Terminology. Terminologia Anatomica: International Anatomical Terminology. 1st ed. Stuttgart ; New York: Thieme; 1998.
28. Sarrafian SK. Biomechanics of the subtalar joint complex. Clin Orthop Relat Res. 1993 May;(290):17–26.
29. Seringe R, Wicart P. The talonavicular and subtalar joints: the “calcaneopedal unit” concept. Orthop Traumatol Surg Res. 2013 Oct;99(6 Suppl):S345-55.
30. S S. Gray’s Anatomy. 39th ed. London, United Kingdom: Elsevier Ltd; 2005.
31. Moore K, Dalley A. Clinically Oriented Anatomy. 5th ed. Baltimore, USA: Lippincott Williams & Wilkins; 2006.
32. Barbaix E, Van Roy P, Clarys JP. Variations of anatomical elements contributing to subtalar joint stability: intrinsic risk factors for post-traumatic lateral instability of the ankle? Ergonomics. 2000 Oct;43(10):1718–25.
33. Jung M-H, Choi BY, Lee JY, Han CS, Lee JS, Yang YC, et al. Types of subtalar joint facets. Surg Radiol Anat. 2015 Aug;37(6):629–38.
34. Bunning PS, Barnett CH. A Comparison of adult and foetal talocalcaneal articulations. J Anat. 1965 Jan;99:71–6.
35. Agarwal S, Garg S, Vasudeva N. Subtalar Joint Instability and Calcaneal Spurs Associated with the Configuration of the Articular Facets of Adult Human Calcaneum in Indian Population. J Clin Diagn Res. 2016 Sep;10(9):AC05–9.
36. Li S-Y, Hou Z-D, Zhang P, Li H-L, Ding Z-H, Liu Y-J. Ligament structures in the tarsal sinus and canal. Foot ankle Int. 2013 Dec;34(12):1729–36.
37. Smith JW. The ligamentous structures in the canalis and sinus tarsi. J Anat. 1958 Oct;92(4):616–20.
38. Bali N, Theivendran K, Prem H. Computed tomography review of tarsal canal anatomy with reference to the fitting of sinus tarsi implants in the tarsal canal. J Foot Ankle Surg. 2013;52(6):714–6.
39. Shultz SJ, Nguyen A-D. Bilateral asymmetries in clinical measures of lower-extremity anatomic characteristics. Clin J Sport Med Off J Can Acad Sport Med. 2007 Sep;17(5):357–61.
40. Islam K, Dobbe A, Komeili A, Duke K, El-Rich M, Dhillon S, et al. Symmetry analysis of talus bone: A Geometric morphometric approach. Bone Joint Res. 2014;3(5):139–45.
41. Tumer N, Arbabi V, Gielis WP, de Jong PA, Weinans H, Tuijthof GJM, et al. Three-dimensional analysis of shape variations and symmetry of the fibula, tibia, calcaneus and talus. J Anat. 2019 Jan;234(1):132–44.
42. Rasmussen O. Stability of the ankle joint. Analysis of the function and traumatology of

the ankle ligaments. Acta Orthop Scand Suppl. 1985;211:1–75.
43. McCullough CJ, Burge PD. Rotatory stability of the load-bearing ankle. An experimental study. J Bone Joint Surg Br. 1980 Nov;62-B(4):460–4.
44. van den Bekerom MPJ, Oostra RJ, Golanó P, van Dijk CN. The anatomy in relation to injury of the lateral collateral ligaments of the ankle: a current concepts review. Clin Anat. 2008 Oct;21(7):619–26.
45. Cooke TD V, Sled EA, Scudamore RA. Frontal plane knee alignment: a call for standardized measurement. Vol. 34, The Journal of rheumatology. Canada; 2007. p. 1796–801.
46. Sheehy L, Felson D, Zhang Y, Niu J, Lam Y-M, Segal N, et al. Does measurement of the anatomic axis consistently predict hip-knee-ankle angle (HKA) for knee alignment studies in osteoarthritis? Analysis of long limb radiographs from the multicenter osteoarthritis (MOST) study. Osteoarthr Cartil. 2011 Jan;19(1):58–64.
47. Duggal N, Paci GM, Narain A, Bournissaint LG, Nazarian A. A computer assessment of the effect of hindfoot alignment on mechanical axis deviation. Comput Methods Programs Biomed. 2014;113(1):126–32.
48. Guichet J-M, Javed A, Russell J, Saleh M. Effect of the foot on the mechanical alignment of the lower limbs. Clin Orthop Relat Res. 2003 Oct;(415):193–201.
49. Mullaji A, Shetty GM. Persistent hindfoot valgus causes lateral deviation of weightbearing axis after total knee arthroplasty. Clin Orthop Relat Res. 2011 Apr;469(4):1154–60.
50. Tanaka T, Takayama K, Hashimoto S, Kanzaki N, Hayashi S, Kuroda R, et al. Radiographic analysis of the lower limbs using the hip-calcaneus line in healthy individuals and in patients with varus knee osteoarthritis. Knee. 2017 Oct;24(5):1146–52.
51. Norton AA, Callaghan JJ, Amendola A, Phisitkul P, Wongsak S, Liu SS, et al. Correlation of knee and hindfoot deformities in advanced knee OA: compensatory hindfoot alignment and where it occurs. Clin Orthop Relat Res. 2015 Jan;473(1):166–74.
52. Yoshimoto K, Noguchi M, Yamada A, Nasu Y. Compensatory Function of the Subtalar Joint for Lower Extremity Malalignment. Adv Orthop. 2019;2019:7656878.
53. Krähenbühl N, Tschuck M, Bolliger L, Hintermann B, Knupp M. Orientation of the Subtalar Joint: Measurement and Reliability Using Weightbearing CT Scans. Foot ankle Int. 2016 Jan;37(1):109–14.
54. Van Bergeyk AB, Younger A, Carson B. CT analysis of hindfoot alignment in chronic lateral ankle instability. Foot ankle Int. 2002 Jan;23(1):37–42.
55. Colin F, Horn Lang T, Zwicky L, Hintermann B, Knupp M. Subtalar joint configuration on weightbearing CT scan. Foot ankle Int. 2014 Oct;35(10):1057–62.
56. Richardson ML, Van Vu M, Vincent LM, Sangeorzan BJ, Benirschke SK. CT measurement of the calcaneal varus angle in the normal and fractured hindfoot. J Comput Assist Tomogr. 1992;16(2):261–4.
57. Frigg A, Nigg B, Hinz L, Valderrabano V, Russell I. Clinical relevance of hindfoot alignment view in total ankle replacement. Foot ankle Int. 2010 Oct;31(10):871–9.
58. Usuelli FG, Di Silvestri CA, D'Ambrosi R, Orenti A, Randelli F. Total ankle replacement: is pre-operative varus deformity a predictor of poor survival rate and clinical and radiological outcomes? Int Orthop. 2019 Jan;43(1):243–9.
59. Nakada I, Nakamura I, Juji T, Ito K, Matsumoto T. Correlation between knee and

hindfoot alignment in patients with rheumatoid arthritis: The effects of subtalar joint destruction. Mod Rheumatol. 2015 Sep;25(5):689–93.
60. Hayashi K, Tanaka Y, Kumai T, Sugimoto K, Takakura Y. Correlation of compensatory alignment of the subtalar joint to the progression of primary osteoarthritis of the ankle. Foot ankle Int. 2008 Apr;29(4):400–6.
61. Tanaka Y, Takakura Y, Fujii T, Kumai T, Sugimoto K. Hindfoot alignment of hallux valgus evaluated by a weightbearing subtalar x-ray view. Foot ankle Int. 1999 Oct;20(10):640–5.
62. Matsumoto T, Hashimura M, Takayama K, Ishida K, Kawakami Y, Matsuzaki T, et al. A radiographic analysis of alignment of the lower extremities--initiation and progression of varus-type knee osteoarthritis. Osteoarthr Cartil. 2015 Feb;23(2):217–23.
63. Reilingh ML, Beimers L, Tuijthof GJM, Stufkens SAS, Maas M, van Dijk CN. Measuring hindfoot alignment radiographically: the long axial view is more reliable than the hindfoot alignment view. Skeletal Radiol. 2010 Nov;39(11):1103–8.
64. Bahrs C, Rolauffs B, Südkamp NP, Schmal H, Eingartner C, Dietz K, et al. Indications for computed tomography (CT-) diagnostics in proximal humeral fractures: a comparative study of plain radiography and computed tomography. BMC Musculoskelet Disord. 2009 Apr;10:33.
65. Marongiu G, Prost R, Capone A. Use of 3D modelling and 3D printing for the diagnostic process, decision making and preoperative planning of periprosthetic acetabular fractures. BMJ Case Rep. 2020 Jan;13(1).
66. Cataño Jimenez S, Saldarriaga S, Chaput CD, Giambini H. Dual-energy estimates of volumetric bone mineral densities in the lumbar spine using quantitative computed tomography better correlate with fracture properties when compared to single-energy BMD outcomes. Bone. 2020 Jan;130:115100.
67. Barg A, Bailey T, Richter M, de Cesar Netto C, Lintz F, Burssens A, et al. Weightbearing Computed Tomography of the Foot and Ankle: Emerging Technology Topical Review. Foot ankle Int. 2018 Mar;39(3):376–86.
68. Ledoux WR, Rohr ES, Ching RP, Sangeorzan BJ. Effect of foot shape on the three-dimensional position of foot bones. J Orthop Res Off Publ Orthop Res Soc. 2006 Dec;24(12):2176–86.
69. Malicky ES, Crary JL, Houghton MJ, Agel J, Hansen STJ, Sangeorzan BJ. Talocalcaneal and subfibular impingement in symptomatic flatfoot in adults. J Bone Joint Surg Am. 2002 Nov;84(11):2005–9.
70. Greisberg J, Hansen STJ, Sangeorzan B. Deformity and degeneration in the hindfoot and midfoot joints of the adult acquired flatfoot. Foot ankle Int. 2003 Jul;24(7):530–4.
71. Ananthakrisnan D, Ching R, Tencer A, Hansen STJ, Sangeorzan BJ. Subluxation of the talocalcaneal joint in adults who have symptomatic flatfoot. J Bone Joint Surg Am. 1999 Aug;81(8):1147–54.
72. Leo CS, Lim CCT S V. An Automated Segmentation Algorithm for Medical Images. In: Lim CT GJ, editor. 13th International Conference on Biomedical Engineering IFMBE Proceedings, vol 23. Heidelberg: Springer, Berlin; 2009.
73. Nozaki S, Watanabe K, Kamiya T, Katayose M, Ogihara N. Three-Dimensional Morphological Variations of the Human Calcaneus Investigated Using Geometric Morphometrics. Clin Anat. 2020 Jul;33(5):751–8.
74. Garrick JG. The frequency of injury, mechanism of injury, and epidemiology of ankle

sprains. Am J Sports Med. 1977;5(6):241–2.
75. Baumhauer JF, Alosa DM, Renström AF, Trevino S, Beynnon B. A prospective study of ankle injury risk factors. Am J Sports Med. 1995;23(5):564–70.
76. Bonnel F, Toullec E, Mabit C, Tourné Y. Chronic ankle instability: biomechanics and pathomechanics of ligaments injury and associated lesions. Orthop Traumatol Surg Res. 2010 Jun;96(4):424–32.
77. Vuurberg G, Wink LM, Blankevoort L, Haverkamp D, Hemke R, Jens S, et al. A risk assessment model for chronic ankle instability: indications for early surgical treatment? An observational prospective cohort - study protocol. BMC Musculoskelet Disord. 2018 Jul;19(1):225.
78. Krause F, Seidel A. Malalignment and Lateral Ankle Instability: Causes of Failure from the Varus Tibia to the Cavovarus Foot. Foot Ankle Clin. 2018 Dec;23(4):593–603.
79. Kobayashi T, Gamada K. Lateral Ankle Sprain and Chronic Ankle Instability: A Critical Review. Vol. 7, Foot & ankle specialist. United States; 2014. p. 298–326.
80. Delco ML, Kennedy JG, Bonassar LJ, Fortier LA. Post-traumatic osteoarthritis of the ankle: A distinct clinical entity requiring new research approaches. J Orthop Res Off Publ Orthop Res Soc. 2017 Mar;35(3):440–53.
81. Henak CR, Anderson AE, Weiss JA. Subject-specific analysis of joint contact mechanics: application to the study of osteoarthritis and surgical planning. J Biomech Eng. 2013 Feb;135(2):21003.

Part 1

Mechanics of the hindfoot

Chapter 2

The relation between geometry and function of the ankle joint complex: a biomechanical review

Roeland P. Kleipool
Leendert Blankevoort

Knee Surg Sports Traumatol Arthrosc. 2010 May; 18(5):618–627
doi: 10.1007/s00167-010-1088-2

'find your feet'
Cambridge dictionary: to become familiar with and confident in a new situation

Abstract

This review deals with the relation between the anatomy and function of the ankle joint complex. The questions addressed are how high do the forces in the ankle joint get, where can the joints go (range of motion) and where do they go during walking and running. Finally the role of the ligaments and the articular surfaces is discussed, i.e. how does it happen. The magnitude of the loads on the ankle joint complex are primarily determined by muscle activity and can be as high as four times the body weight during walking. For the maximal range of motion, plantar and dorsiflexion occurs in the talocrural joint and marginally at the subtalar joint. In-eversion takes place at both levels. The functional range of motion is well within the limits of the maximal range of motion. The ligaments do not contribute to the forces for the functional range of motion but determine the maximal range of motion together with the articular surfaces. The geometry of the articular surfaces primarily determines the kinematics. Clinical studies must include these anatomical aspects to better understand the mechanism of injury, recovery, and interventions. Models can elucidate the mechanism by which the anatomy relates to the function. The relation between the anatomy and mechanical properties of the joint structures and joint function should be considered for diagnosis and treatment of ankle joint pathology.

Introduction

The biomechanics of the ankle joint complex (AJC) has been the subject of numerous studies. This seems warranted, since there is a large incidence of injuries of the AJC and the AJC is of great importance in normal ambulation, sports, and daily activities. The AJC comprises anatomical structures that actively and/or passively contribute to the function of the AJC. Although the anatomy was described in detail, the quantification of function and its relation with anatomy, also referred to as functional anatomy, is sparsely described in previous reviews (1–10). This review aims to address the function of the AJC in terms of loading and motion in relation to the joint's anatomy, more specifically, the role of the passive structures, i.e. the ligaments and articular surfaces.

The issues addressed in this review are the forces acting on the joint, the range of motion, joint function during activities and their relation with anatomy. With respect to the forces, the question is how high can it get? For the range of motion, where can it go? For function where does it go? For the anatomy, how does it happen? The loads on the AJC during daily activities are evaluated. It will be demonstrated what the mechanism is that determines the magnitude of the forces on the AJC. The maximum ranges of motion of the AJC are reviewed with discrimination between the talocrural joint (TCJ) and subtalar joint (STJ). and related to what is required for normal activities. Finally, some aspects of the relations between function and anatomy are reviewed.

Loads: how high can it get?

Simple biomechanical models of the ankle and foot can give realistic but generalized estimates of the magnitude of the forces acting on the ankle joint complex (11–13). These models use a free body diagram (e.g. Fig. 1), that includes only a few of all load bearing structures. The example model represents the end of the stance phase during walking or the stance phase in stair climbing (Fig. 1).

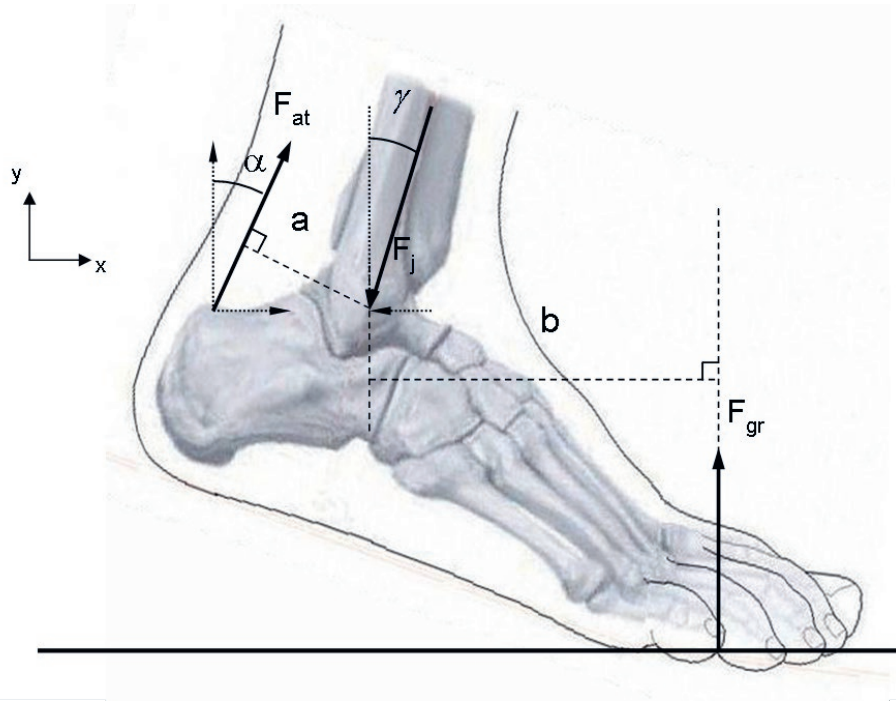

Figure 1. A simple biomechanical model of the foot and ankle for determining the forces acting on the talocrural joint. F_{at} is the Achilles tendon force, F_j the joint contact force and F_{gr} the ground reaction force. Angles α and ϒ represent the angles of the force vectors with the direction of the given y-axis. (Figure adapted from Atlas of Anatomy, General Anatomy and Muscluloskeletal System, Thieme, New York, with permission.)

Included are the ground reaction force F_{gr}, the force in the TCJ joint F_j, and the forces in the Achilles tendon F_{at}. Assuming static equilibrium, the Achilles tendon force F_{at} with known ground reaction force F_{gr} follows from the moment equilibrium.

$$F_{at} \cdot a = F_{gr} \cdot b \quad (1a)$$

$$F_{at} = F_{gr} \cdot \frac{b}{a} \quad (1b)$$

If the angles α and γ of the force vectors with the vertical are small, then the joint contact forces F_j approximately equals the sum of the ground reaction force F_{gr} and the Achilles tendon forces F_{at} :

$$F_j \cong F_{at} + F_{gr} \quad (2a)$$

$$F_j = \left(\frac{b}{a}\right) \cdot F_{gr} + F_{gr} \quad (2b)$$

The Achilles tendon force is greater than the ground reaction force. It can be drastically amplified by the ratio (b/a) of the lever arm of the ground reaction force and lever arm of the tendon force. This is usually the case in the end of the stance phase in walking and stair ascend. For example a F_{gr} of about 1 body weight (BW), a F_{at} lever arm of 5 cm and a F_{gr} lever arm of 15 cm will result in a F_{at} of 3 BW and a F_j of 4 BW. If cocontraction of the antagonist muscles is present, then the joint contact force will be higher (14). The Achilles tendon force was reported to be as high as 12.5 BW during jumping (15).

The model described above reflects the approach used by Stauffer et al. (12) and Walker (13). Procter and Paul (16) incorporated more muscles in their model. Besides the TCJ, also the STJ and talocalcaneonavicular joint were included in the analysis. A mean peak force for the TCJ of 3.9 BW (2.9–4.7 BW range) was reported for the stance phase of gait. This is somewhat smaller than was reported by Brewster et al. (17) (4.5–5.0 BW). For the STJ and talocalcaneonavicular joint loads were 2.43 BW mean (1.6–3.1 BW range) and 2.8 BW mean (2.3–3.4 BW range), respectively (16). At the beginning of the stance phase, AJC loads are lower because of the small moment arm of the ground reaction force.

In the TCJ, the load during the stance phase of gait is primarily carried by the articular contact between talus and tibial plafond, about 98% of the load for the remainder by the lateral (2%) and medial (0.01%) facets, as evaluated in a mathematical model using a discrete element analysis (18). In conclusion, muscle function is the primary determinant for the magnitude of the loads acting on the AJC. The lever arm of the ground reaction force will be the largest during the end of the stance phase and the peak force will be about 4 times the body weight during normal walking.

Ranges of motion: where can it go and where does it go?

Even with high loads, the AJC can move with little effort in plantar-dorsiflexion and in-eversion. If diagnosing and treating the instable or the arthritic ankle, attention must be paid to the maximal range of motion (MROM) of the AJC in relation to the functional range of motion (FROM). Although clinically the motion of the AJC is relatively easy to assess, the distinction between the TCJ and the STJ is essential for proper diagnosis and treatment. Different techniques were used to measure the kinematics of the AJC in vivo and in vitro. Optoelectronic systems that track surface mounted markers are easy to apply in vivo. They are not precise because of skin motion artefacts (19–23). As the talus can not be tracked, the data are limited to motions of the calcaneus relative to the tibia.

An alternative is the use of markers attached to the bone, allowing also the talus to be measured. By placing tantalum markers in the bones in combination with roentgen stereophotogrammetric analysis (RSA), Lundberg (24) was able to determine the 3D positions and orientations of the ankle bones in different joint positions. Another invasive technique is the insertion of intracortical bone pins with markers which was used in vivo (21,23,25–27) and in vitro (28–38). These studies have the advantage over the RSA technique in that the measurements can be performed while the joints moves dynamically.

Imaging techniques, such as magnetic resonance imaging (39–47) and computed tomography (48–50) were used to measure the extremes of motion or the kinematics during specific functions.

Here, the results from the various studies that measured either the MROM or the FROM are reviewed and summarized (Figs. 2, 3, 4, 5). The MROM is the maximal possible range without damaging any joint structure. The FROM in these studies is the range of motion measured during walking or running on even ground. Only those studies were included that reported the rotations in all anatomical planes, i.e. where a rotation is resolved into component rotation about three anatomical axes. Simultaneous motion in more than one anatomical direction within a joint is named coupled motion, whereas combined motion is composed of similar motion components that occur simultaneously in the TCJ and the STJ (50).

Dorsi-plantarflexion in the talocrural joint

The total MROM from dorsiflexion to plantarflexion in the TCJ in the sagittal plane is about 57 degrees (±10 deg. SD) (50) (Fig. 2). As the rotation axis of the TCJ is oblique relative to the anatomical planes, there are coupled rotations in the frontal and

transverse plane. For walking and running the FROM is variable among studies, but much smaller than the MROM (Fig. 2). Relative to the neutral position, i.e. the foot in the sagittal plane at 90 degrees relative to the tibia, the MROM for plantarflexion is about twice that for dorsiflexion (30,50) (Fig. 3). During walking the FROM takes up a large portion of the MROM for dorsiflexion but a small portion of the MROM for plantarflexion (Fig. 3). The differences between the studies can be explained by differences in the methods applied. Furthermore, the definition of the coordinate system has an effect on the resulting rotation components (51). Tuijthof et al. (50) defined a coordinate system based on the anatomical axis of the talus, whereas others used a reference system based on foot anatomy.

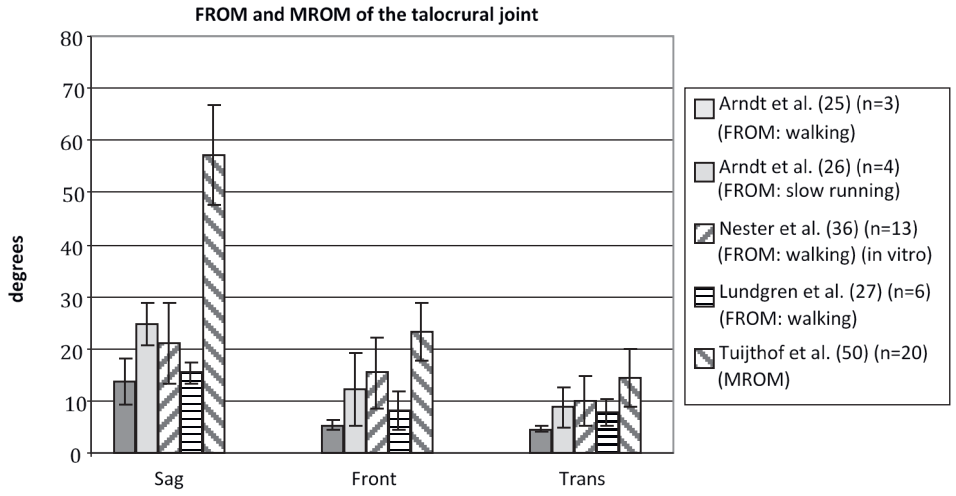

Figure 2. MROM (50) and FROM (25–27,36) of the TCJ. *Sag* sagittal plane (dorsi- and plantarflexion), *Front* frontal plane (eversion and inversion), *Trans* transversal plane (internal and external rotation). Bars represent the different studies. Error bars represent ± one standard deviation.

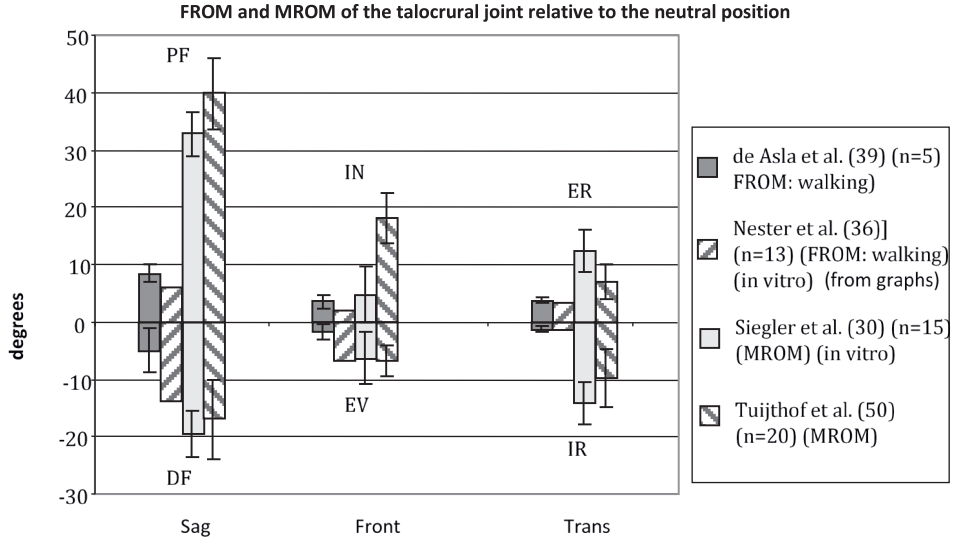

Figure 3. FROM (36,39) and MROM (30,50) of the TCJ. DF dorsiflexion, PF plantarflexion (sagittal plane). EV eversion, IN inversion (frontal plane). IR internal rotation, ER external rotation (transversal plane). 0 degrees correspond to the neutral position. Bars represent the different studies. Error bars represent ± one standard deviation.

In-eversion of the subtalar joint

The reported total MROM from eversion to inversion in the STJ in the frontal plane ranges between about 17 degrees (±4 deg. SD) (52) to 23 degrees (±4 deg. SD) (50) (Fig. 4). Because of the anatomy of the STJ inversion is coupled to internal rotation and eversion is coupled to external rotation (30,50,53). As the articular facets of the STJ have a vertical aspect (10,54), there is marginal plantar and dorsiflexion (50). For walking and running the FROM in the frontal and transverse plane is variable but much smaller than the MROM. The MROM and FROM in the sagittal plane is also variable but the differences between the MROM and FROM is less. Since the sagittal motion in the STJ is marginal this difference is expected to be smaller. Relative to the neutral position the MROM for inversion is about equal to eversion (30,50) (Fig. 5). During walking the FROM takes up a small portion of the MROM (Fig. 5). The reported FROM for in-eversion of the STJ are rather small. This might be because the walking activity was on even ground. The role of the STJ has been described to be responsible for accommodation to uneven ground (1,5,39,55). Higher values of in-eversion are to be expected if the foot is placed on uneven grounds (e.g. (41)).

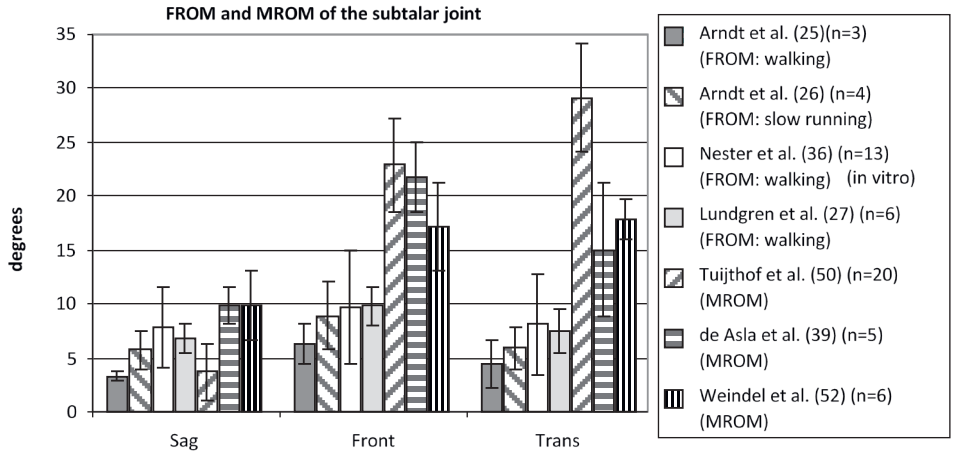

Figure 4. FROM (27,36,39,40) and MROM (39,50,52) of the STJ. *Sag* sagittal plane (dorsi- and plantarflexion), *Front* frontal plane (eversion and inversion), *Trans* transversal plane (internal and external rotation). Bars represent the different studies. Error bars represent ± one standard deviation.

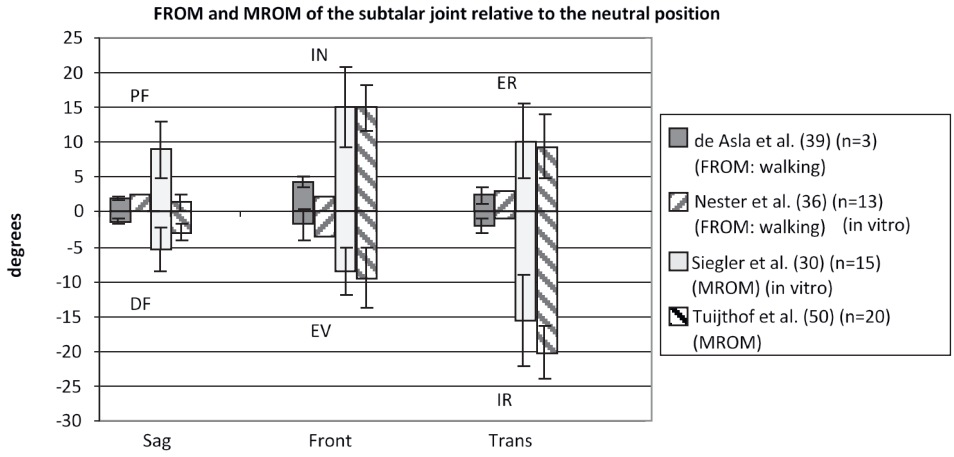

Figure 5. FROM (36,39) and MROM (30,50) of the STJ. DF dorsiflexion, PF plantarflexion (sagittal plane). EV eversion, IN inversion (frontal plane). IR internal rotation, ER external rotation. Bars represent the different studies. Error bars represent ± one standard deviation.

Motion at two levels

The motion of the AJC is the combination of motion at two levels. Flexion is primarily at the level of the TCJ, with little or no motion in the STJ (50). The MROM for in-eversion is reported to occur as a combined motion in both joints (50), whereby approximately two-third is at the level of the STJ and one-third at the level of the TCJ. The general orientation of the two rotational axes leads to coupling of inversion to internal rotation and eversion to external rotation in both joints (30,50,53). The motion within the limits of the MROM was also described to occur within the so-called neutral zone, where the moment required to rotate the joints is small (56–58). The implication is that muscle forces and muscle coordination are required to stabilize the joints during activities.

Relation between geometry and function: how does it happen?

It can be hypothesized that the morphology of the joint complex, i.e. geometry of articular surfaces and of the ligaments, is the primary determinant of the MROM and the kinematics for the FROM (59). This is, to some extent supported, by Imhauser et al. (34) who made models of the AJC of six specimens based on morphological data obtained by MR images (Fig. 6). The mechanical properties of cartilage and ligaments were the same for all models and were estimated from literature data. Forced inversion (3.4 Nm) and forced anterior drawer (150 N) were compared between the specimen-specific model and the experiment on the specimen (Fig. 7). Apparently, for inversion more than for anterior drawer, the maximum range is determined by geometric differences. If extrapolating this, geometrical differences between subjects may explain differences in MROM and FROM of the AJC between subjects. Secondary to the geometry, the stiffness of the ligaments determines the stiffness of the joint at the limits of the MROM and the stiffness of the cartilage determines the contact area and stresses and strains in the articular contact.

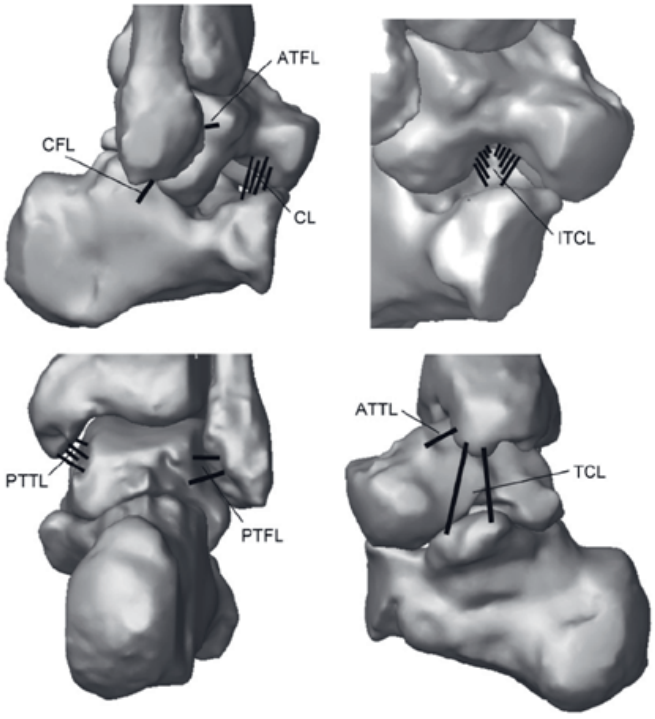

Figure 6. A 3D representation of the specimen specific model of an ankle joint used in the study of Imhauser et al. (34) to predict the forced inversion range of motion and anterior drawer translation with experimentally determined values (Reproduced with permission)

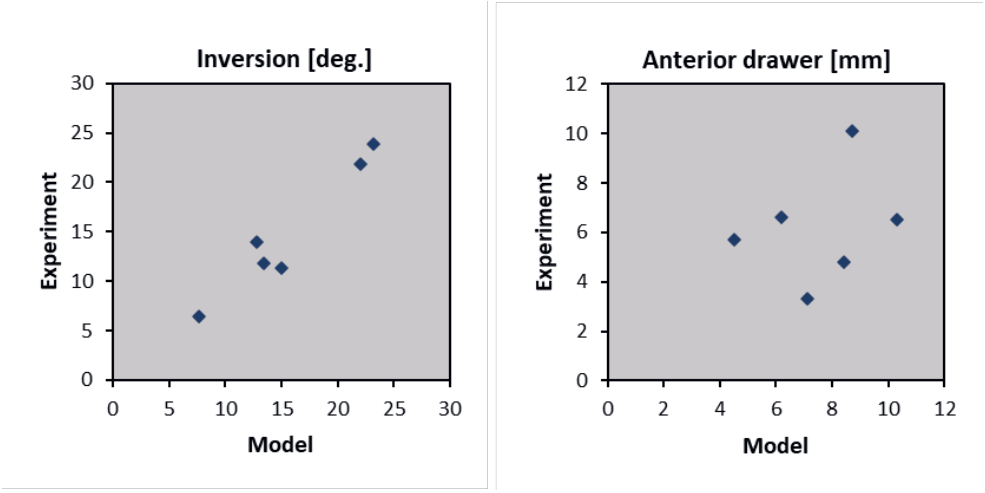

Figure 7. Scatter diagram of the one-to-one comparison between model predictions and the corresponding experimentally determined forced inversion (3.4 Nm) and forced anterior drawer (150 N) in 6 ankle joint specimen in the study of Imhauser et al. (34)

In extension to the results of Imhauser et al. (34), the function of ligaments and articular surfaces are further discussed.

Ligaments

The main ligaments of the AJC are the laterally situated anterior talofibular (ATFL), calcaneofibular (CFL), and posterior talofibular ligament (PTFL) and the medially situated deltoid ligament. Ligaments between the talus and calcaneus (e.g. interosseous talocalcaneal and posterior talocalcaneal ligament) are beyond the scope of this review.

The function of the ankle joint ligaments is thought to control and limit the motions between the bones that comprise one or more joints. Many studies have shown that the ankle ligaments determine the MROM. Usually this was demonstrated by in vitro experiments where the effect is measured of ligament dissection on the MROM (e.g. (60–64)).

The ATFL restrains inversion and anterior talar translation at all positions of flexion (4). The CFL limits inversion together with the ATFL in plantarflexion and neutral position, and together with the PTFL in dorsiflexion (62). The PTFL restraints external rotation in dorsiflexion (62).

The deltoid ligament is a large fan-shaped ligament originating from the medial malleolus. Because of the many variations and different insertions, it is difficult to discuss

the function of the deltoid ligament as a whole. The most frequently reported function is the restraint against eversion (4).

Alternatives to cutting experiments are measurements of ligament length (40,55,65), strain (66–71) or force (29,67,69,72). Data on ligament forces are scarce, but give some clue as to the function in controlling and restraining ankle joint motion (29,67,69,72,73). The interpretation of the data on ligament length or strain as function of joint motion is hampered by the problem of defining the zero-load length of the ligaments. So is ligament strain, which is defined as

$$\varepsilon = \frac{[(L - L_0)]}{L_0} \qquad (3)$$

where ε is the strain, L the current length and L_0 the zeroload length. The length of a ligament is a function of the distance between its origin and insertion and is thus a function of the relative motion between the bones. A strain smaller than zero means that a ligament is slack and does not function. Only ligament strains greater than zero result in a force in the ligament.

Studies that used a reference length that is equal to the length in the neutral position of the AJC, usually with the foot in 90 degrees relative to the tibia, report relative length changes with joint motion for which it is not clear whether ligaments are actually tensioned (e.g. (67,68,71,74)).

There are few studies that address the determination of the zero-load length and report estimates of the strain in ankle ligaments (69,70,75,76). These studies show that not all ligaments are taut in the neutral position of the ankle. Ozeki et al. (70) reported zero-load lengths of the four major ankle ligaments and also reported joint positions in dorsal-plantar flexion for the transition from slack to taut (Table 1).

Table 1. Zero-load length L_0 (in mm) of the ankle ligaments derived from Ozeki et al. (70) and the joint position for the transition between slack and taut

	L_0 (mm)	Joint position as slack-taut transition
ATFL	20.4	16.2 ± 2.6° PF
CFL	24.6	17.2 ± 6.4° DF
PTFL	30.5	18.0 ± 7.5° DF
TCL	27.4	9.5.2 ± 8.9° PF

ATFL anterior talofibular ligament, CFL calcaneofibular ligament, PTFL posterior talofibular ligament, TCL tibiocalcaneal ligament. The following abbreviations indicate the motion direction for which the ligaments becomes taut: DF dorsiflexion, PF plantarflexion

The finding that the reported ankle ligaments are slack for neutral joint position and taut after a certain level of plantar or dorsiflexion, is in agreement with earlier findings of Nigg et al. (69) and Bahr et al. (29). The latter showed that in a range of 10 degrees of dorsiflexion and 20 degrees of plantarflexion the force in the ATFL and CFL are zero or very small.

Studies that evaluated ligament function during walking confirm that the four ankle ligaments are slack (18,76). So within the FROM the ligaments are slack and towards the MROM they are tensioned (76). Because of the low stiffness of ligaments for small strains (66,74,75,77) and the small moment arms, it questionable that the ligaments play an important role in guiding and limiting joint motion for normal functional activities. Also, the maximal forces in the ligaments as reported in literature (29,67–69,71) during motion and in the extreme end of motion are rather small if compared to the tendon loads. However, at the extremes of joint motion, plantar-dorsiflexion and in-eversion, but also forced anterior drawer (3) the ligaments act as motion constraints jointly with the articular contact.

The ligament may have a sensory function, hypothesized as early as 1900 (78). Mechanoreceptors are found not only in the AJC ligaments (79–81), but also in other joints and can control muscle activity (81,82). Assuming there is a proprioceptive role for ligaments, then damage or rupture will result in a loss of neurosensory information.

Articular contacts

As elaborated above, the ligaments of the AJC do not contribute to the mechanics of the TCJ and STJ within the FROM. Therefore, the mechanics are primarily determined by the geometry of the articulating surfaces (4,10,18,41). The TCJ and STJ are highly congruent joints with a total contact area of 1.5–9.4 cm2 (4). The geometry of the articulating surfaces determine the kinematics and stability of the joints. If contact is

maintained, the TCJ and STJ appear to function as joints with one degree of freedom of motion (41). However, towards the limits of motion and in functional stress tests, like forced anterior drawer or forced in or eversion, congruent contact is not maintained. The motion will then deviate from the normal kinematics within the MROM. The question here is how much evidence exist for the relation between articular contact geometry and the kinematics for the FROM and beyond that but within the MROM. The second question is how the articular contact geometry contributes to the stability of the joints for the extremes of motion and for stress tests.

If the TCJ is statically compressed than the restraint against dislocating torques is primarily provided by the articular surfaces (18,58,63,83). The reported contribution levels accounted for 100% (58) and 70% (83) of anterior/posterior stability, 100% (63) and 50% (83) of in-eversion stability, and 30% (63,83) or 60% (58) of internal/external rotation stability. Tochigi et al. (83) did not include the talomalleolar articulation and this might explain the lower contribution percentages in in-eversion and anterior–posterior stability.

The ankle mortise comprises the tibia and fibula with both malleoli. The talus is thus tightly packed. There is considerable variation in the shape of the TCJ (84–86) and STJ (54) among subjects. The shape of the tibial plafond in combination with the curvature of the trochlea tali (87,88) determines the stability in the anterior posterior direction (89,90) and the varus tilt of the tibial plafond is related to chronic ankle instability (91). In agreement with this finding is that a simulated fracture, by an osteotomy of the anterior part of the distal tibia results in an increased anterior laxity of the TCJ (92). An altered joint geometry, such as after malunion of a fracture, can result in joint instability (92,93). Also, an additional joint contact, e.g. a Stieda process, can result in different kinematics (44). Barbaix et al. (54) hypothesized a same contribution of the anatomy of the STJ and subtalar instability, but no literature was found to proof this.

Discussion

This review addressed four questions concerning the ankle joint complex. The first was on the loading of the joint. How high can it get? The second was on the MROM. Where can it go? This was followed by the FROM. Where does it go? Finally, the relation between function and morphology was addressed. How does it happen? The literature was reviewed, such that answers were obtained on the above questions and, where possible quantitative data was presented. The review was limited to addressing the above questions.

The load on the ankle joint is high, amounting to several times the body weight. The primary determinants of the magnitude of the joint contact force are the ground reaction force of the foot and the moment arm of this force. Literature data on joint loading show variability among subjects or joint specimens. This may be the effect of variable geometry, i.e. moment arms of the muscles, but also of differences in muscle coordination and cocontraction of antagonist muscles.

The MROM of the AJC, i.e. the calcaneus relative to the tibia is achieved by the ROM of the TCJ and the STJ. It can be concluded that dorsi and plantarflexion is only at the level of the TCJ, whereas in-eversion is both at the level of the STJ and TCJ. A great variability is present between individuals.

Quantitative data on the FROM at the level of the TCJ and the STJ are limited to simple activities like walking and running on even ground. This may have underestimated the FROM for in-eversion. At any rate, the FROM are well within the MROM of the joints.

The mechanics of the AJC is not only a function of the geometry, but also of the mechanical properties of the ligaments and articular surfaces. It appears however, that ligament and articular geometry are the primary determinants of the MROM and FROM. Cutting ligaments affects the MROM, but if intact, their stiffness only affects the stiffness at the limits of the MROM and not so much the ROM itself. No or little contribution of the ligaments is to be expected for motion and loading within the MROM. Stability is then determined by the congruency of the articular surfaces and stabilizing function of the muscles. Various studies have shown that differences in articular geometry may explain the differences in function and even differences in susceptibility to ligament injury. In the future, much more need to be uncovered in this regard. Studies should aim for including geometric characteristics of the joints that are studied to be correlated with functional measures. Advanced mechanical models may find the mechanisms that govern the relations between geometry and function.

The AJC is a passive mechanical system that connects the foot to the lower leg. The ankle joint complex has interactions with the mid and forefoot, both passively through articular contacts and ligaments and actively by the tendons crossing the ankle.

Conversely, there is no passive mechanical interaction with the knee joint. So it is a simplification to describe the mechanics of the AJC in isolation, though many studies have done this. The interaction with the mid and forefoot is more relevant for the STJ than for the TCJ, but the function of the latter cannot be considered in isolation from the former, because of the ligaments that span both joints. So in this respect, the review is limited by not addressing explicitly the interactions with mid and forefoot.

The clinical consequences are diverse. For developing diagnostic and treatment techniques for ankle ligament injuries, the contributions came from the studies on ligament function at the extremes of the range of motion. However, ligament function during sports activities, strenuous exercises or for near accidents remains to be uncovered. This may give guidelines for ligament reconstruction and postoperative rehabilitation. More importantly, future diagnostic techniques and treatments should include subject specific parameters, preferably to be included in personalized models, that not only include the passive mechanics but also the function of the dynamic stabilizing function of the muscles. These are the scientific challenges.

Clinicians can use these results to better understand the joint contact force determining factors. The values of FROM and MROM are helpful in diagnosing and interventions such as arthrodesis and the clinician should take into account that during normal ambulation motion takes place at both levels. Also, the clinician must understand the function of ligaments, i.e. it is not a limiting structure in the FROM, because the ligaments do not contribute to the stability within the FROM. Ligament reconstruction should take into account the zero-slack length for it determines at which joint angles the ligament is tensed and contributes to the force balance.

Conclusion

During walking the maximal joint contact force is about four times the body weight. This value is reached at the end of the stance phase where the moment arm of the ground reaction force is high. There is large variability between subjects in both MROM and FROM. The motion in the sagittal plane is primarily the result of the TCJ, but in the frontal plane both joint levels contribute. There is evidence that the geometry of the articular surfaces determines the kinematics. Also the susceptibility to ankle injury might be explained in terms of AJC geometry. The ligaments are only restraining the motion near the MROM, so articular surfaces, alternatively in combination with muscle activity, must provide the stability within the FROM.

References

1. Budny A. Subtalar joint instability: current clinical concepts. Clin Podiatr Med Surg. 2004 Jul;21(3):449–60, viii.
2. Chan CW, Rudins A. Foot biomechanics during walking and running. Mayo Clin Proc. 1994 May;69(5):448–61.
3. Kerkhoffs GM, Blankevoort L, van Poll D, Marti RK, van Dijk CN. Anterior lateral ankle ligament damage and anterior talocrural-joint laxity: an overview of the in vitro reports in literature. Clin Biomech (Bristol, Avon). 2001 Oct;16(8):635–43.
4. Leardini A, O'Connor JJ, Catani F, Giannini S. The role of the passive structures in the mobility and stability of the human ankle joint: a literature review. Foot ankle Int. 2000 Jul;21(7):602–15.
5. Michael JM, Golshani A, Gargac S, Goswami T. Biomechanics of the ankle joint and clinical outcomes of total ankle replacement. J Mech Behav Biomed Mater. 2008 Oct;1(4):276–94.
6. Morris JM. Biomechanics of the foot and ankle. Clin Orthop Relat Res. 1977;(122):10–7.
7. Nester CJ. Rearfoot complex: a review of its interdependent components, axis orientation and functional model. Foot. 1997;8:86–96.
8. Nester CJ. Review of literature on the axis of rotation at the subtalar joint. Foot1. 1998;8:111–8.
9. Perry J. Anatomy and biomechanics of the hindfoot. Clin Orthop Relat Res. 1983;(177):9–15.
10. Sarrafian SK. Biomechanics of the subtalar joint complex. Clin Orthop Relat Res. 1993 May;(290):17–26.
11. Kim W, Voloshin AS. Role of plantar fascia in the load bearing capacity of the human foot. J Biomech. 1995 Sep;28(9):1025–33.
12. Stauffer RN, Chao EY, Brewster RC. Force and motion analysis of the normal, diseased, and prosthetic ankle joint. Clin Orthop Relat Res. 1977;(127):189–96.
13. Walker P. Human joints and their artificial replacement. Springfield: Charles C. Thomas; 1977.
14. Potthast W, Lersch C, Segesser B, Koebke J, Bruggemann G-P. Intraarticular pressure distribution in the talocrural joint is related to lower leg muscle forces. Clin Biomech (Bristol, Avon). 2008 Jun;23(5):632–9.
15. Komi P V. Relevance of in vivo force measurements to human biomechanics. J Biomech. 1990;23 Suppl 1:23–34.
16. Procter P, Paul JP. Ankle joint biomechanics. J Biomech. 1982;15(9):627–34.
17. Brewster RC. Force analysis of the ankle joint during the stance phase of gait. In: 27th ACEMB Alliance for Engineers, editor. Philadelphia; 1974.
18. Haraguchi N, Armiger RS, Myerson MS, Campbell JT, Chao EYS. Prediction of three-dimensional contact stress and ligament tension in the ankle during stance determined from computational modeling. Foot ankle Int. 2009 Feb;30(2):177–85.
19. Cappozzo A, Catani F, Leardini A, Benedetti MG, Croce U Della. Position and orientation in space of bones during movement: experimental artefacts. Clin Biomech (Bristol, Avon). 1996 Mar;11(2):90–100.

20. Leardini A, Chiari L, Della Croce U, Cappozzo A. Human movement analysis using stereophotogrammetry. Part 3. Soft tissue artifact assessment and compensation. Gait Posture. 2005 Feb;21(2):212–25.
21. Reinschmidt C, van Den Bogert AJ, Murphy N, Lundberg A, Nigg BM. Tibiocalcaneal motion during running, measured with external and bone markers. Clin Biomech (Bristol, Avon). 1997 Jan;12(1):8–16.
22. Stacoff A, Nigg BM, Reinschmidt C, van den Bogert AJ, Lundberg A. Tibiocalcaneal kinematics of barefoot versus shod running. J Biomech. 2000 Nov;33(11):1387–95.
23. Westblad P, Hashimoto T, Winson I, Lundberg A, Arndt A. Differences in ankle-joint complex motion during the stance phase of walking as measured by superficial and bone-anchored markers. Foot ankle Int. 2002 Sep;23(9):856–63.
24. Lundberg A. Kinematics of the ankle and foot. In vivo roentgen stereophotogrammetry. Acta Orthop Scand Suppl. 1989;233:1–24.
25. Arndt A, Westblad P, Winson I, Hashimoto T, Lundberg A. Ankle and subtalar kinematics measured with intracortical pins during the stance phase of walking. Foot ankle Int. 2004 May;25(5):357–64.
26. Arndt A, Wolf P, Liu A, Nester C, Stacoff A, Jones R, et al. Intrinsic foot kinematics measured in vivo during the stance phase of slow running. J Biomech. 2007;40(12):2672–8.
27. Lundgren P, Nester C, Liu A, Arndt A, Jones R, Stacoff A, et al. Invasive in vivo measurement of rear-, mid- and forefoot motion during walking. Gait Posture. 2008 Jul;28(1):93–100.
28. Astion DJ, Deland JT, Otis JC, Kenneally S. Motion of the hindfoot after simulated arthrodesis. J Bone Joint Surg Am. 1997 Feb;79(2):241–6.
29. Bahr R, Pena F, Shine J, Lew WD, Engebretsen L. Ligament force and joint motion in the intact ankle: a cadaveric study. Knee Surg Sports Traumatol Arthrosc. 1998;6(2):115–21.
30. Siegler S, Chen J, Schneck CD. The three-dimensional kinematics and flexibility characteristics of the human ankle and subtalar joints--Part I: Kinematics. J Biomech Eng. 1988 Nov;110(4):364–73.
31. Fujii T, Kitaoka HB, Luo Z-P, Kura H, An K-N. Analysis of ankle-hindfoot stability in multiple planes: an in vitro study. Foot ankle Int. 2005 Aug;26(8):633–7.
32. Hamel AJ, Sharkey NA, Buczek FL, Michelson J. Relative motions of the tibia, talus, and calcaneus during the stance phase of gait: a cadaver study. Gait Posture. 2004 Oct;20(2):147–53.
33. Hurschler C, Emmerich J, Wulker N. In vitro simulation of stance phase gait part I: Model verification. Foot ankle Int. 2003 Aug;24(8):614–22.
34. Imhauser CW, Siegler S, Udupa JK, Toy JR. Subject-specific models of the hindfoot reveal a relationship between morphology and passive mechanical properties. J Biomech. 2008;41(6):1341–9.
35. Kerkhoffs G, Blankevoort L, Kingma I, van Dijk N. Three-dimensional bone kinematics in an anterior laxity test of the ankle joint. Knee Surg Sports Traumatol Arthrosc. 2007 Jun;15(6):817–24.
36. Nester CJ, Liu AM, Ward E, Howard D, Cocheba J, Derrick T, et al. In vitro study of foot kinematics using a dynamic walking cadaver model. J Biomech. 2007;40(9):1927–37.
37. Okita N, Meyers SA, Challis JH, Sharkey NA. An objective evaluation of a segmented

foot model. Gait Posture. 2009 Jul;30(1):27–34.
38. Rosenbaum D, Becker HP, Wilke HJ, Claes LE. Tenodeses destroy the kinematic coupling of the ankle joint complex. A three-dimensional in vitro analysis of joint movement. J Bone Joint Surg Br. 1998 Jan;80(1):162–8.
39. de Asla RJ, Wan L, Rubash HE, Li G. Six DOF in vivo kinematics of the ankle joint complex: Application of a combined dual-orthogonal fluoroscopic and magnetic resonance imaging technique. J Orthop Res. 2006 May;24(5):1019–27.
40. de Asla RJ, Kozanek M, Wan L, Rubash HE, Li G. Function of anterior talofibular and calcaneofibular ligaments during in-vivo motion of the ankle joint complex. J Orthop Surg Res. 2009 Mar;4:7.
41. Goto A, Moritomo H, Itohara T, Watanabe T, Sugamoto K. Three-dimensional in vivo kinematics of the subtalar joint during dorsi-plantarflexion and inversion-eversion. Foot ankle Int. 2009 May;30(5):432–8.
42. Mattingly B, Talwalkar V, Tylkowski C, Stevens DB, Hardy PA, Pienkowski D. Three-dimensional in vivo motion of adult hind foot bones. J Biomech. 2006;39(4):726–33.
43. Ringleb SI, Udupa JK, Siegler S, Imhauser CW, Hirsch BE, Liu J, et al. The effect of ankle ligament damage and surgical reconstructions on the mechanics of the ankle and subtalar joints revealed by three-dimensional stress MRI. J Orthop Res. 2005 Jul;23(4):743–9.
44. Sheehan FT, Seisler AR, Siegel KL. In vivo talocrural and subtalar kinematics: a non-invasive 3D dynamic MRI study. Foot ankle Int. 2007 Mar;28(3):323–35.
45. Siegler S, Udupa JK, Ringleb SI, Imhauser CW, Hirsch BE, Odhner D, et al. Mechanics of the ankle and subtalar joints revealed through a 3D quasi-static stress MRI technique. J Biomech. 2005 Mar;38(3):567–78.
46. Stindel E, Udupa JK, Hirsch BE, Odhner D. An in vivo analysis of the motion of the peri-talar joint complex based on MR imaging. IEEE Trans Biomed Eng. 2001 Feb;48(2):236–47.
47. Wolf P, Luechinger R, Boesiger P, Stuessi E, Stacoff A. A MR imaging procedure to measure tarsal bone rotations. J Biomech Eng. 2007 Dec;129(6):931–6.
48. Beimers L, Tuijthof GJM, Blankevoort L, Jonges R, Maas M, van Dijk CN. In-vivo range of motion of the subtalar joint using computed tomography. J Biomech. 2008;41(7):1390–7.
49. Imai K, Tokunaga D, Takatori R, Ikoma K, Maki M, Ohkawa H, et al. In vivo three-dimensional analysis of hindfoot kinematics. Foot ankle Int. 2009 Nov;30(11):1094–100.
50. Tuijthof GJM, Zengerink M, Beimers L, Jonges R, Maas M, van Dijk CN, et al. Determination of consistent patterns of range of motion in the ankle joint with a computed tomography stress-test. Clin Biomech (Bristol, Avon). 2009 Jul;24(6):517–23.
51. Blankevoort L, Huiskes R, de Lange A. The envelope of passive knee joint motion. J Biomech. 1988;21(9):705–20.
52. Weindel S, Schmidt R, Rammelt S, Claes L, v Campe A, Rein S. Subtalar instability: a biomechanical cadaver study. Arch Orthop Trauma Surg. 2010 Mar;130(3):313–9.
53. Leardini A, Stagni R, O'Connor JJ. Mobility of the subtalar joint in the intact ankle complex. J Biomech. 2001 Jun;34(6):805–9.
54. Barbaix E, Van Roy P, Clarys JP. Variations of anatomical elements contributing to subtalar joint stability: intrinsic risk factors for post-traumatic lateral instability of the

ankle? Ergonomics. 2000 Oct;43(10):1718–25.
55. Martin LP, Wayne JS, Monahan TJ, Adelaar RS. Elongation behavior of calcaneofibular and cervical ligaments during inversion loads applied in an open kinetic chain. Foot ankle Int. 1998 Apr;19(4):232–9.
56. Ching RP, Tencer AF, Anderson PA, Daly CH. Comparison of residual stability in thoracolumbar spine fractures using neutral zone measurements. J Orthop Res. 1995 Jul;13(4):533–41.
57. Panjabi MM, Summers DJ, Pelker RR, Videman T, Friedlaender GE, Southwick WO. Three-dimensional load-displacement curves due to forces on the cervical spine. J Orthop Res. 1986;4(2):152–61.
58. Watanabe K, Crevoisier XM, Kitaoka HB, Zhao KD, Berglund LJ, Kaufman KR, et al. Analysis of joint laxity after total ankle arthroplasty: cadaver study. Clin Biomech (Bristol, Avon). 2009 Oct;24(8):655–60.
59. Franci R, Parenti-Castelli V, Belvedere C, Leardini A. A new one-DOF fully parallel mechanism for modelling passive motion at the human tibiotalar joint. J Biomech. 2009 Jul;42(10):1403–8.
60. Fujii T, Luo ZP, Kitaoka HB, An KN. The manual stress test may not be sufficient to differentiate ankle ligament injuries. Clin Biomech (Bristol, Avon). 2000 Oct;15(8):619–23.
61. Kjaersgaard-Andersen P, Wethelund JO, Helmig P, Soballe K. The stabilizing effect of the ligamentous structures in the sinus and canalis tarsi on movements in the hindfoot. An experimental study. Am J Sports Med. 1988;16(5):512–6.
62. Rasmussen O. Stability of the ankle joint. Analysis of the function and traumatology of the ankle ligaments. Acta Orthop Scand Suppl. 1985;211:1–75.
63. Stormont DM, Morrey BF, An KN, Cass JR. Stability of the loaded ankle. Relation between articular restraint and primary and secondary static restraints. Am J Sports Med. 1985;13(5):295–300.
64. Tochigi Y, Takahashi K, Yamagata M, Tamaki T. Influence of the interosseous talocalcaneal ligament injury on stability of the ankle-subtalar joint complex--a cadaveric experimental study. Foot ankle Int. 2000 Jun;21(6):486–91.
65. Stagni R, Leardini A, Ensini A. Ligament fibre recruitment at the human ankle joint complex in passive flexion. J Biomech. 2004 Dec;37(12):1823–9.
66. Butler AM, Walsh WR. Mechanical response of ankle ligaments at low loads. Foot ankle Int. 2004 Jan;25(1):8–12.
67. Cawley PW, France EP. Biomechanics of the lateral ligaments of the ankle: an evaluation of the effects of axial load and single plane motions on ligament strain patterns. Foot Ankle. 1991 Oct;12(2):92–9.
68. Colville MR, Marder RA, Boyle JJ, Zarins B. Strain measurement in lateral ankle ligaments. Am J Sports Med. 1990;18(2):196–200.
69. Nigg BM, Skarvan G, Frank CB, Yeadon MR. Elongation and forces of ankle ligaments in a physiological range of motion. Foot Ankle. 1990 Aug;11(1):30–40.
70. Ozeki S, Yasuda K, Kaneda K, Yamakoshi K, Yamanoi T. Simultaneous strain measurement with determination of a zero strain reference for the medial and lateral ligaments of the ankle. Foot ankle Int. 2002 Sep;23(9):825–32.
71. Renstrom P, Wertz M, Incavo S, Pope M, Ostgaard HC, Arms S, et al. Strain in the lateral ligaments of the ankle. Foot Ankle. 1988 Oct;9(2):59–63.

72. Shybut, GT Hayes, WC White A. Normal patterns of ligament loading among the collateral ligaments. 29th Annual ORS; 1993.
73. Beumer A, van Hemert WLW, Swierstra BA, Jasper LE, Belkoff SM. A biomechanical evaluation of the tibiofibular and tibiotalar ligaments of the ankle. Foot ankle Int. 2003 May;24(5):426–9.
74. Siegler S, Block J, Schneck CD. The mechanical characteristics of the collateral ligaments of the human ankle joint. Foot Ankle. 1988 Apr;8(5):234–42.
75. Funk JR, Hall GW, Crandall JR, Pilkey WD. Linear and quasi-linear viscoelastic characterization of ankle ligaments. J Biomech Eng. 2000 Feb;122(1):15–22.
76. Tochigi Y, Rudert MJ, Amendola A, Brown TD, Saltzman CL. Tensile engagement of the peri-ankle ligaments in stance phase. Foot ankle Int. 2005 Dec;26(12):1067–73.
77. Attarian DE, McCrackin HJ, DeVito DP, McElhaney JH, Garrett WEJ. Biomechanical characteristics of human ankle ligaments. Foot Ankle. 1985 Oct;6(2):54–8.
78. Pyar E. Der Heutige Stand der Gelenckchirurgic. Arch Klin Chir. 1900;48:404–51.
79. Michelson JD, Hutchins C. Mechanoreceptors in human ankle ligaments. J Bone Joint Surg Br. 1995 Mar;77(2):219–24.
80. Moraes MRB, Cavalcante MLC, Leite JAD, Ferreira FV, Castro AJO, Santana MG. Histomorphometric evaluation of mechanoreceptors and free nerve endings in human lateral ankle ligaments. Foot ankle Int. 2008 Jan;29(1):87–90.
81. Takebayashi T, Yamashita T, Minaki Y, Ishii S. Mechanosensitive afferent units in the lateral ligament of the ankle. J Bone Joint Surg Br. 1997 May;79(3):490–3.
82. Solomonow M, Lewis J. Reflex from the ankle ligaments of the feline. J Electromyogr Kinesiol. 2002 Jun;12(3):193–8.
83. Tochigi Y, Rudert MJ, Saltzman CL, Amendola A, Brown TD. Contribution of articular surface geometry to ankle stabilization. J Bone Joint Surg Am. 2006 Dec;88(12):2704–13.
84. Fessy MH, Carret JP, Bejui J. Morphometry of the talocrural joint. Surg Radiol Anat. 1997;19(5):299–302.
85. Hayes A, Tochigi Y, Saltzman CL. Ankle morphometry on 3D-CT images. Iowa Orthop J. 2006;26:1–4.
86. Stagni R, Leardini A, Ensini A, Cappello A. Ankle morphometry evaluated using a new semi-automated technique based on X-ray pictures. Clin Biomech (Bristol, Avon). 2005 Mar;20(3):307–11.
87. Barnett CH, Napier JR. The axis of rotation at the ankle joint in man; its influence upon the form of the talus and the mobility of the fibula. J Anat. 1952 Jan;86(1):1–9.
88. Inman VT. The joints of the ankle. Baltimore: Williams and Wilkins;
89. Frigg A, Frigg R, Hintermann B, Barg A, Valderrabano V. The biomechanical influence of tibio-talar containment on stability of the ankle joint. Knee Surg Sports Traumatol Arthrosc. 2007 Nov;15(11):1355–62.
90. Kanbe K, Hasegawa A, Nakajima Y, Takagishi K. The relationship of the anterior drawer sign to the shape of the tibial plafond in chronic lateral instability of the ankle. Foot ankle Int. 2002 Feb;23(2):118–22.
91. Sugimoto K, Samoto N, Takakura Y, Tamai S. Varus tilt of the tibial plafond as a factor in chronic ligament instability of the ankle. Foot ankle Int. 1997 Jul;18(7):402–5.
92. Tochigi Y, Rudert MJ, McKinley TO, Pedersen DR, Brown TD. Correlation of dynamic cartilage contact stress aberrations with severity of instability in ankle incongruity. J

Orthop Res. 2008 Sep;26(9):1186–93.
93. Michelson JD, Hamel AJ, Buczek FL, Sharkey NA. Kinematic behavior of the ankle following malleolar fracture repair in a high-fidelity cadaver model. J Bone Joint Surg Am. 2002 Nov;84(11):2029–38.

Chapter 3

The dimensions of the tarsal sinus and canal in different foot positions and its clinical implications

Roeland P. Kleipool
Leendert Blankevoort
Jan M. Ruijter
Gino M.M.J. Kerkhoffs
Roelof-Jan Oostra

Clin Anat. 2017 Nov;30(8):1049-1057.
doi: 10.1002/ca.22908

'put your best foot forward'
Cambridge dictionary: to try as hard as you can

Abstract

This study presents a reference for the dimensions of the tarsal sinus and canal in healthy adults in different foot positions to facilitate understanding of the kinematics of the subtalar joint, the effect of an implant, and other clinical issues. In a 3D CT stress test on 20 subjects, the right foot was forced into a neutral and eight different extreme foot positions while CT scans were obtained. The bones were segmented in the neutral foot position. The kinematics of the bones in the extreme positions were determined relative to the neutral position. The dimensions of the tarsal sinus and canal were calculated by determining the radii of the maximal inscribed spheres at 20 equidistant locations along an axis in 3D surface models of the tali and calcanei in each foot position. The radii were small on the medial side and increased laterally. Medial from the middle, the radii were small and not significantly different among the various foot positions. At the lateral side, the dimensions were affected mainly by eversion or inversion and less by dorsiflexion or plantarflexion. The pattern was reproducible among subjects, but there were between-subject differences. The dimensions are mostly determined by rotation in the frontal plane. A pivot point was found medial from the middle. These data serve as a reference and model for predicting the effect of sinus implants and understanding such clinical problems as sinus tarsi syndrome. Between-subjects differences have to be taken into account.

Introduction

Tarsal sinus implants are placed for treating hyperpronation or (flexible) flatfoot (1,2) in a procedure called arthroereisis. The size of the implant should fit the patient to restrain excessive motion but also allow a normal range of motion at the subtalar joint. Only an implant of the correct size, neither too large nor too small, can fulfill both goals. A reference of normal dimensions at different foot positions can help to understand and plan the arthroereisis. Recently, Bali et al. (3) studied these dimensions in plantarflexion (based on the figures) in children for this procedure. To our knowledge, no studies have documented the dimensions of the tarsal sinus and canal (TSC) of adults in more than one position of the foot relative to the shank.

The tarsal sinus is the lateral continuation of the medial tarsal canal. The TSC lies between the posterior and anterior facets of the subtalar joint and is formed by the talar and calcaneal sulci. The sinus on the lateral side is conical and is bounded by the lateral process and neck of the talus and by the anterosuperior aspect of the calcaneus. It continues in the posteromedial direction as a funnel-shaped canal that opens medially posterior of the sustentaculum tali (4,5). The space contains blood vessels, nerves, fat, and ligaments.

The subtalar region is complex in anatomy and function. A lack of external landmarks makes it difficult to examine the function of the subtalar joint (6). Furthermore, motions in the subtalar joint are difficult to conceptualize as the joint axis is not in line with the anatomical axes (6,7). The motions between the calcaneus and talus in the subtalar joint contribute to the total range of motion of the hindfoot (8,9) and the dimensions of the TSC probably change with these motions. For example, on lateral radiographs, the sinus 'opens' or 'closes' from supination to pronation, respectively (7). The TSC anatomy has been studied macroscopically (10–16), microscopically (17), and by medical imaging, mostly magnetic resonance imaging (MRI) (13,18,19).

Impingements and undue tensioning of the TSC structures resulting from different foot positions have been described as causes of pain in sinus tarsi syndrome (13,19,20), but the causes have not been related to the dimensions of the TSC in different foot positions. In surgery, the patient lies down and the surgeon cannot see the actual alignment of the hindfoot. A reference of the size of the TSC to the foot position, at different locations along the medial to lateral axis of the TSC, can help to estimate the alignment. Subtalar arthroscopy uses medial and lateral portals at the sinus and canal, respectively (21). Knowledge of the dimensions of the TSC in different foot positions can help the surgeon to maneuver in this tight space. The subtalar region is receiving increased attention in the field of orthopedics. The present study is designed to build a reference of the dimensions of the TSC in different foot positions. It can elucidate this

part of the complex anatomy and functioning of the subtalar region and can help to bridge basic science with clinical practice. The dimensions along the medial to lateral axis of the TSC will be registered in different foot positions. The hypothesis is that the dimensions of the TSC change between foot positions.

Materials and methods

Dataset

Kinematic data from an earlier study, approved by our hospital Ethics Committee, were used and processed (22). It was therefore a convenience sample; see Beimers et al. (22) for a full description of the methods. Briefly, in a 3D computer tomography (CT) stress test on 20 healthy individuals with no history of ankle pathology, the right foot was forced into eight different maximally tolerated foot positions. First, in the neutral foot position, a high dose scan was made for segmentation of the tibia, talus, and calcaneus. Next, a low dose CTscan was obtained at each extreme foot position. The extreme foot positions were dorsiflexion (DF), combined dorsiflexion and eversion (DF+EV), eversion (EV), combined plantarflexion and eversion (PF+EV), plantarflexion (PF), combined plantarflexion and inversion (PF+IN), inversion (IN), and combined dorsiflexion and inversion (DF+IN). Using custom-made software the contours of the segmented tibia, talus, and calcaneus were matched to the foot positions of these bones in the CT-data set for each extreme foot position. The translations and rotations of each bone were registered relative to its position in the neutral foot position in a local coordinate system based on the principal axes of the surface geometry of the talus. In the processing of the kinematic data (translations and rotations) the calcaneus moved relative to a fixed talus.

Sphere Fitting

The dimensions at 20 equidistant locations along the axis of the TSC were determined by fitting maximum inscribed spheres (MIS). A MIS is the largest possible sphere contained in the TSC. For this, the original meshes of the surfaces of the segmented talus and calcaneus were simplified and represented as triangulated surfaces. An arbitrary tracking line was drawn on the basis of sulcus tali geometry (Fig. 1). The medial and lateral margins of the TSC were identified by moving medial to lateral in a plane perpendicular to the tracking line. A beginning and an end point were set as, respectively, the first and last points where the plane intersected with the talus. The 20 locations were numbered from medial to lateral.

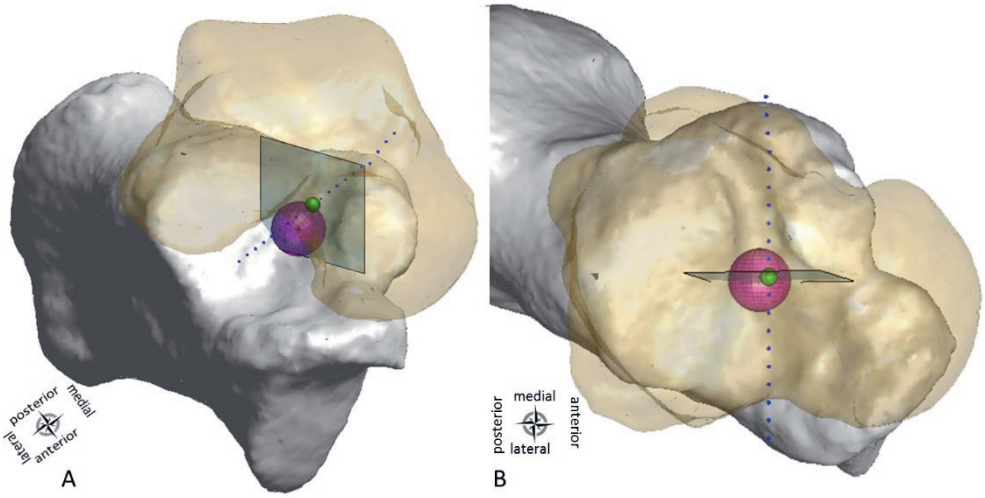

Figure 1. Graphical representation of the 'growth' of a maximal inscribed sphere in the tarsal sinus and canal shown from two directions (A and B). An iterative process started at one of the equidistant 20 points on the tracking line (in this case point 10) with a starting sphere with a radius equal to the distance to the nearest point on either of the two surfaces (small green sphere). At each iterative step the center of the sphere moved in a plane perpendicular to the tracking line (in the equatorial plane, the transparent square in the figure) such that the radius increased without growing into the bones. The iterative processed stopped if the sphere could not grow larger (pink sphere). This result is the maximal inscribed sphere at that location. A: Anterolateral view of talus and calcaneus. B: Superior view of talus and calcaneus. The talus is transparent.

Next, an iterative growing algorithm to determine the MIS was started. This algorithm can be interpreted as inflating a spherical balloon in the TSC. At each point, the center of the growing sphere started on the tracking line with a starting radius equal to the distance of the nearest boundary point of the TSC. With each iteration, the center of the sphere moved in the plane perpendicular to each starting position on the tracking line (in the equatorial plane) such that the diameter of the inscribed sphere was larger than the sphere before without growing into the bones (Fig. 1). The iteration stopped when the radius could no longer increase or when the center of the MIS moved >10 mm from the starting point. In the latter case the MIS gave 'Not a Number' (NaN). MISs were determined at 20 equidistant locations within the TSC, at each position of the foot including neutral (nine positions altogether), and for each of the 20 subjects, generating a total of 3600 MIS radii. The MIS was inspected visually. All data were processed with custom-made routines in Matlab (MATLAB Release 2014a, The MathWorks, Inc., Natick, Massachusetts, United States).

Statistical Analyses

No power analysis was performed. Variations in the original data are visualized by box plots. For this, the median, interquartile range and minimal and maximal values were determined after filtering for outliers, defined as >1.5 times the interquartile range from the median.

Descriptive analysis revealed systematic differences in MIS radii among subjects. These systematic differences were removed using factor correction (23) to prevent them from confounding the analysis of the relationship between foot position, location, and TSC radius. After this correction, the differences in TSC radius at each of the 20 locations could be attributed to the change in foot position. A correction factor was determined for each subject and all data for that subject were divided by that factor to remove the systematic difference. This correction does not affect the random variation in TSC radius, so the resulting dataset reflects the biological variation in the pattern of changes in TSC radius per location and foot position.

SPSS (IBM SPSS Statistics for Windows, Version 23.0. Released 2015. IBM Corp. Armonk, NY: IBM Corp) was used for statistical analyses. Statistically significant interactions between foot position and location were tested using a two-way analysis of variance (ANOVA), with position and location as factors. If there was a significant interaction, a one-way ANOVA followed by a post-hoc Student–Newman–Keuls test between foot positions was used to identify in which foot positions the MIS radii differed significantly from each other at every location; $p < 0.05$ was considered to indicate statistical significance.

Results

Overall, for all foot positions, radii were smaller in the medial locations and larger in the lateral locations (Figs. 2 and 3A, and Table 1 for the number of outliers per location). The radii increased gradually from medial to lateral. At the lateral side of the TSC, the largest radii were observed in foot positions IN and DF+IN, and the smallest in EV and DF+EV. At the medial side, the largest radii were in positions DF and DF+EV and the smallest in IN and PF.

Descriptive statistics showed that the prime source of variation (Fig. 2) per location and position was systematic differences in MIS radii between subjects. Relative to the overall pattern per location and foot position, the systematic effect of the subjects ranged from 0.90 to 1.18. To remove this systematic difference, factor correction (23) was applied. The variation in TSC radius was small (Fig. 3A; Table 2 for means and SEMs). At the medial side (locations 1–3) the number of missing data was notably high (Table 1). Further analysis was therefore restricted to locations 4–20. The factor-corrected data showed a significant interaction between foot position and location (two-way ANOVA). This interaction means that the difference in radii between positions depends on the location on the medial to lateral axis that is studied (Fig. 3A). Comparison of the radii per foot position showed several patterns (by one-way analysis with post-hoc Student- Newman-Keuls test). At locations 8 and 9 there were no significant differences among any of the foot positions (Fig. 3A). The mean length of the tracking line between the beginning and end points was 47 mm (SD 2.0 mm) in the 20 individuals. Thus, on average, locations 8 and 9 were 17.3 mm and 19.8 mm, respectively, from the medial margin.

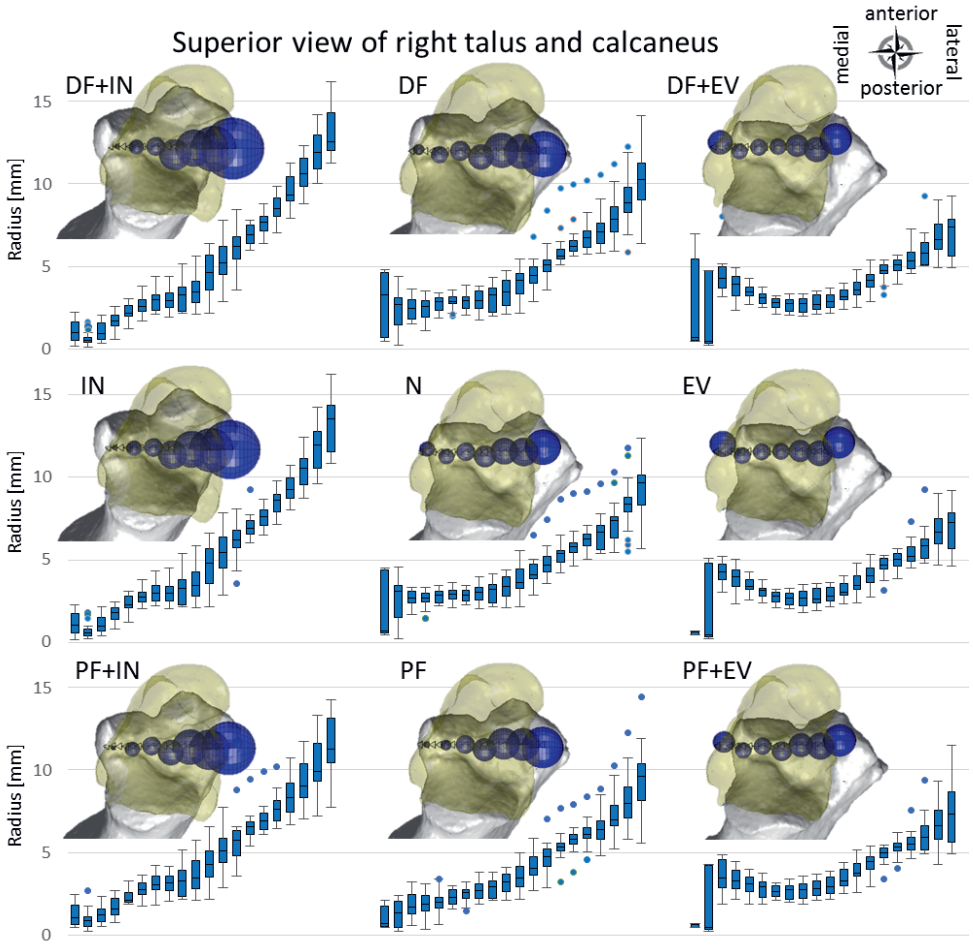

Figure 2. Box plots of the radii (in mm) of the maximal inscribed spheres at 20 locations in the tarsal sinus and canal (TSC) per foot position. The box plots illustrate the variation among the 20 subjects. Also, a graphical representation of the maximal inscribed spheres in a typical subject is shown in each of the nine positions. For clarity, only seven of the 20 maximal inscribed spheres that could be fitted per foot position are shown as a superior view with a transparent talus. N, neutral; DF, dorsiflexion; EV, eversion; PF, plantarflexion; IN, inversion.

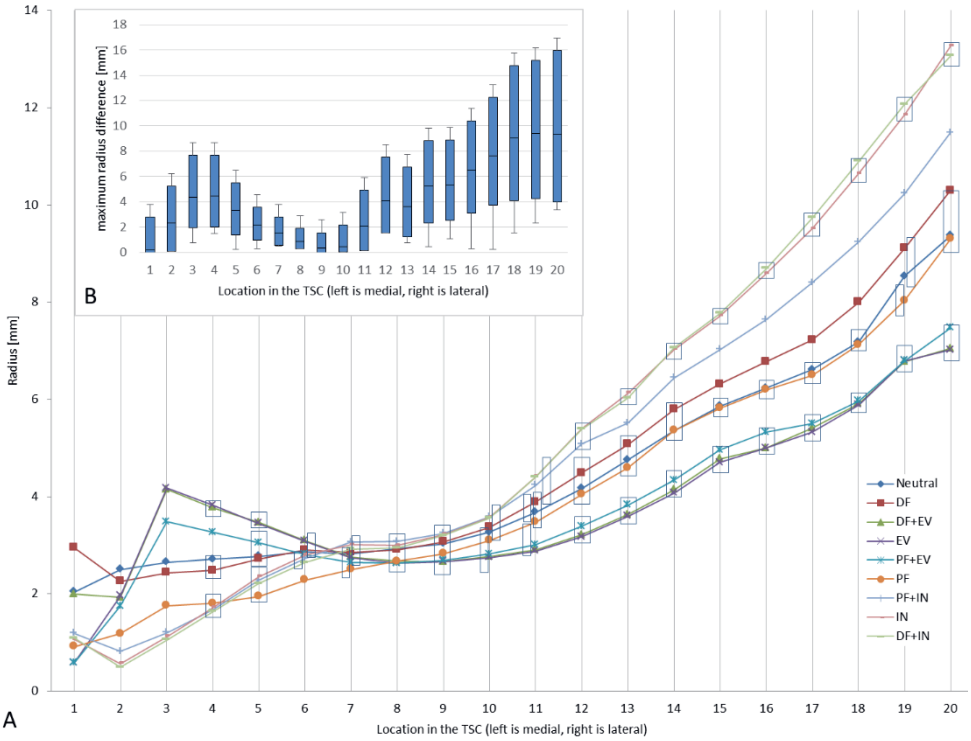

Figure 3. A. Line graphs of the mean radii in the nine positions at the 20 locations in the tarsal sinus and canal (TSC) (n=20 subjects) after factor correction. The boxes indicate the sets of two or more positions that did not differ significantly between locations. Note that positions can be included in overlapping sets (narrow boxes). For example, at location 19, no differences were found between PF and neutral, or between neutral and DF. Radii are filtered from outliers. No analysis was performed at locations 1–3 because of the large number of missing values here. N, neutral; DF, dorsiflexion; EV, eversion; PF, plantarflexion; IN, inversion (to avoid crowding of the figure, no error bars are drawn in Figure 3 A; see Table 2 for means and SEMs). **B.** Box plot of the median and interquartile range of observed radii (in mm) pooled for the nine positions at each of the 20 locations in the TSC (n=20) in the original data (before factor correction).

Table 1. Number of outliers and maximal inscribed spheres that were out of range during the growing algorithm

Location	1	2	3	4	5	6	7	8	9	10	11	12	13	14	15	16	17	18	19	20
#NaN's[a]	112	71	41	11	0	0	0	0	0	0	0	0	2	3	4	5	6	7	13	32
#negative outliers[b]	0	0	0	2	0	2	1	0	0	0	0	0	1	1	6	3	0	0	0	4
#positive outliers[c]	0	8	3	0	1	0	0	0	0	0	0	2	4	6	5	4	5	7	4	1

[a] NaN's, Number of NaN's at each position (a NaN was given to the MIS if the center was out of range of the tracking line).
[b] Negative outliers, number of negative outliers (< 1.5* interquartile range).
[c] Positive outliers, number of positive outliers (>1.5* interquartile range).

At locations 12 to 20 several other foot positions were identified that were not significantly different from each other. The first set of these positions comprised DF+EV, EV, and PF+EV, which share an eversion component (right column in Fig. 2). This set had small radii at these locations (Fig. 3A). A second set of such foot positions comprised DF, neutral, and PF, which have no eversion or inversion components (middle column in Fig. 2). The radii were on average 1.5 times larger than the foot positions with an eversion component. The foot positions IN and PF+IN made a third set of foot positions in this category. The foot position DF+IN differed significantly from all the others (Fig.3A). In these three sets of positions the mean radii were more than four times (foot positions with inversion), about three times (foot positions with no inversion or eversion) and less than twice (foot positions with eversion) as big as in the region with the more constant radius (locations 8 and 9). At locations 6–10, or 12.4–22.2 mm from the medial margin, the range between the minimum and maximum observed radii was low, <1.22 mm (Fig. 3B). Several foot positions did not differ significantly from each other at these locations. The largest range of observed radii was found in the lateral area (Fig. 3B), which is where the radii per location are significantly different per set of foot positions. At the medial side, foot positions DF+EV and EV formed a set in which no significant differences were found. The foot positions neutral and DF also showed no significant differences. None of the foot positions with an inversion component differed significantly from each other at locations 4–7.

Table 2. Mean and standard error of the mean (SEM) for each location at each position after factor correction to eliminate between-subjects variation

	N			DF			DF+EV			EV			PF+EV			PF			PF+IN			IN			DF+IN		
LOC	mean	SEM	n	mean	SEM	n	mean	SEM	n	mean	SEM	n	mean	SEM	n	mean	SEM	n	mean	SEM	n	mean	SEM	n	mean	SEM	n
1	2.04	0.893	5	2.952	0.645	9	1.993	1.408	4	0.586	0.085	3	0.586	0.085	3	0.919	0.338	4	1.193	0.204	11	1.064	0.176	14	1.088	0.178	15
2	2.501	0.378	13	2.263	0.297	15	1.93	0.944	5	1.959	0.966	5	1.751	0.834	5	1.182	0.278	8	0.816	0.095	17	0.565	0.051	17	0.496	0.049	16
3	2.652	0.136	17	2.438	0.146	20	4.15	0.275	8	4.179	0.25	9	3.487	0.309	9	1.756	0.208	14	1.201	0.119	19	1.126	0.102	20	1.053	0.114	20
4	2.713	0.108	18	2.483	0.139	20	3.778	0.201	16	3.827	0.193	16	3.266	0.175	18	1.808	0.166	19	1.668	0.128	20	1.72	0.114	20	1.639	0.13	20
5	2.777	0.082	20	2.723	0.096	20	3.47	0.111	20	3.449	0.113	20	3.052	0.141	20	1.951	0.151	20	2.278	0.079	20	2.355	0.112	20	2.21	0.099	20
6	2.869	0.087	20	2.905	0.078	18	3.1	0.098	20	3.087	0.105	20	2.814	0.135	20	2.284	0.094	20	2.732	0.087	20	2.799	0.096	20	2.649	0.105	20
7	2.831	0.076	20	2.859	0.099	20	2.764	0.077	20	2.746	0.083	20	2.644	0.082	20	2.505	0.072	19	3.066	0.108	20	3.011	0.132	20	2.923	0.13	20
8	2.937	0.098	20	2.909	0.114	20	2.672	0.087	20	2.635	0.077	20	2.631	0.082	20	2.67	0.09	20	3.081	0.121	20	2.997	0.12	20	2.945	0.121	20
9	3.029	0.119	20	3.074	0.14	20	2.659	0.099	20	2.665	0.098	20	2.693	0.094	20	2.827	0.089	20	3.25	0.177	20	3.22	0.182	20	3.199	0.174	20
10	3.269	0.128	20	3.368	0.152	20	2.767	0.095	20	2.747	0.099	20	2.822	0.095	20	3.099	0.097	20	3.586	0.193	20	3.575	0.2	20	3.558	0.192	20
11	3.683	0.15	20	3.895	0.17	20	2.91	0.098	20	2.88	0.1	20	3.01	0.1	20	3.481	0.133	20	4.235	0.232	20	4.413	0.251	20	4.409	0.248	20
12	4.167	0.108	19	4.488	0.12	19	3.216	0.099	20	3.177	0.107	20	3.389	0.112	20	4.045	0.137	20	5.084	0.189	20	5.396	0.201	20	5.389	0.207	20
13	4.755	0.12	19	5.077	0.118	19	3.631	0.134	20	3.597	0.135	20	3.83	0.134	20	4.596	0.138	19	5.519	0.168	19	6.134	0.174	18	6.029	0.211	19
14	5.359	0.125	19	5.792	0.117	18	4.145	0.15	20	4.074	0.149	20	4.341	0.133	20	5.358	0.086	18	6.445	0.132	19	7.025	0.122	18	7.058	0.138	18
15	5.86	0.147	19	6.314	0.143	18	4.781	0.132	18	4.704	0.133	19	4.962	0.109	18	5.82	0.116	18	7.025	0.16	19	7.719	0.18	18	7.771	0.186	18
16	6.238	0.164	19	6.773	0.194	19	5.005	0.129	20	5.004	0.125	20	5.324	0.113	18	6.198	0.151	18	7.643	0.196	19	8.588	0.201	18	8.689	0.225	17
17	6.612	0.185	19	7.225	0.223	19	5.411	0.134	20	5.33	0.126	19	5.504	0.131	19	6.502	0.189	19	8.4	0.242	20	9.51	0.24	17	9.736	0.259	17
18	7.183	0.231	18	8	0.252	19	5.915	0.173	19	5.891	0.175	19	5.967	0.207	19	7.126	0.232	19	9.238	0.28	20	10.647	0.283	17	10.898	0.313	16
19	8.537	0.19	15	9.112	0.273	18	6.776	0.277	19	6.795	0.279	19	6.798	0.328	19	8.036	0.292	19	10.233	0.332	19	11.855	0.321	16	12.069	0.318	15
20	9.372	0.377	19	10.299	0.355	20	7.05	0.428	13	7.02	0.402	14	7.473	0.474	15	9.301	0.376	19	11.487	0.388	19	13.271	0.41	15	13.068	0.328	12

Abbreviations: LOC, location in the tarsal sinus and canal (1=medial, 20=lateral); SEM, standard error of the mean; n, number of subjects; N, neutral; DF,dorsiflexion; EV, eversion; PF, plantarflexion; IN, inversion

Discussion

This study measured the dimensions of the tarsal sinus and canal (TSC) and the changes in those dimensions among different (extreme) foot positions. Overall, the TSC space is narrow at the medial side and gradually increases laterally. The dimensions of the TSC change among foot positions. The dimensions at the lateral side are mainly determined by rotation in the frontal plane: that is, eversion, inversion or an absence of both. Motions in the sagittal plane, that is plantar flexion or dorsiflexion, hardly contribute to the dimensions.

Just medial from the middle of the TSC, a region was identified where for all foot positions (Fig. 3A) and subjects (Fig. 3B) the radii are relatively small and constant among positions. For most of the foot positions, if the sphere radii increased at one end of the region then the sphere sizes decreased at the
opposite end, or vice versa (Figs. 2 and 3A). Thus, this region seems to act as a pivot point for the subtalar joints. This effect could be seen between opposite foot positions, such as PF+EV to DF+IN, and IN to EV, but not DF to PF.

The range between the maximum and minimum radii at a location pooled over positions (Fig. 3B) is a measure of the amount of movement at that location. A large range means that the TSC radii change markedly among foot positions, and the movements of the joint elements are large. The opposite is true for a small range of radii. This range was largest at the lateral side, which implies that the joint elements move the most. The smallest range coincided with the region where there were no significant differences among foot positions.

The individual measurements showed that individuals differed systematically, ranging from 0.9 to 1.18 times the mean pattern. However, after this systematic difference was eliminated, the small variations among subjects for each position and location (Table 2) showed that the relative effects of foot position are highly reproducible. The remaining small random difference among individuals allowed the foot positions and sets of positions at locations 4 to 20 to be distinguished (Fig. 3A). The relative width of the 95% confidence interval per foot position and location was 0.13 (Table 2), whereas the relative difference in radii between (sets of) foot positions ranged from 1.2 to 1.9 (average 1.6). Thus, any difference among foot positions would become evident from the measured radii. These large differences among the sets of foot positions therefore enable the position of the foot of an individual to be predicted from the ratio of the size of the TSC at a more lateral location to the size at the medial, constant, region. For locations 6 to 10 the ratios for confidence interval and relative differences were lower (0.15 and 1.2 to 1.3 respectively), so there was more overlap among the sets (Fig. 3A, narrow boxes).

The pattern of changes in the radii can be related to the kinematics of the subtalar joint. The subtalar joint axis mainly runs in an anterior-posterior direction (8,24). Because of this orientation, imposed by the vertical orientation of the articular facets (25,26), there is only marginal plantarflexion and dorsiflexion between the talus and calcaneus. Between these extreme foot positions there is only a small change in the radii of the MIS. During pronation the talus will adduct, plantar flex and invert relative to the calcaneus. The lateral talar process will slide anteriorly and inferiorly along the posterior articular facet of the calcaneus. Maximal pronation is reached when the lateral talar process comes into contact with the floor of the sinus. The position DF+EV corresponds best to pronation. From this position to an EV or a PF+EV there is hardly any movement between the talus and calcaneus (22); the motion is mainly
between the talus and tibia. This explains why there were only small differences in radii among positions DF+EV, EV, and PF+EV. The same holds for the positions with an inversion component or the positions without inversion or eversion components.

The purpose of an arthroereisis is to restrict the abnormal excessive pronation and restore normal alignment of the hindfoot. A tarsal sinus implant should therefore supinate the pronated hindfoot to some extent. What happens if a space-filling implant is placed in the lateral part of the TSC can be virtually imaged on the basis of the current results: the talus will abduct, dorsiflex and evert relative to the calcaneus. This is the same as supination and corresponds to the desired effect. It also corresponds to the findings of an earlier study of the kinematic effects of such an implant (27). An overcorrection caused by placing an oversized implant causes the hindfoot to invert with or without dorsiflexion. The largest radii at the lateral side were found in these two foot positions. The location just medial to the middle, which varied little, acts as a pivot point. An implant placed too far medially, in the tarsal canal, will cause the medial side to open and thus the lateral side to close. This is undesirable. A large enough implant will open the sinus and close the canal and thereby prevent over-insertion of the implant. Implants that occupy both sinus and canal require the stabilizing ligaments to be removed. It is difficult to predict the effect of this removal and subsequent placing of the implant. If for whatever reason the implant has to be removed, this is expected to result in instability of the subtalar joint because the stabilizing ligaments have been removed (28).

Several studies have documented the anatomy of the ligaments in and around the TSC (4,10,11,15,16). None of these studies has quantified the location of the insertions of those ligaments. The figures in these publications suggest that the interosseous talocalcaneal ligament is located in the area where the TSC dimensions change little among foot positions. This is in agreement with Van Langelaan (29), who tried to correlate the determined helical axes to the location of the ligaments. This area of little

variation in TSC radii is where the short fibers of the interosseous talocalcaneal ligament span between the talus and calcaneus (29). These ligaments can be a reference for locating the region with constant diameter during movement of the joint, for example to determine the ratio of the diameter at this location and at a more lateral side to predict the foot position as described above.

Sinus tarsi syndrome presents clinically as pain over the lateral opening of the sinus tarsi that is eliminated by local anesthesia, sometimes with a feeling of hindfoot instability (30). The pain in sinus tarsi syndrome is more severe during standing, walking on uneven ground, and movements of supination and adduction of the foot (13,20). The pain usually disappears at rest and is eased by a firm bandage or a support holding the heel in pronation or a valgus position (20). However, pain in pronation or valgus has also been reported (31). These findings suggest that the position of the foot is important for the experience of pain. It is clear that sinus tarsi syndrome is not a single clinical entity. From the findings of the current study we can see that in eversion positions the medial side of the TSC becomes very narrow. The radii decrease up to one fifth of the highest values. Impingement of the containing structures can be expected. At the lateral side it is difficult to determine whether the soft tissues inside the canal are likely to suffer from impingement. The lateral side shows a relative change in radius of no more than 1.9 times and still leaves a large passage. However, locally, certain structures can be trapped between the two bones, especially by the lateral talar process. This is likely to occur in EV or DF+EV. From a neutral position to EV or DF+EV the opening of the sinus will move anteriorly and the orientation of the space becomes more anteroposterior than medial to lateral. On the other hand, undue tensioning has also been described as a cause for pain in the sinus region. This could be provoked by IN and DF+IN as in these positions the radii were the largest. One can use this information during physical examination.

Several comments can be made about the methods used in this study. First, we should emphasize that we used only data from healthy subjects. The presented data can be used as reference in a follow-up study that analyses pathologically-affected feet. Second, when the geometry of the TSC is studied, it becomes clear that the space is not fully conical or tunnel-shaped. The radius of the minimal inscribed sphere at discrete locations along the TSC-axis is a simplification of the complex shape, which also changes with the motions of the hindfoot. However, a sphere is easy to conceptualize and therefore a good representation of the dimensions. Because we used multiple spheres along the TSC the results reflect the shape of the TSC. Moreover, the narrow 95% confidence limits of the MIS radii per location and position show that the TSC shape is very reproducible among healthy subjects. Lastly, fringe effects occurred, mostly at the medial side, when the calcaneus came into such a position that no lower bound was

present under the upper talar sulcus. At such a location, the sphere kept on growing and the center went beyond the defined limits (<10 mm from the starting point on the tracking line). We discarded these MISs in our analyses, which could have resulted in negatively-biased lower values for those locations.

Conclusions

This study demonstrated that the dimensions of the tarsal sinus and canal differ among foot positions. Overall, the medial side is narrow and the size increases laterally. Around the middle, the dimensions do not change much among foot positions. If the size increases on one end of this region with constant dimensions, then it decreases on the opposite side. The dimension is mainly determined by the motion if eversion or inversion. The pattern is consistent among healthy subjects but there are systematic between-subjects differences. These data can serve as a reference to help the clinician choose an implant and can explain certain pathologies such as impingement and stretching.

References

1. Maxwell J, Cerniglia M. Subtalar joint arthroereisis. Downey MS: Banks AS; 2001.
2. Needleman RL. Current topic review: subtalar arthroereisis for the correction of flexible flatfoot. Foot ankle Int. 2005 Apr;26(4):336–46.
3. Bali N, Theivendran K, Prem H. Computed tomography review of tarsal canal anatomy with reference to the fitting of sinus tarsi implants in the tarsal canal. J Foot Ankle Surg. 2013;52(6):714–6.
4. Cahill DR. The anatomy and function of the contents of the human tarsal sinus and canal. Anat Rec. 1965 Sep;153(1):1–17.
5. Sarrafian SK. Biomechanics of the subtalar joint complex. Clin Orthop Relat Res. 1993 May;(290):17–26.
6. Jastifer JR, Gustafson PA. The subtalar joint: biomechanics and functional representations in the literature. Foot (Edinb). 2014 Dec;24(4):203–9.
7. Maceira E, Monteagudo M. Subtalar anatomy and mechanics. Foot Ankle Clin. 2015 Jun;20(2):195–221.
8. Tuijthof GJM, Zengerink M, Beimers L, Jonges R, Maas M, van Dijk CN, et al. Determination of consistent patterns of range of motion in the ankle joint with a computed tomography stress-test. Clin Biomech (Bristol, Avon). 2009 Jul;24(6):517–23.
9. Kleipool RP, Blankevoort L. The relation between geometry and function of the ankle joint complex: a biomechanical review. Knee Surg Sports Traumatol Arthrosc. 2010 May;18(5):618–27.
10. Smith JW. The ligamentous structures in the canalis and sinus tarsi. J Anat. 1958 Oct;92(4):616–20.
11. Schmidt HM. [Form and attachment of the human sinus tarsi and canalis tarsi ligaments]. Acta Anat (Basel). 1978;102(2):184–94.
12. Schwarzenbach B, Dora C, Lang A, Kissling RO. Blood vessels of the sinus tarsi and the sinus tarsi syndrome. Clin Anat. 1997;10(3):173–82.
13. Lektrakul N, Chung CB, Ym L, Theodorou DJ, Yu J, Haghighi P, et al. Tarsal sinus: arthrographic, MR imaging, MR arthrographic, and pathologic findings in cadavers and retrospective study data in patients with sinus tarsi syndrome. Radiology. 2001 Jun;219(3):802–10.
14. Rab M, Ebmer J, Dellon AL. Innervation of the sinus tarsi and implications for treating anterolateral ankle pain. Ann Plast Surg. 2001 Nov;47(5):500–4.
15. Jotoku T, Kinoshita M, Okuda R, Abe M. Anatomy of ligamentous structures in the tarsal sinus and canal. Foot ankle Int. 2006 Jul;27(7):533–8.
16. Li S-Y, Hou Z-D, Zhang P, Li H-L, Ding Z-H, Liu Y-J. Ligament structures in the tarsal sinus and canal. Foot ankle Int. 2013 Dec;34(12):1729–36.
17. Rein S, Hanisch U, Zwipp H, Fieguth A, Lwowski S, Hagert E. Comparative analysis of inter- and intraligamentous distribution of sensory nerve endings in ankle ligaments: a cadaver study. Foot ankle Int. 2013 Jul;34(7):1017–24.
18. Klein MA, Spreitzer AM. MR imaging of the tarsal sinus and canal: normal anatomy, pathologic findings, and features of the sinus tarsi syndrome. Radiology. 1993 Jan;186(1):233–40.
19. Lee K-B, Bai L-B, Park J-G, Song E-K, Lee J-J. Efficacy of MRI versus arthroscopy for

evaluation of sinus tarsi syndrome. Foot ankle Int. 2008 Nov;29(11):1111–6.
20. Taillard W, Meyer JM, Garcia J, Blanc Y. The sinus tarsi syndrome. Int Orthop. 1981;5(2):117–30.
21. Lui TH, Tong SC. Subtalar arthroscopy: When, why and how. World J Orthop. 2015 Jan;6(1):56–61.
22. Beimers L, Tuijthof GJM, Blankevoort L, Jonges R, Maas M, van Dijk CN. In-vivo range of motion of the subtalar joint using computed tomography. J Biomech. 2008;41(7):1390–7.
23. Ruijter JM, Thygesen HH, Schoneveld OJLM, Das AT, Berkhout B, Lamers WH. Factor correction as a tool to eliminate between-session variation in replicate experiments: application to molecular biology and retrovirology. Retrovirology. 2006 Jan;3:2.
24. Siegler S, Chen J, Schneck CD. The three-dimensional kinematics and flexibility characteristics of the human ankle and subtalar joints--Part I: Kinematics. J Biomech Eng. 1988 Nov;110(4):364–73.
25. Sarrafian SK. Anatomy of the foot and ankle, descriptive, topographic, functional. 2nd ed. Philadelphia: J.B. Lipincott Co.; 1993.
26. Barbaix E, Van Roy P, Clarys JP. Variations of anatomical elements contributing to subtalar joint stability: intrinsic risk factors for post-traumatic lateral instability of the ankle? Ergonomics. 2000 Oct;43(10):1718–25.
27. Christensen JC, Campbell N, DiNucci K. Closed kinetic chain tarsal mechanics of subtalar joint arthroereisis. J Am Podiatr Med Assoc. 1996 Oct;86(10):467–73.
28. Tochigi Y, Takahashi K, Yamagata M, Tamaki T. Influence of the interosseous talocalcaneal ligament injury on stability of the ankle-subtalar joint complex--a cadaveric experimental study. Foot ankle Int. 2000 Jun;21(6):486–91.
29. van Langelaan E. Relative talotibial movements and relative tarsal movements. Acta Orthop Scand. 1983;54:135–265.
30. O'Connor D. Sinus tarsi syndrome: A clinical entity. J Bone Jt Surg. 1958;40:720–6.
31. Shear MS, Baitch SP, Shear DB. Sinus tarsi syndrome: the importance of biomechanically-based evaluation and treatment. Arch Phys Med Rehabil. 1993 Jul;74(7):777–81.

Chapter 4

The mechanical functionality of the EXO-L ankle brace: assessment with a 3-dimensional computed tomography stress test

Roeland P. Kleipool
Jerry J. Natenstedt
Geert J. Streekstra
Johannes G.G. Dobbe
Rogier M. Gerards
Leendert Blankevoort
Gabriëlle J.M. Tuijthof

Am J Sports Med. 2016 Jan;44(1):171-176.
doi: 10.1177/0363546515611878

'put your foot down'
Cambrigde dictionary: to use your authority to stop something happening

Abstract

Background: A new type of ankle brace (EXO-L) has recently been introduced. It is designed to limit the motion of most sprains without limiting other motions and to overcome problems such as skin irritation associated with taping or poor fit in the sports shoe.

Purpose: To evaluate the claimed functionality of the new ankle brace in limiting only the motion of combined inversion and plantar flexion.

Study Design: Controlled laboratory study.

Methods: In 12 patients who received and used the new ankle brace, the mobility of the joints was measured with a highly accurate and objective in vivo 3-dimensional computed tomography (3D CT) stress test. Primary outcomes were the ranges of motion as expressed by helical axis rotations without and with the ankle brace between the following extreme positions: dorsiflexion to plantar flexion, and combined eversion and dorsiflexion to combined inversion and plantar flexion. Rotations were acquired for both talocrural and subtalar joints. A paired Student t test was performed to test the significance of the differences between the 2 conditions ($p \leq .05$).

Results: The use of the ankle brace significantly restricted the rotation of motion from combined eversion and dorsiflexion to combined inversion and plantar flexion in both the talocrural ($p = .004$) and subtalar joints ($p < .001$). No significant differences were found in both joints for the motion from dorsiflexion to plantar flexion.

Conclusion: The 3D CT stress test confirmed that under static and passive testing conditions, the new ankle brace limits the inversion–plantar flexion motion that is responsible for most ankle sprains without limiting plantar flexion or dorsiflexion.

Clinical Relevance: This test demonstrated its use in the objective evaluation of braces.

Introduction

After a first inversion injury of the ankle, the joints can be protected during sports activity by using a brace or tape (1). The preference for tape or a brace differs among individual athletes and among sports disciplines. Both are effective in preventing recurrent inversion injuries (2). However, they also present discomfort, with the braces demonstrating a poor fit, limitation of motions other than only inversion, and reduction of the fit of the sports shoe (3–7). Sports tape can lead to skin irritation, requires a professional for correct application, and loses function within a short period of time in the course of sports activity (5,8,9). An alternative type of ankle brace was developed to overcome these disadvantages. The product name is EXO-L (EXO Ligament BV). It comprises a custom-fit shell that encloses the distal leg just above the malleoli, an attachment to the sports shoe at the lateral side, and a cord that attaches the shell to the sports shoe and acts as an additional external ligament (Fig. 1).

Figure 1. The EXO-L ankle brace consists of a custom made shell that encloses the distal tibia and fibula, an attachment to the sports shoe, and a cord that connects the shell to the sports shoe.

The design of this new ankle brace is such that it is intended to only limit the combined plantar flexion and inversion motion, which is the most common motion mechanism to sustain an ankle sprain.(10)19

The effectiveness of ankle supports in preventing an ankle sprain has been studied intensely (eg, reviews (11,12)), but direct measurement of the restricting effect in the

range of motion (ROM) has also been assessed.(4,13–25).These studies are either ex vivo (cadaveric specimens) or use superficial markers to capture the motion. The former are limited in reflecting the true complex motion pattern in vivo. The latter lack the possibility to discriminate between talocrural and subtalar joint motion. This is relevant as lateral ankle instability can be attributable to both levels, with 10% to 25% of patients having subtalar instability (26).

The objective of this study was to investigate the claimed functionality of the new ankle brace. It was hypothesized that the brace would exclusively limit the combined plantar flexion and inversion motion and not affect the other ankle joint complex motions. This functionality was tested with our previously developed 3-dimensional computed tomography (3D CT) stress technique that allows the in vivo determination of both talocrural and subtalar motion (27–29). An analysis of the limits of joint motion by the brace per joint level was performed.

Methods

The study was approved by the medical ethics committee of our hospital (NL47339.018.14). Twelve volunteers signed informed consent forms before participation. Inclusion criteria were age ≥ 18 years, a clinical history of ankle inversion instability longer than 2 months before participation, and the participant having acquired and used an EXO-L brace in combination with an appropriately customized sports shoe. Exclusion criteria were a sustained ankle injury in the past 2 months, history of rheumatic disease, history of surgical intervention in the ankle or foot, or constitutional laxity. Additional exclusion criteria for female participants were present gravidity or the intent to become pregnant, as CT was part of the study setup.

Power Analysis

Using the same 3D stress test as applied in this study, Tuijthof et al. (29) determined that the mean helical axis rotation (∈) from combined eversion and dorsiflexion to combined inversion and plantar flexion was 49.4 ± 6 9.0° for the talocrural joint in a healthy population of adults. If the ankle brace performs as intended, that is, gives a clinically relevant effect (30), we assumed that ∈ would show a difference of at least 7° between the braced and unbraced condition, with ∈ being smaller in the ankle brace condition. With an SD of 9.0° and a clinically relevant difference of 7°, a power analysis was performed for a 1-sided t test with a power of 80% and a significance level of .05 (31). This gave a required sample size of 12 participants.

Participants

The mean age of the study patients was 27.3 ± 10.9 years (range, 19-59 years); 8 were male, and 4 were female. The medical history was reviewed, and a physical examination of the ankle and hindfoot was performed by a single clinician (R.R.M.G.) to determine if the patient was eligible for participation. Swelling as well as pain with passive motion and resistance were contraindications. If both sides were affected, the side with the highest incidence of sprains was chosen. Eight right and 4 left sides were measured. The Dutch version of the American Orthopaedic Foot and Ankle Society (AOFAS) score (32) was used to classify the status of the ankle.

3D Stress Test

To determine the relative motion of the bones of the ankle joint complex of all participants with and without the use of the ankle brace, our previously developed and validated 3D CT stress technique was applied (27–29). We made a slight modification to this earlier used protocol to keep the radiation doses limited to 1 high-dose CT scan and 8 low-dose CT scans (27–29).

The following protocol was used for the 3D stress test. A high-dose CT scan (Brilliance 64 CT scanner with voxel size of 0.3 x 0.3 x 0.3 mm^3, 120 kV, and 150 mA; Philips) was obtained in the neutral position with no shoe or ankle brace to allow detailed segmentation of the tibia, talus, and calcaneus bones. Subsequently, low-dose CT scans (voxel size of 0.3 x 0.3 x 0.3 mm^3, 120 kV, and 25 mA) were obtained with the foot in the sports shoe in each of the following 4 extreme positions: dorsiflexion (DF), plantar flexion (PF), combined eversion–dorsiflexion (EVDF), and combined inversion–plantar flexion (INPF) (Fig. 2). Subsequently, the patients were asked to put on their own EXO-L brace in the same manner as they would in the field. Finally, 4 low-dose CT scans were obtained with the ankle in the brace in the same 4 extreme positions with the same loads as used in the first set. The loads applied in the loading device to force the foot in the 4 extreme positions relative to the lower leg varied between 5 and 8 kg. The loads were gradually increased to a maximum load that was tolerated by the participant.

The tibia, talus, and calcaneus were segmented using the high-dose CT scan with custom-made software (33). The 3 bones of the neutral position scan were matched to the bones of the low-dose CT scans for the extreme positions per participant (Fig. 3; 3B and 3D show this for plantar flexion with the ankle brace). This way, the translations and rotations (or transformations) for the individual bones from the high-dose scan to the extreme positions in the low-dose CT scans were determined. The accuracy and

precision of the Euler angles as determined from the image analysis method were previously shown to be 0.2° and 0.1°, respectively (33).

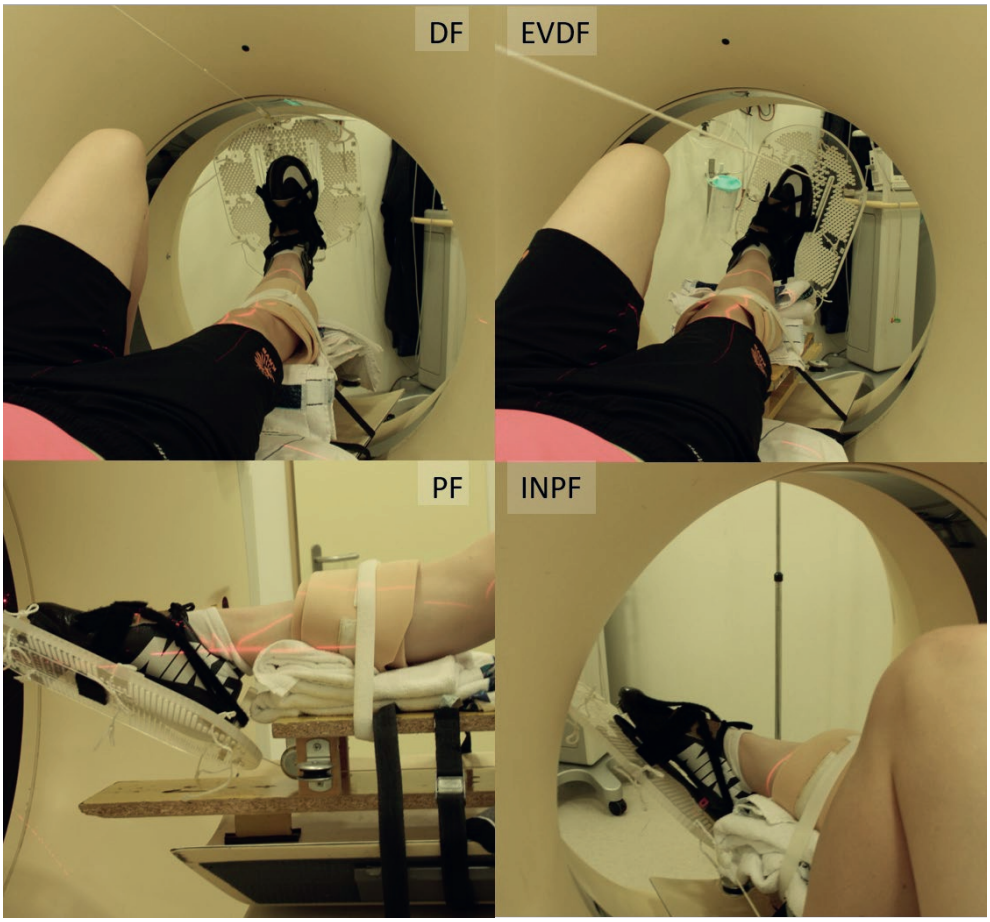

Figure 2. Photographs of the loading protocol for 4 extreme positions: (A) dorsiflexion, (B) combined eversion and dorsiflexion, (C) plantar flexion, and (D) combined inversion and plantar flexion. The leg is attached to a support, while the foot is pulled into 4 different positions by a pulley system at the head of the participant (not in the photographs).

Next, the joint kinematics of the talocrural and subtalar joints were computed for 2 motion directions: DF to PF and EVDF to INPF for both conditions with and without the ankle brace. The motions in these 2 directions were expressed by helical axis rotations with respect to the principal axes of the talus (for more detail, see Beimers et al. (27)). The helical axis of a joint is defined as the line along which a body (in our case, the tibia or calcaneus) both translates and rotates when it moves with respect to another body (in our case, the talus).

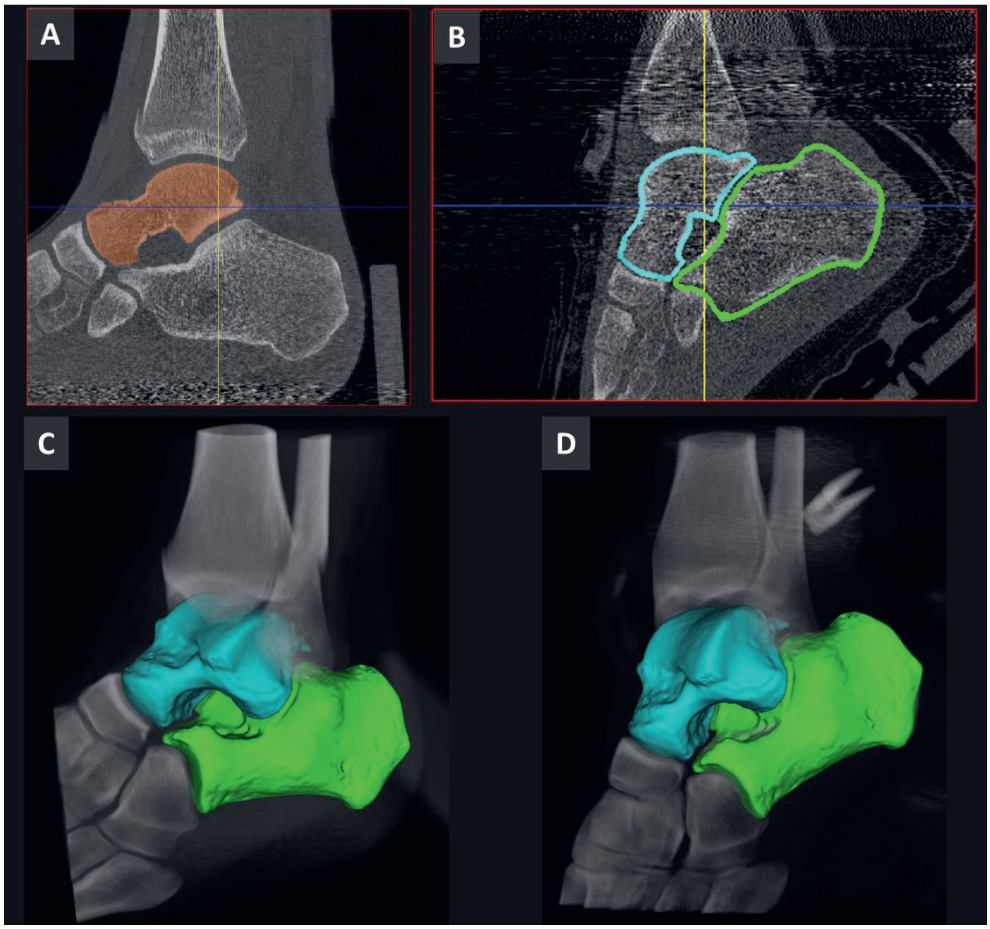

Figure 3. Segmentation and matching of bones. (A) The talus of a patient is segmented in a computed tomography image of the high-dose scan. (B) The contours of the segmented tibia, talus, and calcaneus (from the high-dose scan) are matched to those of a low-dose scan of the ankle with the ankle brace in plantar flexion. (C, D) Surface rendering of the tibia, talus, and calcaneus superimposed on a digitally reconstructed radiograph of the ankle (C) in a neutral position and (D) with the ankle brace in plantar flexion (corresponding to B).

The calculations were performed with custom-made routines in Matlab software (version 8.1; MathWorks Inc). In total, 8 helical axes were determined (Table 1).

Table 1. Overview of helical axis rotations outcome.

Rotation θ	Comparison
Talocrural DF to PF[a]	Without vs. With ankle brace
Talocrural EVDF to INPF[b]	Without vs. With ankle brace
Subtalar DF to PF	Without vs. With ankle brace
Subtalar EVDF to INPF	Without vs. With ankle brace

[a]DF to PF, dorsiflexion to plantarflexion. [b]EVDF to INPF, combined eversion and dorsiflexion to combined inversion and plantarflexion

Statistical Analysis

Statistical analysis was performed using SPSS software (version 21.0; IBM Corp). The helical axis rotations with and without the ankle brace were analyzed using paired Student t tests. Statistical significance was set at $p < .05$.

Results

The mean AOFAS score was 92.8 ± 8.4 (range, 77-100), indicating that the patients had no or little impairment (32,34). The ankle brace significantly decreased the helical axis rotation for the motion EVDF to INPF in the talocrural joint ($p = .004$) and in the subtalar joint ($p < .001$) (Fig. 4). The mean decrease in the talocrural joint was 9.2° (18.7%) and in the subtalar joint was 8.8° (36.1%).

No significant differences were found in the talocrural or subtalar joint for the motion DF to PF. A relatively high SD was found in the motion DF to PF for the subtalar joint for both conditions without and with the ankle brace (Fig. 4).

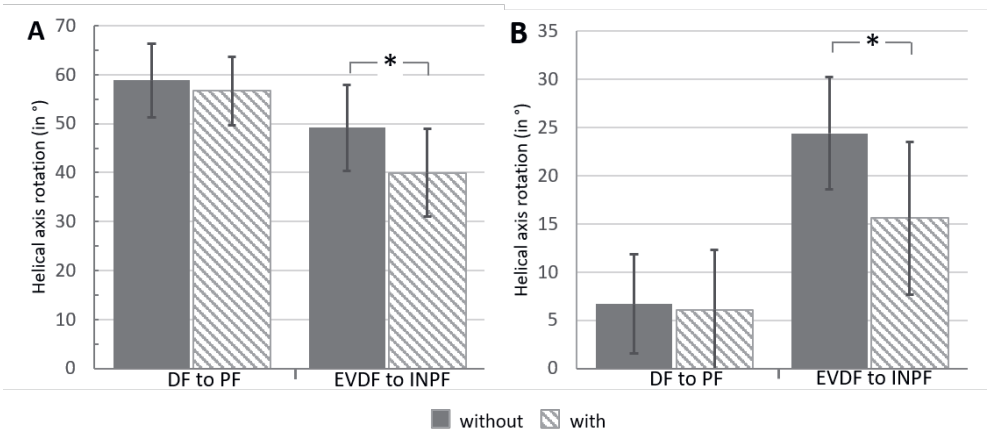

Figure 4. Helical axis rotation (∈) (mean ± SD) for dorsiflexion to plantar flexion (DF to PF) and combined eversion and dorsiflexion to combined inversion and plantar flexion (EVDF to INPF) for conditions without and with the ankle brace. (A) Talocrural joint (talus and tibia). (B) Subtalar joint (talus and calcaneus). *Significant difference between the without and with ankle brace conditions.

Discussion

The functionality of a new ankle brace was evaluated with a 3D CT stress technique that allows the in vivo determination of both talocrural and subtalar ROM. The brace was designed to only limit the combined motion of inversion and plantar flexion, which is the dominant motion to sustain an ankle sprain. Our results and observations support this claim because no significant differences were found for the motion PF to DF, while significant differences were found for the motion EVDF to INPF in both joints. Relatively, most limitations occurred in the subtalar joint (−36.1% and −18.7%, respectively, for the subtalar and talocrural joints with the brace), but the mean decrease in absolute values was comparable (−8.8° and −9.2° for the subtalar and talocrural joints, respectively). Because instability might be attributable to either the talocrural or subtalar joint (26), it is favorable that for this motion, the restriction is at both levels.

A limitation of this study was that it used only 4 extreme positions. The developed, validated, and applied methodology (27–29) originally utilized 8 different positions and thus evaluated a more complete, potential ROM than this study. We had to reduce the number of different positions to 4, measured both twice (without and with the ankle brace), to limit the radiation dose. We chose to evaluate the motion DF to PF because in normal gait and slow running, this is the most important motion with the highest ROM (35–38). The new ankle brace was designed not to limit this essential motion. The other motion, EVDF to INPF, was relevant as this is the motion of most sprains. A secondary motivation to limit the amount of different positions was the time to complete the whole protocol. Another limitation was that we used passive and static conditions. As the concept and design of this device are very different from other devices, we chose this protocol for a first evaluation of the functionality instead of a dynamic and/or active setting. A direct comparison with other frequently applied commercial braces would imply a double radiation dose per brace, which was one reason why such a direct comparison would be difficult.

There are no available data on the durability of the brace over time, but material fatigue is expected to have a marginal influence on the performance of the brace. The attachment of the loop to the shoe was by conventional stitching, and there was no potential for the attachment to the shoe to loosen over time other than normal fatigue of the material (Fig. 1). The cord (English Braids) is made from pre-stretched polyester. The user can tighten or loosen the cord using the Clamcleat (Clamcleats Ltd) that is positioned in the shell, thereby adjusting the effectiveness of the brace as needed.

Our group of patients had a history of ankle instability, but this was not reflected in their ROM data as compared with the healthy participants in our earlier studies (27–29). Our group of patients were physically active, some at professional levels of sporting,

and had little or no impairment as represented by the high AOFAS score (32,34). One explanation for the comparable ROMs between the 2 groups is that instability was functional and not mechanical (39).

Tohyama et al. (15) concluded that in evaluating the functionality of ankle braces, there is a difference between weightbearing and nonweightbearing conditions. This is in accordance with the conclusions of Stormont et al. (40) who concluded that in weightbearing conditions, the articular surfaces of the joints can account for a large to total contribution of the stability of the joints. In our protocol, weightbearing was simulated by the stress applied by the pulley system.

An earlier study also used stereophotogrammetry to evaluate talus and calcaneus motion in vivo with orthoses (41). Yet, as Tuijthof et al. (28) mentioned, this technique requires specific equipment and is invasive (implanted tantalum markers), and accuracy is dependent on several factors such as the type and quality of the calibration equipment, image quality, and film flatness.

The strength of our study was that we used an objective, highly accurate, and noninvasive methodology that was able to discriminate between the 2 levels of joints of the ankle joint complex and simulated weightbearing conditions. This 3D CT stress test will be useful in a first evaluation of orthoses such as ankle braces, which can help to construct future orthoses with specific focus.

In conclusion, our results demonstrate the claimed functionality of the new ankle brace. Although this is promising, we acknowledge that the findings were determined under static conditions, which are not representative of the dynamic ankle sprain mechanism during sports. Additional study is needed to evaluate the dynamic functioning of the ankle brace, such that insight into the effect of application during motions in a laboratory or in the field is obtained.

Acknowledgment

The authors thank the volunteers for their participation in this study.

References

1. Kerkhoffs GM, van den Bekerom M, Elders LAM, van Beek PA, Hullegie WAM, Bloemers GMFM, et al. Diagnosis, treatment and prevention of ankle sprains: an evidence-based clinical guideline. Br J Sports Med. 2012 Sep;46(12):854–60.
2. Verhagen EALM, Bay K. Optimising ankle sprain prevention: a critical review and practical appraisal of the literature. Br J Sports Med. 2010 Dec;44(15):1082–8.
3. Beriau MR, Cox WB, Manning J. Effects of ankle braces upon agility course performance in high school athletes. J Athl Train. 1994 Sep;29(3):224–30.
4. Eils E, Demming C, Kollmeier G, Thorwesten L, Volker K, Rosenbaum D. Comprehensive testing of 10 different ankle braces. Evaluation of passive and rapidly induced stability in subjects with chronic ankle instability. Clin Biomech (Bristol, Avon). 2002 Aug;17(7):526–35.
5. Lardenoye S, Theunissen E, Cleffken B, Brink PR, de Bie RA, Poeze M. The effect of taping versus semi-rigid bracing on patient outcome and satisfaction in ankle sprains: a prospective, randomized controlled trial. BMC Musculoskelet Disord. 2012 May;13:81.
6. Papadopoulos ES, Nikolopoulos CS, Athanasopoulos S. The effect of different skin-ankle brace application pressures with and without shoes on single-limb balance, electromyographic activation onset and peroneal reaction time of lower limb muscles. Foot (Edinb). 2008 Dec;18(4):228–36.
7. Rosenbaum D, Becker HP, Wilke HJ, Claes LE. Tenodeses destroy the kinematic coupling of the ankle joint complex. A three-dimensional in vitro analysis of joint movement. J Bone Joint Surg Br. 1998 Jan;80(1):162–8.
8. Greene TA, Hillman SK. Comparison of support provided by a semirigid orthosis and adhesive ankle taping before, during, and after exercise. Am J Sports Med. 1990;18(5):498–506.
9. Verhagen EA, van der Beek AJ, van Mechelen W. The effect of tape, braces and shoes on ankle range of motion. Sports Med. 2001;31(9):667–77.
10. Kerkhoffs GMMJ, Van Dijk CN. Acute lateral ankle ligament ruptures in the athlete: the role of surgery. Foot Ankle Clin. 2013 Jun;18(2):215–8.
11. Dizon JMR, Reyes JJB. A systematic review on the effectiveness of external ankle supports in the prevention of inversion ankle sprains among elite and recreational players. J Sci Med Sport. 2010 May;13(3):309–17.
12. Handoll HH, Rowe BH, Quinn KM, de Bie R. Interventions for preventing ankle ligament injuries. Cochrane database Syst Rev. 2001;(3):CD000018.
13. Bruns J, Staerk H. Mechanical ankle stabilisation due to the use of orthotic devices and peroneal muscle strength. An experimental investigation. Int J Sports Med. 1992 Nov;13(8):611–5.
14. Tang YM, Wu ZH, Liao WH, Chan KM. A study of semi-rigid support on ankle supination sprain kinematics. Scand J Med Sci Sports. 2010 Dec;20(6):822–6.
15. Tohyama H, Yasuda K, Beynnon BD, Renstrom PA. Stabilizing effects of ankle bracing under a combination of inversion and axial compression loading. Knee Surg Sports Traumatol Arthrosc. 2006 Apr;14(4):373–8.
16. Ubell ML, Boylan JP, Ashton-Miller JA, Wojtys EM. The effect of ankle braces on the prevention of dynamic forced ankle inversion. Am J Sports Med. 2003;31(6):935–40.

17. Zhang S, Wortley M, Chen Q, Freedman J. Efficacy of an ankle brace with a subtalar locking system in inversion control in dynamic movements. J Orthop Sports Phys Ther. 2009 Dec;39(12):875–83.
18. Choisne J, Hoch MC, Bawab S, Alexander I, Ringleb SI. The effects of a semi-rigid ankle brace on a simulated isolated subtalar joint instability. J Orthop Res. 2013 Dec;31(12):1869–75.
19. Eils E, Imberge S, Volker K, Rosenbaum D. Passive stability characteristics of ankle braces and tape in simulated barefoot and shoe conditions. Am J Sports Med. 2007 Feb;35(2):282–7.
20. Kamiya T, Kura H, Suzuki D, Uchiyama E, Fujimiya M, Yamashita T. Mechanical stability of the subtalar joint after lateral ligament sectioning and ankle brace application: a biomechanical experimental study. Am J Sports Med. 2009 Dec;37(12):2451–8.
21. Lee WCC, Kobayashi T, Choy BTS, Leung AKL. Comparison of custom-moulded ankle orthosis with hinged joints and off-the-shelf ankle braces in preventing ankle sprain in lateral cutting movements. Prosthet Orthot Int. 2012 Jun;36(2):190–5.
22. Nishikawa T, Kurosaka M, Mizuno K, Grabiner M. Protection and performance effects of ankle bracing. Int Orthop. 2000;24(5):285–8.
23. Raikin SM, Parks BG, Noll KH, Schon LC. Biomechanical evaluation of the ability of casts and braces to immobilize the ankle and hindfoot. Foot ankle Int. 2001 Mar;22(3):214–9.
24. Shapiro MS, Kabo JM, Mitchell PW, Loren G, Tsenter M. Ankle sprain prophylaxis: an analysis of the stabilizing effects of braces and tape. Am J Sports Med. 1994;22(1):78–82.
25. Siegler S, Liu W, Sennett B, Nobilini RJ, Dunbar D. The three-dimensional passive support characteristics of ankle braces. J Orthop Sports Phys Ther. 1997 Dec;26(6):299–309.
26. Karlsson J, Eriksson BI, Renstrom PA. Subtalar ankle instability. A review. Sports Med. 1997 Nov;24(5):337–46.
27. Beimers L, Tuijthof GJM, Blankevoort L, Jonges R, Maas M, van Dijk CN. In-vivo range of motion of the subtalar joint using computed tomography. J Biomech. 2008;41(7):1390–7.
28. Tuijthof GJM, Beimers L, Jonges R, Valstar ER, Blankevoort L. Accuracy of a CT-based bone contour registration method to measure relative bone motions in the hindfoot. J Biomech. 2009 Apr;42(6):686–91.
29. Tuijthof GJM, Zengerink M, Beimers L, Jonges R, Maas M, van Dijk CN, et al. Determination of consistent patterns of range of motion in the ankle joint with a computed tomography stress-test. Clin Biomech (Bristol, Avon). 2009 Jul;24(6):517–23.
30. Vaes PH, Duquet W, Casteleyn PP, Handelberg F, Opdecam P. Static and dynamic roentgenographic analysis of ankle stability in braced and nonbraced stable and functionally unstable ankles. Am J Sports Med. 1998;26(5):692–702.
31. O'Brein R, Muller K. Unified power analysis for t-tests through multivariate hypotheses. In: Edwards LK, editor. Applied Analysis of Variance in the Behavioral Sciences. New York: Marcel Dekker; 1993. p. 297–344.
32. Kitaoka HB, Alexander IJ, Adelaar RS, Nunley JA, Myerson MS, Sanders M. Clinical rating systems for the ankle-hindfoot, midfoot, hallux, and lesser toes. Foot ankle Int. 1994 Jul;15(7):349–53.

33. Dobbe JGG, Strackee SD, Schreurs AW, Jonges R, Carelsen B, Vroemen JC, et al. Computer-assisted planning and navigation for corrective distal radius osteotomy, based on pre- and intraoperative imaging. IEEE Trans Biomed Eng. 2011 Jan;58(1):182–90.
34. Ibrahim T, Beiri A, Azzabi M, Best AJ, Taylor GJ, Menon DK. Reliability and validity of the subjective component of the American Orthopaedic Foot and Ankle Society clinical rating scales. J Foot Ankle Surg. 2007;46(2):65–74.
35. Arndt A, Westblad P, Winson I, Hashimoto T, Lundberg A. Ankle and subtalar kinematics measured with intracortical pins during the stance phase of walking. Foot ankle Int. 2004 May;25(5):357–64.
36. Arndt A, Wolf P, Liu A, Nester C, Stacoff A, Jones R, et al. Intrinsic foot kinematics measured in vivo during the stance phase of slow running. J Biomech. 2007;40(12):2672–8.
37. Hamel AJ, Sharkey NA, Buczek FL, Michelson J. Relative motions of the tibia, talus, and calcaneus during the stance phase of gait: a cadaver study. Gait Posture. 2004 Oct;20(2):147–53.
38. Westblad P, Hashimoto T, Winson I, Lundberg A, Arndt A. Differences in ankle-joint complex motion during the stance phase of walking as measured by superficial and bone-anchored markers. Foot ankle Int. 2002 Sep;23(9):856–63.
39. Hertel J. Functional Anatomy, Pathomechanics, and Pathophysiology of Lateral Ankle Instability. J Athl Train. 2002 Dec;37(4):364–75.
40. Stormont DM, Morrey BF, An KN, Cass JR. Stability of the loaded ankle. Relation between articular restraint and primary and secondary static restraints. Am J Sports Med. 1985;13(5):295–300.
41. Lofvenberg R, Karrholm J. The influence of an ankle orthosis on the talar and calcaneal motions in chronic lateral instability of the ankle. A stereophotogrammetric analysis. Am J Sports Med. 1993;21(2):224–30.

Part 2

Morphology of the hindfoot

Chapter 5

Study on the three-dimensional orientation of the posterior facet of the subtalar joint using simulated weight-bearing CT

Roeland P. Kleipool
Jari Dahmen
Gwen Vuurberg
Roelof-Jan Oostra
Leendert Blankevoort
Markus Knupp
Sjoerd A.S. Stufkens

J Orthop Res. 2019 Jan;37(1):197-204.
doi: 10.1002/jor.24163

'take the weight off your feet'
Cambridge dictionary: If you take the weight off your feet/legs, you sit down, especially after standing or walking for a long time

Abstract

The purpose of this study was to describe the normal 3D orientation and shape of the subtalar calcaneal posterior facet. This is not adequately described in current literature. In a supine position both feet of 20 healthy subjects were imaged in a simulated weight-bearing CT. A cylinder and plane were fitted to the posterior facet of the surface model. The orientation of both shapes was expressed by two angles in (1) the CT-based coordinate system with the axis of the foot aligned with the sagittal axis and (2) a coordinate system based on the geometric principal axes of the subject's calcaneus. The subtalar vertical angle was determined in the intersection in three different coronal planes of the cylinder. The cylinder's axis oriented from supero-postero-laterally to infero-anteromedially. The plane's normal directed supero-antero-medially in the CT-based coordinate system, and supero-antero-laterally in the other coordinate system. The subtalar vertical angle was significantly different ($p<0.001$) between the three defined coronal planes and increased from anterior to posterior. The mean diameter of the fitted cylinder was 42.0 ± 7.7 mm and the root mean square error was 0.5 ± 0.1 mm. The posterior facet can be modelled as a segment of a cylinder with a supero-postero-lateral to infero-antero-medial orientation. The morphometry of the posterior facet in a healthy population serves as a reference in identifying abnormal subtalar joint morphology. More generally this study shows the need to include the full 3D morphology in assessing the orientation of the subtalar posterior facet.

Introduction

The hindfoot is a complex biomechanical unit that must support the whole body weight and has a crucial contribution in gait and propulsion (1,2). The subtalar joint (or talocalcaneal joint) has variation in the number and connections between the articulating facets on the superior surface of the calcaneus (3,4). The posterior facet of the subtalar joint is the largest and is always present. There is variation in its orientation and this has been linked to the development and progression of osteoarthritis (5,6), and to adult-acquired flatfoot deformity (7). The posterior facet is convex in a sagittally oriented plane and flat or slightly concave in a coronally oriented plane (8).

Previous studies that addressed the orientation of the posterior facet used the angle of the facet with the proximo-distal axis, also known as the subtalar vertical angle (SVA), in one or multiple coronal planes (6,9,10). In other literature, such as the frequently cited review of Sarrafian in 1993, the orientation was presented only in a sagittal plane (8). All these studies are limited by their two dimensional approach. The complex 3D morphology seems to be the reason that imaging of the subtalar joint to date is highly unreliable; the joint cannot be visualized in an adequate manner on plain radiographs (11,12). Computed Tomography (CT) scans give a better impression of the morphology (11). However, even in this imaging modality the determination of angles is dependent on the selected plane(s). This is illustrated by the finding that SVA values are different between coronal planes through the facet at different locations along the anteroposterior axis (6,10). Until recently, CT was limited to non-weight-bearing conditions, but weight-bearing CT scans have shown advantages above plain radiographs and non-weight-bearing CT (13,14). In this loaded condition the bones are orientated differently than in the unloaded condition (13). The foot and the joints are in a physiological and meaningful plantigrade position, other than a typically non-weight bearing equinus inversion-supination orientation. Weight-bearing CT will potentially broaden the functional and morphological understanding of the largest joint in the foot (13,14). However, many institutions do not have a weight-bearing CT facility and simulated weight bearing has been used as an alternative (15).

In order to express an orientation, one must choose a coordinate system. The choice can influence the outcome and thus has to be reproducible (6). The orientation can be expressed in reference to the coordinate system of the 3D CT image. It is obvious that the orientation in reference to a CT coordinate system is dependent on the alignment of the foot in the scanner, but no standard protocol for the assessment of the 3D images has been established for clinical CT scans. In order to overcome the introduced variation of foot positioning it is possible to define a coordinate system based on the morphometric features of the calcaneus itself. A reference based on the calcaneus itself

could be a temporary solution in future research. We used a method to standardize the orientation of the foot in simulated weight bearing CT and express the orientation of the posterior facet both in a CT based coordinate system of the standing foot and in a calcaneus based coordinate system.

Kapandji described the posterior facet as a segment of a cylinder with its axis orientated obliquely anteroposteriorly, lateromedially and slightly superoinferiorly (16). We used this description as a starting point to more fully account for the 3D morphology.

The main purpose of this study was to assess the orientation and the curvature of the posterior facet in a healthy population. We believe this will serve future investigation on the influence of the subtalar joint on the evolution of ankle joint arthritis in valgus and varus hindfoot deformities. The second objective was to identify the relation between the 3D morphology and the SVA in different coronal planes. The third goal was to compare the orientation of the posterior facet of the subtalar joint using both the 3D CT image coordinate system and the coordinate system based on the anatomy of the calcaneus on simulated weight-bearing CT scans.

Methods

This study was approved by our IRB (registration number NL60684.018.17). For this study healthy volunteers were recruited through public flyers distributed in our hospital. Inclusion criteria were that the volunteers were healthy, and symptoms free in their lower extremities at the time of study inclusion. Females who were pregnant or wanting to become pregnant at the time of volunteer recruitment were excluded. Additionally, participants who had a history of lower extremity trauma and/or surgery were excluded. Also participants who had undergone a CT scan in the previous year or were planned to undergo a CT scan in the upcoming year at the time of the study inclusion were excluded from the study.

Image Acquisition

A simulated weight-bearing device was custom made for the present study as our hospital does not have a standing weight-bearing CT scanner (Fig. 1). The subject was seated on the device in a horizontal standing position and the upper body resting against a back rest at an inclination angle of 53 degrees, similar to a study performed by to Zhang et al (15). The subjects were asked to place their feet on the movable footplate and to extend both legs in order to push away the moveable footplate. Between the footplate and the fixated frame a cord with a digital spring balance was attached (Type HCB200K500, KERN & SOHN GmbH, Balingen, Germany). The stretch in the cord allowed the extension of the legs and the force that was required for this stretch was assessed through the digital spring balance. This was repeated and the length of the cord adjusted until the desired force (equal to the body weight as measured in Newton) was reached. Through this manner an active simulated body weight loaded situation was created. In this final position and loading a CT scan was made from the footplate up to the level of the knee joint (Brilliance 64 CT scanner with voxel size of 0.4557 x 0.4557 x 0.45mm3, 120kV, and 160mA; Philips).

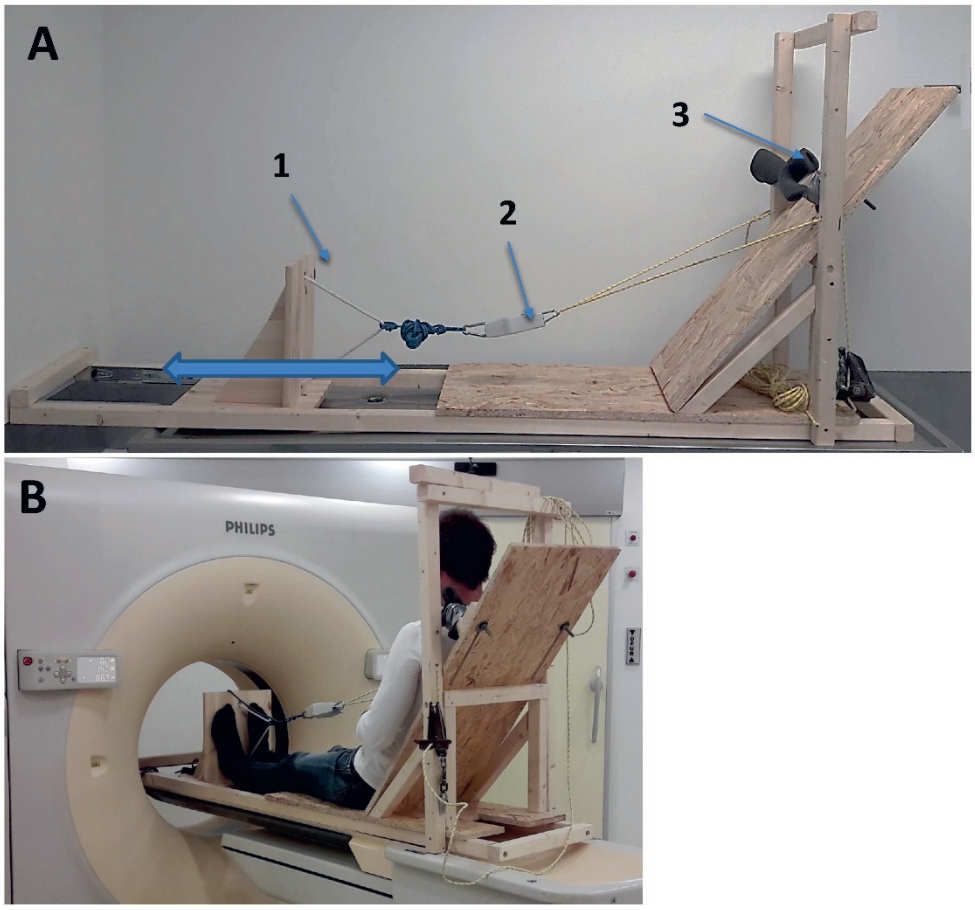

Figure 1. (A) Depiction of the device used for simulated weight-bearing. 1. moveable footplate, the bidirectional arrow illustrates the direction of movement. 2. digital spring balance to measure the force of the footplate on the legs. 3. extra shoulder supports that can be adjusted in height. (B) Depiction of the CT scanning protocol. The subject seated on the device with extended legs with a pressure on their legs equal to the body weight (see text for more detailed information).

Shape Analysis of the Posterior Facet

The talus and calcaneus were segmented in the CT images with custom made software, which was developed at our academic hospital (17). This resulted in virtual 3D surface models of the talus and calcaneus. The surface of the posterior facet of the calcaneus was defined as that area of the calcaneal surface where the smallest distance of each point to any surface point of the talus was less than 4 mm, with the restriction that the angle between the normal vectors of the surface at these points (i.e., perpendicular to the bone surface) was less than 30 degrees (18). The optimal threshold was determined by visual inspection for several feet and with several different thresholds. In the software the areas of both the calcaneus and talus are highlighted with these thresholds and the chosen thresholds resulted in the best result. The effect of a variation of the 4mm distance threshold and 30 degrees angle threshold on the cylinder fit (see further) was evaluated by repeating the cylinder fit with 3.5 and 4.5 distance thresholds and 25 and 35 degrees angle thresholds on the data set of two randomly selected feet. The left calcanei and facets were mirrored to right calcanei and facets for further analyses in a corresponding orientation.

The shape and orientation of the posterior facet was modelled as a segment of a cylinder.16 This gives information about the orientation and curvature of the facet by means of the orientation of the cylinder's axis and the diameter, respectively. Additionally, the facet was modelled as a plane. The plane's normal (i.e., the vector perpendicular to the plane) was positioned in the centroid (calculated as the mean of the 3D points) of the facet. The plane's normal gives a rough approximation of the orientation of the facet, but also gives information concerning the location of the segment in the fitted cylinder which is not defined otherwise.

The cylinder was fit to the point cloud of the posterior facet (the point cloud consists of the 3D points or vertices that are connected in the 3D surface model) using a nonlinear least-squares optimization process with the axis in a predominantly transverse orientation. The plane was fit to the point cloud of the facet by minimizing the normal quadratic distance. The root mean square errors for the cylinder and plane were calculated as a measure for the accuracy of the fit.

Plane and cylinder fitting, and determination of the angles (see further) were processed with custom made routines in Matlab (MATLAB Release 2016a, The MathWorks, Inc., Natick, MA).

Expression of the Orientation and Coordinate Systems

The cylinder's axis and the plane's normal were determined in 1) the CT-based coordinate system and 2) in reference to the principal axis of the calcaneus (Fig. 2). For each foot in the CT-based coordinate system the 3D image was virtually rotated around the proximo-distal axis (Z-axis) such that the line between the center of the heel and the base of the 2nd metatarsal (representing the axis of the foot) directed anteriorly (6). The position of the calcaneus in the CT-based coordinate system, after rotating the axis of the foot in the anterior direction, was considered a standing position and in reference to the principle axis of the calcaneus was considered an anatomical position. The origin of both coordinate systems was placed in the centroid of the calcaneus. The centroid was calculated as the mean of all vertices.

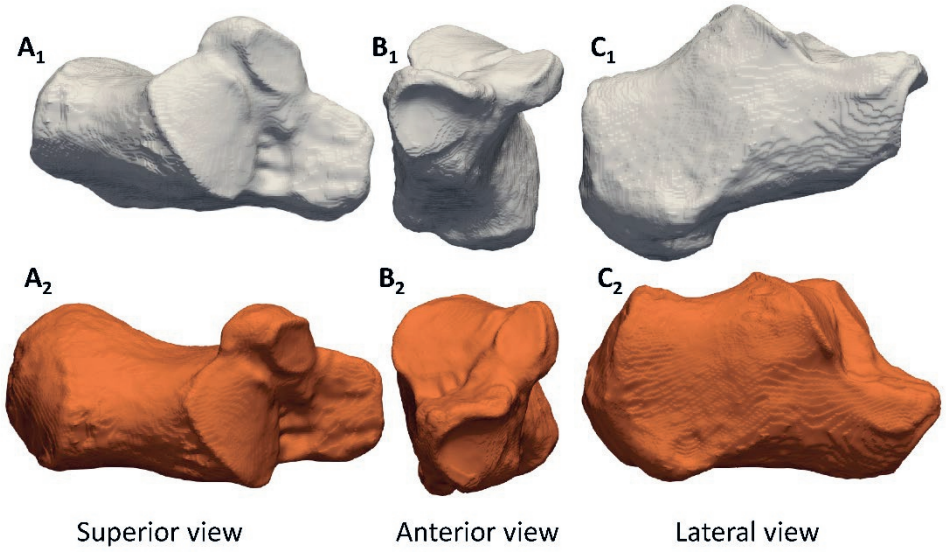

Figure 2. Graphical representation of the right calcaneus of one subject in both coordinate systems. (A) proximal view, (B) anterior view, (C) lateral view. Top row is the calcaneus in the CT coordinate system after aligning the axis of the foot with a sagittal axis. Bottom row is the calcaneus in the coordinate system based on its principal axes (For a better conception of the 3D aspects, the reader is encouraged to consult the interactive 3D figures in the supplementary file (Fig. S-1, doi: 10.1002/jor.24163).

The orientation of the cylinder's axis and plane's normal were expressed with two angles. The first was the inclination angle: The angle between the cylinder's axis or plane's normal and the XY-plane. The second was the deviation angle: The angle between the projection of the cylinder's axis or plane's normal on the XY-plane and the Y-axis, or the sagittal plane. A negative inclination angle corresponds to an inferiorly or plantarly orientated axis or normal. A negative deviation angle corresponds to a medially orientated axis or normal (Fig. 3).

Determining the Subtalar Vertical Angle

In analogy to previous studies, the SVA was determined in three coronal planes (Fig. 4) (6,9,10). A middle coronal plane of the posterior facet was defined by the midpoint between its most posterior and anterior points. Two additional planes, respectively 5mm anterior and posterior to the middle coronal plane, were defined. A part of the cylinder was selected within the boundaries of the facet (boundary box). This part was cut by the three coronal planes. At each coronal plane a line was fitted to the curvature of the selected part of the cylinder. The angle of this line with the vertical or Z-axis was calculated as the SVA. The SVA was only determined in reference to the standing position.

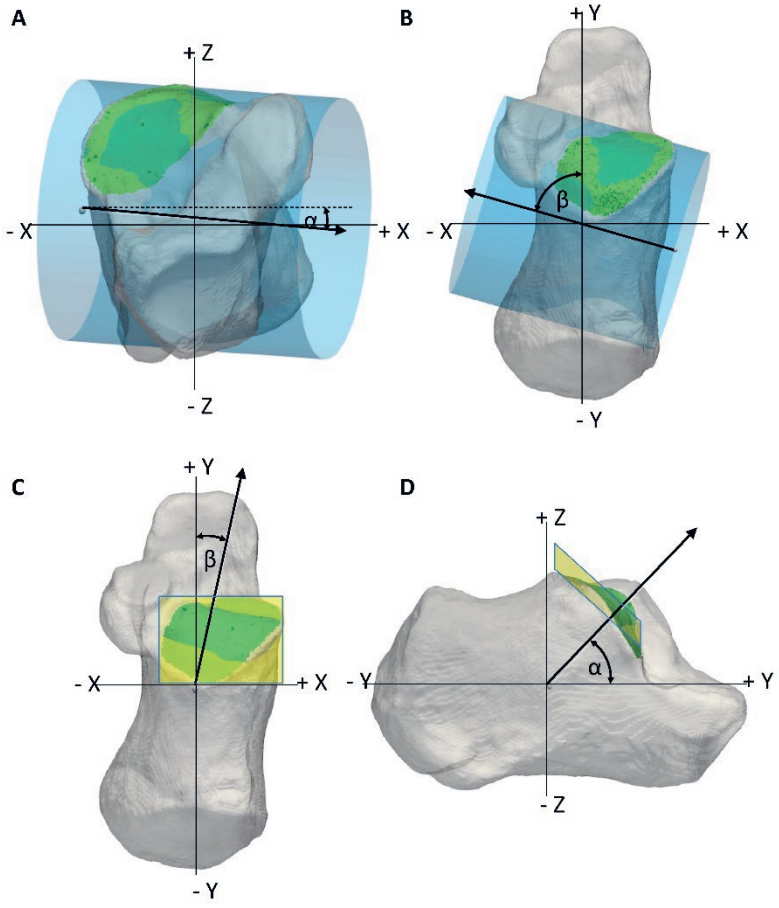

Figure 3. Graphical representation of the cylinder and plane fit parameters of one right calcaneus with the posterior facet (in green), the fitted cylinder (in blue), and the fitted plane (in yellow). (A) frontal view, (B) proximal view, (C) proximal view, (D) lateral view. The origin of the XYZcoordinate system was located in the centroid of the calcaneus. The positive X-axis is directed laterally. The positive Y-axis is directed anteriorly. The positive Z-axis is directed proximally. The orientation within this coordinate system of the cylinder's axis and the plane's normal is expressed as an inclination angle (alpha in the figure A and D) and a deviation angle (beta in the figure B and C, the dashed line in A is a line parallel to the X-axis). The inclination angle is the angle of the cylinder's axis or plane's normal with the XY-plane. The deviation angle is the angle of the projection of the cylinder's axis or plane's normal on the XY-plane with the Y-axis (For a better conception of the 3D aspects, the reader is encouraged to consult the interactive 3D figures in the supplementary file (Fig. S-1, doi: 10.1002/jor.24163).

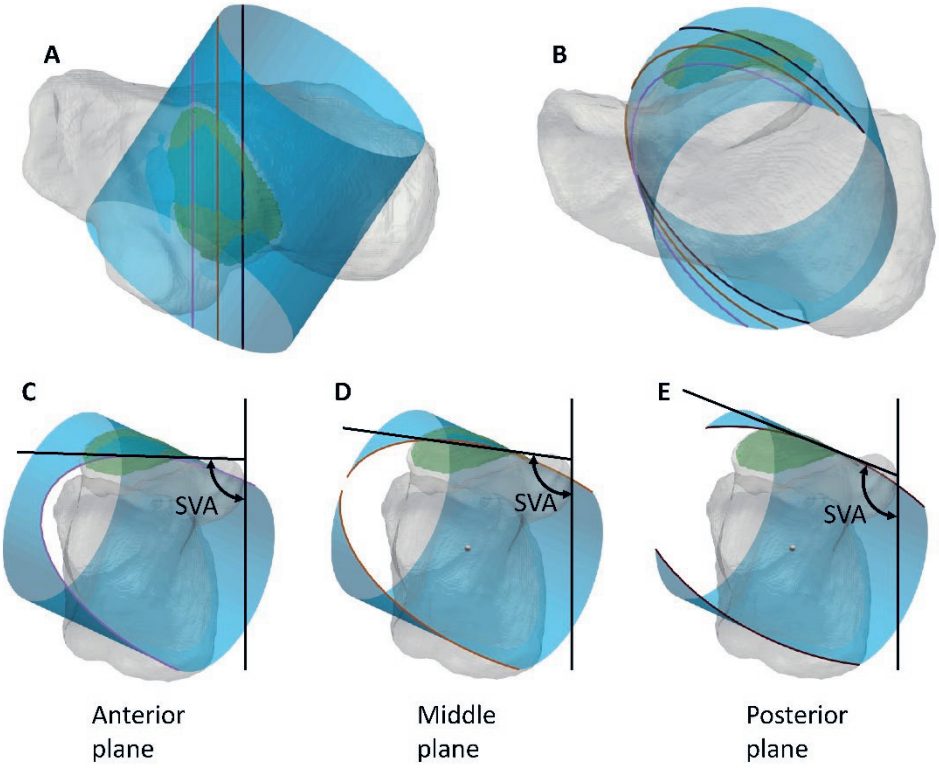

Figure 4. Graphical representation of a right calcaneus with the posterior facet (in green) and the fitted cylinder (in blue). (A) proximal view, (B) medial view, (C–E) anterior view. In A the level of three coronal planes, where the Subtalar Vertical Angles (SVAs) were determined, are represented with the three lines. In C–E a line was fitted to the curvature of that part of the cylinder that is within the boundaries of the facet. The angle of this line with the vertical or Z-axis was calculated as the SVA (For a better conception of the 3D aspects, the reader is encouraged to consult the interactive 3D figures in the supplementary file (Fig. S-1, doi: 10.1002/jor.24163).

Determining the Rotation Angles From One Coordinate System to the Other

The principal axes of the calcaneus in standing position were determined. The rotation angles to place the principal axes parallel to the axes of the (global) CT coordinate system were calculated. This is the position of the calcaneus in an anatomical position. The rotation sequence was XYZ.

Determining Foot Shape

The foot shape was analyzed with the Meary's Angle (19). A digitally reconstructed radiograph of the lateral ankle was made based on the 3D CT image with the axis of the foot in sagittal direction (the same orientation as for the determination of the posterior facet in standing position). Feet with indexes outside the range of <-5 degrees (pes cavus) or >8 degrees (pes planus) were excluded from further analysis (20).

Statistical Analyses

All data of the cylinder and plane fit parameters and SVAs were analyzed for normal distribution with the Shapiro–Wilk Test. Statistical differences between the orientation angles of the cylinder, plane and the principal axes between the standing position and anatomical position were tested with a paired Student t-test. Statistical differences between the SVAs at the three coronal planes was tested with a repeated measures ANOVA with a Bonferroni correction applied. Statistical differences of the distribution of the inclination angle and the deviation angle of the plane's normal and the cylinder's axis between the two coordinate systems was tested after standardization (xnew = (x - mean)/SD) with the Kolmogorov–Smirnov's test. Statistical level of significance was set at $p = 0.05$. Statistical analysis was performed with SPSS (IBM SPSS Statistics for Windows, Version 24.0. Released 2016. IBM Corp. Armonk, NY: IBM Corp). Data is presented as mean ± standard deviation.

Results

Twenty volunteers participated, 10 male and 10 female, and signed informed consent. The mean age was 35.9 ± 11.1 (range, 23–59) years and the mean weight was 76.9 ± 11.1 (range, 58–95) kg. The mean Meary's Angle was 0.4 ± 3.3 (range, -4.9 to 6.9) degrees, thus no foot had an abnormal longitudinal curvature aside from a very mild form of pes planus or pes cavus. Based on this measurement all feet were included in further analyses (n= 40).

3D Orientation of the Posterior Facet and the Curvature

The direction of the cylinder's axis was in a superopostero-lateral to infero-antero-medial direction for both the standing and anatomical positions. In the standing position the inclination angle of the cylinder's axis was more negative compared to the anatomical position (Table 1). This corresponds to a more plantarly directed orientation. The inclination angle in the anatomical position was only a few degrees, almost lying in the axial plane. The deviation angle was less negative in the standing position relative to the anatomical position. This corresponds to a more anteriorly directed orientation. Both angles were significantly different between the two positions ($p<0.001$). The diameter of the fitted cylinder for the left side was 41.9 ± 7.4 (range, 30.5–56.6) mm and for the right side 42.2 ± 8.2 (range, 31.8–58.9) mm.

In the standing position, the plane's normal was directed in an anterior, superior and medial direction (Table 1). In the anatomical position the mean inclination angle was lower and the normal was orientated laterally. Both angles were significantly different between the two positions ($p<0.001$). The plane's normal at the centroid of the posterior facet was approximately perpendicular to the cylinder's axis (90.4 ± 1.6 degrees).

The average root mean square errors for the plane fit was 1.52 ± 0.19 and 1.57 ± 0.27mm for the left and right facets respectively. The cylinder fit had lower average root mean square errors: 0.51 ± 0.10 and 0.5 ± 0.10 mm for the left and right facets respectively. Both angles of the cylinder's axis and plane's normal was normally distributed (Shapiro–Wilk Test, p>0.05), except for the deviation angle of the cylinder's axis in the standing position for the left side ($p = 0.048$).

Table 1. Inclination and deviation angles (in degrees) of the cylinder's axis and plane's normal for 20 pairs of calcanei (the left calcanei were mirrored to right for a corresponding orientation)

Coordinate system:		CT 3D image (Functional position)				Principal axes calcaneus (Anatomical position)			
		Inclination		Deviation		Inclination		Deviation	
		L	R	L	R	L	R	L	R
Cylinder fit	Mean	-17.4	-17.3	-51.4	-48.0	-2.4	-4.1	-70.1	-68.6
	SD	5.7	4.9	8.2	7.0	6.9	7.9	5.6	4.4
	Min	-29.7	-30.4	-60.0	-58.1	-15.8	-17.9	-77.9	-75.7
	Max	-8.2	-4.3	-24.4	-34.8	9.4	7.4	-56.7	-60.9
Plane fit	Mean	65.4	66.7	-4.1	-2.7	44.7	46.7	17.8	17.4
	SD	5.1	5.4	11.6	13.3	4.3	3.6	6.3	8.8
	Min	56.9	55.6	-20.9	-22.2	34.2	41.3	6.4	3.9
	Max	76.5	77.9	13.4	27.6	53.6	54.7	28.9	32.9

L is left side, R is right side.

A variation of the 4mm distance threshold, for the isolation of the posterior facet from the whole calcaneal surface model, by +0.5 and -0.5mm did not change the cylinder's diameter, inclination angle or deviation angle. Variation of the 30 degrees angle threshold by +5 and -5 degrees resulted in a maximal change of 0.8 mm for the diameter, 0.2 degrees for the inclination angle, and 0.8 degrees for the deviation angle.

Subtalar Vertical Angle

The SVA showed an increase from anterior to posterior (Table 2 and Fig. 4 for a graphical representation). The SVA for the left and right side at all three coronal planes had a normal distribution. Mauchly's test showed that for the left side the assumption of sphericity was violated. Therefore the degrees of freedom were corrected with Greenhouse-Geisser. Results showed there were statistically significant differences in SVA between the three (-5/0/+5mm from the middle) coronal planes for both the left side ($F(1.502, 28.547) = 323.041$, $p<0.001$) and the right side ($F(2,38) = 594.616$, $p<0.001$). Post hoc analyses showed that at both the left and right sides all three SVAs differed significantly from each other ($p<0.001$, also see Table 2).

Table 2. Subtalar Vertical Angle SVA, (in degrees) at an anterior, middle, and posterior coronal plane based on the cylinder fitted to the posterior facet of the calcaneus of the talocalcaneal joint (see text) for 20 pairs of calcanei (the left calcanei were mirrored to right for a corresponding orientation)

	Anterior**		Middle*		Posterior**	
	L	R	L	R	L	R
Mean	85.0	85.4	97. 1	95.8	109.6	109.7
SD	5.5	4.5	7.2	6.6	7.8	8.0

L is left side, R is right side. *Indicates that the SVA in the middle plane was significantly different from the anterior and posterior plane with $p = 0.005$ for both left and right side. ** Indicates that the SVA was significantly different between the anterior and posterior plane with $p<0.001$ for both left and right side.

Rotations Between the Two Coordinate Systems

The calcaneus had a different orientation between its standing and anatomical position, in reference to the CT coordinate system (after rotating the axis of the foot in anterior direction) and its principal axes, respectively. In the standing position the anterior process of the calcaneus was orientated more laterally in the axial plane (mean rotation about the Z-axis of 5.2 ± 4.1 degrees), more superiorly in the sagittal plane (mean rotation about the X-axis of 16.7 ± 4.1 degrees), and the calcaneus was tilted medially in the coronal plane (mean rotation about the Y-axis of 25.8 ± 6.6 degrees), in comparison to the anatomical position (with a rotation sequence XYZ). All angles were significantly different between the two positions ($p<0.001$). This difference in orientation was, as expected, also reflected in the orientations of the cylinder's axis and plane's normal. The distribution of the inclination and deviation angle of the cylinder's axis and the plane's normal was not significantly different between the two coordinate systems.

Discussion

The most important finding of the present study is that the posterior facet of the calcaneus of the subtalar joint can be described as a cut out of a cylinder with a supero-postero-lateral to infero-antero-medial axis in a healthy population. The facet directs, as expressed by the normal of a plane fit, in an anterior, medial and superior direction. The plane fit resulted in higher values for root mean square errors, thus in a poorer fit, than the cylinder fit and only gives a rough approximation of the orientation. Moreover, the acquired accuracy of the cylinder fit was comparable to that of a cylinder fit to the trochlea tali surface in a related study by Huang et al (21). Also, the visual inspection

confirmed that a segment of a cylinder is an appropriate representation for the shape and orientation of the posterior facet. These findings closely resemble the descriptions of Inman and Kapandji which were used as a starting point of our analysis (16,22). Since this present study is a survey of the normally shaped feet, all included feet were asymptomatic and were subsequently classified by the Meary's Angle (19). The angles were within normal ranges with only very mild pes planus or pes cavus feet at the extremes (20). This selection makes the assumption that the feet were normal trustworthy. The average orientation of the axis of rotation of the subtalar joint as reported in the literature has an inclination angle of 42 degrees and a deviation angle of -23 degrees in a standing position with the sagittal axis parallel to the midline of the foot (8). The axis of rotation runs from the superomedial aspect of the talar neck, through the medial aspect of the tarsal canal to the posterolateral corner of the calcaneus (8). Based on the orientations of the rotation axis and the cylinder's axis of the present study we can postulate that parts of the joint surfaces cannot maintain contact through the whole range of motion. For instance, during supination the talus will abduct, dorsiflex, evert and posteriorly translate relative to the calcaneus. This motion will result in a gap at the posterolateral side. This proposed mechanism is in line with previous descriptions of motion of the posterior subtalar joint (8,16,22).

Our method with advanced 3D imaging and shape analysis was applied to more fully account for the 3D morphology. Previous studies are limited in their assessment of the 3D orientation because the studies solely utilized a single anatomical plane (6,8–10,12).

The oblique orientation of the facet or cylinder has a direct relation to the SVA at different coronal planes along an anteroposterior direction. To fully appreciate this relationship, one is advised to consult Figure 4 (or preferably online the supplemental figures [Fig. S-1]). Posteriorly the SVA will be greater than anteriorly. Our acquired values by the virtual models are in line with the angles determined on true weight-bearing CT images with the same foot orientation of the study of Krahenbuhl et al (6). They found SVAs in a healthy control cohort (n=20, 10 male and 10 female) with a median of 85, 96, and 107 degrees for the anterior, middle and posterior coronal plane respectively (based on Fig. 3 of their article). These findings confirm the appropriateness of the chosen geometrical shape model in the present study and demonstrates that the simulated weight-bearing was a proper alternative for true weight-bearing CTs.

Additionally, the present study showed that the orientation is dependent on the particular chosen coordinate system. The principal axes of the calcaneus are calculated and are dependent on the whole geometry of the calcanei, as Parr et al. discussed for the talus (23). The calcanei were superimposed over one another by using their principal axes, and by visual inspection the alignment appeared to be comparable. However, no

quantitative analyses were performed on this issue. In the CT scanner the subject can place their feet in a variable manner and this obviously has an influence on the orientation of the foot relative to the CT coordinate system. The subjects were instructed to place their feet on the footplate as they would when they were standing normally. In the postprocessing the position of each foot was standardized by virtually rotating the feet in the axial plane such that the line from the center of the heel to the base of the 2nd metatarsal directs anteriorly (6). Thus the feet were in a normal physiological position, but were virtually aligned for a matching orientation. This makes that the results are reproducible and makes translation possible to further research. In order to interpret the relationship of the subtalar joint orientation to the development of pathological conditions such as tibiotalar varus and valgus asymmetrical osteoarthritis, it will be necessary to develop a new reference coordinate system based on the tibia or on a larger segment of the lower extremity. The orientation of the ankle joint and subtalar joint with reference to the tibial axes, ideally the kinematics in a 4D description included, could provide an insight in the role of pathoanatomy in the coupled motions of the hindfoot. The comparison between a standing and an anatomical position showed no reason to state that the standing position was more variable. The acquired values for rotations over the three axes from the anatomical position (based on the principal axes of the calcaneus) to the weight-bearing 'standing' position can be used to transform any calcaneus from a random position to approximate the orientation in a standing position. This makes it possible to use also other (non-weight bearing) CT images of feet in different positions, although this transformation requires further research. We advise to use the standing position in future studies as this is a physiological meaningful position, and to use the anatomical position when weight-bearing is not possible. Weight-bearing ensures physiological alignment of the hindfoot and therefore allows measurements that represent clinical practice.

The method to isolate the posterior articular surface from the whole calcaneal surface model was based on an algorithm with chosen thresholds. The software allowed a clear visualization of the selected area. For example, a distance threshold of 3mm resulted in holes in the surface of the facet. Our analysis of the threshold variations within a realistic range from the chosen values resulted in small changes compared to the standard deviation of the cohort and can be considered of minor influence on the outcomes. Apart from a first identification of appropriate thresholds the method is objective and reproducible, and appears to be robust.

The present study does have some limitations. Although the facet was analyzed in 3D and our approach is new, it should be noted that a geometrical shape analysis, a cylinder and a plane in our case, is still a simplification of the true morphology, which inevitably yields a residual error. It is demonstrated that, obviously, a plane is a too simple

representation for this complex anatomical structure. Another geometrical shape, such as a cut out of a conus or a saddle shaped surface might result in smaller residual error (21). However, a saddle shape is difficult to interpret. Furthermore, the present study was not designed to change the decision making in a clinical setting. The results are not easily acquired and no pathological feet were analyzed. Simulated weight bearing also has its limitations and is second best to a true physiological load. The next steps will be to use full weight bearing CTs and include patients with malalignment.

In conclusion, this study showed that the posterior facet of the calcaneus of healthy subjects can be modeled as a segment of a cylinder of which the orientation is oblique in all three anatomical planes; anteroposteriorly, lateromedially and slightly superoinferiorly. Because of this oblique nature, any determination of the orientation in 2 dimensions, as in plain radiographs or CT slices, is prone to errors. As the facet is three dimensional we advise to take this into consideration in clinical practice, such as when determining the SVA and when conducting future studies. Furthermore, the orientation depends on the chosen coordinate system. The present study demonstrated this and quantified the differences between a standing position of the calcaneus and an anatomical position. Finally, our simulated weight-bearing CT protocol provides a suitable alternative for those institutes that do not have a standing weight-bearing CT facility.

Acknowledgements

We would like to acknowledge J.G.G. Dobbe (PhD) and G.J. Streekstra (PhD) of the department of Biomedical Engineering and Physics, UMC Amsterdam, location AMC, for methodological support and assistance in conducting this study. We would like to acknowledge the Musculoskeletal Imaging Quantification Center (MIQC) Amsterdam, The Netherlands, and Marti-Keuning Eckhardt Stichting Amsterdam, The Netherlands for their financial support enabling radiological imaging. We would like to acknowledge Mr. J. Hagoort of the Medical Biology department, UMC Amsterdam, location AMC, for the technical support in constructing the supplemental figures.

References

1. Benink RJ. The constraint-mechanism of the human tarsus. A roentgenological experimental study. Acta Orthop Scand Suppl. 1985;215:1–135.
2. Maceira E, Monteagudo M. Subtalar anatomy and mechanics. Foot Ankle Clin. 2015 Jun;20(2):195–221.
3. Bruckner J. Variations in the human subtalar joint. J Orthop Sports Phys Ther. 1987;8(10):489–94.
4. Drayer-Verhagen F. Arthritis of the subtalar joint associated with sustentaculum tali facet configuration. J Anat. 1993 Dec;183 (Pt 3:631–4.
5. Hayashi K, Tanaka Y, Kumai T, Sugimoto K, Takakura Y. Correlation of compensatory alignment of the subtalar joint to the progression of primary osteoarthritis of the ankle. Foot ankle Int. 2008 Apr;29(4):400–6.
6. Krähenbühl N, Tschuck M, Bolliger L, Hintermann B, Knupp M. Orientation of the Subtalar Joint: Measurement and Reliability Using Weightbearing CT Scans. Foot ankle Int. 2016 Jan;37(1):109–14.
7. Probasco W, Haleem AM, Yu J, Sangeorzan BJ, Deland JT, Ellis SJ. Assessment of coronal plane subtalar joint alignment in peritalar subluxation via weight-bearing multiplanar imaging. Foot ankle Int. 2015 Mar;36(3):302–9.
8. Sarrafian SK. Biomechanics of the subtalar joint complex. Clin Orthop Relat Res. 1993 May;(290):17–26.
9. Van Bergeyk AB, Younger A, Carson B. CT analysis of hindfoot alignment in chronic lateral ankle instability. Foot ankle Int. 2002 Jan;23(1):37–42.
10. Colin F, Horn Lang T, Zwicky L, Hintermann B, Knupp M. Subtalar joint configuration on weightbearing CT scan. Foot ankle Int. 2014 Oct;35(10):1057–62.
11. Cody EA, Williamson ER, Burket JC, Deland JT, Ellis SJ. Correlation of Talar Anatomy and Subtalar Joint Alignment on Weightbearing Computed Tomography With Radiographic Flatfoot Parameters. Foot ankle Int. 2016 Aug;37(8):874–81.
12. Ebraheim NA, Mekhail AO, Yeasting RA. Components of the posterior calcaneal facet: anatomic and radiologic evaluation. Foot ankle Int. 1996 Dec;17(12):751–7.
13. Hirschmann A, Pfirrmann CWA, Klammer G, Espinosa N, Buck FM. Upright cone CT of the hindfoot: comparison of the non-weight-bearing with the upright weight-bearing position. Eur Radiol. 2014 Mar;24(3):553–8.
14. Richter M, Seidl B, Zech S, Hahn S. PedCAT for 3D-imaging in standing position allows for more accurate bone position (angle) measurement than radiographs or CT. Foot Ankle Surg. 2014 Sep;20(3):201–7.
15. Zhang Y, Xu J, Wang X, Huang J, Zhang C, Chen L, et al. An in vivo study of hindfoot 3D kinetics in stage II posterior tibial tendon dysfunction (PTTD) flatfoot based on weight-bearing CT scan. Bone Joint Res. 2013;2(12):255–63.
16. Kapandji IA. The Physiology of the Joints: Lower Limb, Volume 2. Churchill: Livingstone; 1987.
17. Dobbe JGG, Pre KJ du, Kloen P, Blankevoort L, Streekstra GJ. Computer-assisted and patient-specific 3-D planning and evaluation of a single-cut rotational osteotomy for complex long-bone deformities. Med Biol Eng Comput. 2011 Dec;49(12):1363–70.

18. Foumani M, Strackee SD, van de Giessen M, Jonges R, Blankevoort L, Streekstra GJ. In-vivo dynamic and static three-dimensional joint space distance maps for assessment of cartilage thickness in the radiocarpal joint. Clin Biomech (Bristol, Avon). 2013 Feb;28(2):151–6.
19. Meary R. On the measurement of the angle between the talus and the first metatarsal. Rev Chir Orthop. 1967;53(389).
20. Arunakul M, Amendola A, Gao Y, Goetz JE, Femino JE, Phisitkul P. Tripod index: a new radiographic parameter assessing foot alignment. Foot ankle Int. 2013 Oct;34(10):1411–20.
21. Huang J, Liu H, Wang D, Griffith JF, Shi L. Talar dome detection and its geometric approximation in CT: Sphere, cylinder or bi-truncated cone? Comput Med Imaging Graph. 2017 Apr;57:62–6.
22. Inman VT. The joints of the ankle. Baltimore: Williams and Wilkins;
23. Parr WCH, Chatterjee HJ, Soligo C. Calculating the axes of rotation for the subtalar and talocrural joints using 3D bone reconstructions. J Biomech. 2012 Apr;45(6):1103–7.

Chapter 6

Difference in orientation of the talar articular facets between healthy ankle joints and ankle joints with chronic instability

Roeland P. Kleipool
Sjoerd A.S. Stufkens
Jari Dahmen
Gwendolyn Vuurberg
Geert J. Streekstra
Johannes G.G. Dobbe
Leendert Blankevoort
Markus Knupp

J Orthop Res. 2021 Apr 29
doi: 10.1002/jor.25068

'the boot is on the other foot'
Cambrigde dictionary: the situation is now the opposite of what it was, especially because someone who was weak now has power

Abstract

Since both the talocrural and subtalar joints can be involved in chronic ankle instability, the present study assessed the talar morphology as this bone is the key player between both joint levels. The 3D orientation and curvature of the superior and the posteroinferior facet between subjects with chronic ankle instability and healthy controls were compared. Hereto, the talus was segmented in the CT images of a control group and a chronic ankle instability group, after which they were reconstructed to 3D surface models. A cylinder was fitted to the subchondral articulating surfaces. The axis of a cylinder represented the facet orientation, which was expressed by an inclination and deviation angle in a coordinate system based on the cylinder of the superior talar facet and the geometric principal axes of the subject's talus. The curvature of the surface was expressed as the radius of the cylinder. The results demonstrated no significant differences in the radius or deviation angle. However, the inclination angle of the posteroinferior talar facet was significantly more plantarly orientated (by 3.5 degrees) in the chronic instability group (14.7 ± 3.1 degrees) compared to the control group (11.2 ± 4.9 degrees) ($p < 0.05$). In the coronal plane this corresponds to a valgus orientation of the posteroinferior talar facet relative to the talar dome. In conclusion, a more plantarly and valgus orientated posteroinferior talar facet may be associated to chronic ankle instability.

Clinical Significance. The present study identified the talar morphology to be associated with chronic ankle instability.

Introduction

Identifying factors that are related to chronic ankle instability (CAI) can decrease unnecessary delay in diagnosis and treatment, increase the effectiveness of treatment as well as reduce the direct costs of medical care, and decrease the high socio-economic burden associated with ankle sprains (1). CAI is defined as instability of the ankle joint with the sense of giving way, episodes of recurrent ankle sprains, with or without the presence of joint laxity (2,3). Varus malalignment of the lower leg or the hindfoot has shown to increase the risk of CAI (4–11). The malalignment of the hindfoot is radiographically defined as the calcaneal offset in relation to the longitudinal axis of the tibia. A varus malalignment shifts the axial load laterally compared to a neutral alignment, which subsequently creates an inversion moment that can result in a lateral ankle sprain if not timely countered at foot landing (12). While the correlation of tibial malalignment and ankle joint instability has been extensively analyzed (5), only few studies assess the importance of hindfoot varus alignment on the development of CAI.

The alignment of the hindfoot is influenced by the shape of the bones. In particular, the orientation of the articulating surfaces as well as the deformation in the mid- and forefoot induced by foot loading play an important role in this alignment. Both the talocrural and subtalar joints can be involved in CAI. (2). The talus is a key player between both joint levels and therefore also regarding the alignment of the hindfoot. Malalignment can be present at any level in the mechanical chain from tibia to the ground (7,13). The influence of the morphology of the talocrural joint on the development of CAI is well documented. For example, the radius of the talar dome was shown to be larger in patients with CAI than in controls (14). However, controversies exist on the role of the morphology of the subtalar joint in the relationship with CAI. Furthermore, abnormal orientation at one joint level in the mechanical chain of the hindfoot can be compensated by an adaptation at another joint level (7,14). This makes it important to determine the morphology per joint level and the interrelationships in orientation at these joint levels.

A three-dimensional (3D) analysis of the orientation of the articulating facets in the mechanical chain of the hindfoot is currently missing in present literature. Previously, the determination of subtalar joint orientation was reported in a two-dimensional (2D) manner (e.gg. (4,13,15,16)), however, this is prone to errors and has limitations (9,17,18).

As a result, the present study was designed to address the potentially present differences in the morphology of the talar facets between subjects with CAI and those without (i.e., healthy controls). A comparison was made between healthy controls and patients with CAI to assess the differences in orientation of the posteroinferior subtalar

joint relative to the talar dome in 3D space, and of the curvature of these facets. The hypothesis is that this orientation and curvature is significantly different between patients with CAI and healthy controls.

Materials and Methods

Datasets

For this retrospective case controlled study three datasets from three previous studies were used (18–20). Each study was approved by the local Institutional Review Board. In all three studies the distal tibia, talus, and calcaneus of the participants were imaged in supine position with Computed Tomography (CT) (0.3 < voxel size < 0.4557 mm, tube charge of 120 kV, and radiation dose of 150 to 160 mAs, Brilliance 64 CT scanner, Philips Healthcare, Amsterdam, The Netherlands). A total of 40 ankles from two groups of 20 healthy volunteers each, with non-symptomatic feet/ankles were included to form the control group for the present study (18,19). In case both sides were scanned an arbitrary choice was made for one of the sides assuming that the differences within a subject is smaller than the differences between subjects (18). The CAI group included 12 patients with CAI (Table 1) (20). If both sides of the patient were affected, the side with the highest incidence of previous ankle sprains was selected. No a-priori power analysis was performed since there were no data available to perform such analysis.

Table 1. Participant characteristics of the control group and group of patients with chronic ankle instability (CAI)

Group	Number of tali	Number of Male / Female	Mean age (years)	Standard deviation (years)	Minimal age (years)	Maximal age (years)	Range (years)
Control (18,19)	40	20 / 20	31.1	9.5	22	59	37
CAI (20)	12	8 / 4	27.3	10.9	19	59	40

Image analysis

The talus was segmented from the 3D-CT image and modelled as 3D polygons using custom made software (21), which was developed and validated at our academic hospital (22). The following subchondral articular joint surfaces of the talus were selected using the selection tool in Blender (software version 2.79, GNU General Public

License): the talar superior facet (the facet of the talus that articulates with the tibial plafond, also known as the talar dome), and the talar posteroinferior facet (the facet that articulates with the posterior facet of the calcaneus). Selection of these surfaces was done by one researcher (RPK, who has more than five years of experience in segmentations and 3D modelling of the hindfoot). No blinding for study group was performed for a possible bias, since the observer had no overview of the end results. In the first step segmentation was performed. Secondly, the selection of the surface of the talar dome was performed. Lastly, the selection of the posterior subtalar surface was performed without the presence of images of the talar dome. Subsequent analysis was performed by computer algorithms not requiring any user intervention.

Data processing

The facets were modelled as a segment of a cylinder (18). Hereto, a cylinder was fit to the points in each selected polygon surface using a nonlinear least-squares optimization process (Fig. 1). The cylinders were named TalusSF and TalusIF, for the superior and posteroinferior talar facet, respectively. The radius of the cylinder represents the curvature of the facet. To quantify to what extent the facet matches with the cylindrical shape the root mean square error between the points of the facet and cylinder was calculated. A large error indicates that the articulating surface does not fit well to the cylinder, for example because the surface is flat. On the other hand, a small error indicates a good match with a cylindrical surface.

Another outcome of the present study was the interrelationship between the two facets of the talus. The orientation of TalusIF in respect to TalusSF describes (a part of) the talar morphology. To align all tali uniformly and reproducibly, a local orthogonal right-handed coordinate system was defined with the following steps. All left tali were mirrored to right tali for further analyses in a corresponding orientation. The X-axis was set parallel with the cylinder's axis of TalusSF and was in a medial-lateral direction. Next, the geometric principal axes of the subject's talus were determined. The Y-axis was defined using the Gram-Schmidt process with the determined X-axis and the talar principal axis in antero-posterior direction (23). The Z-axis was defined perpendicular to the X- and Y-axis with the positive direction orientated superiorly. The orientation of a cylinder was defined by a direction vector, which was chosen in approximately the medial direction in this study. From this, it follows that the direction vector of TalusSF was parallel to the X-axis, pointing in the negative direction.

The orientation of TalusIF was defined by two angles (Fig. 1B,C). The inclination (α) angle was determined between the direction vector and the XY plane, and the deviation (β) angle was determined between the negative X-axis and the projection of the direction vector in the XY plane. Cylinder fitting and determination of the angles were

processed with custom made routines in Matlab (MATLAB Release 2019a, The MathWorks, Inc., Natick, MA).

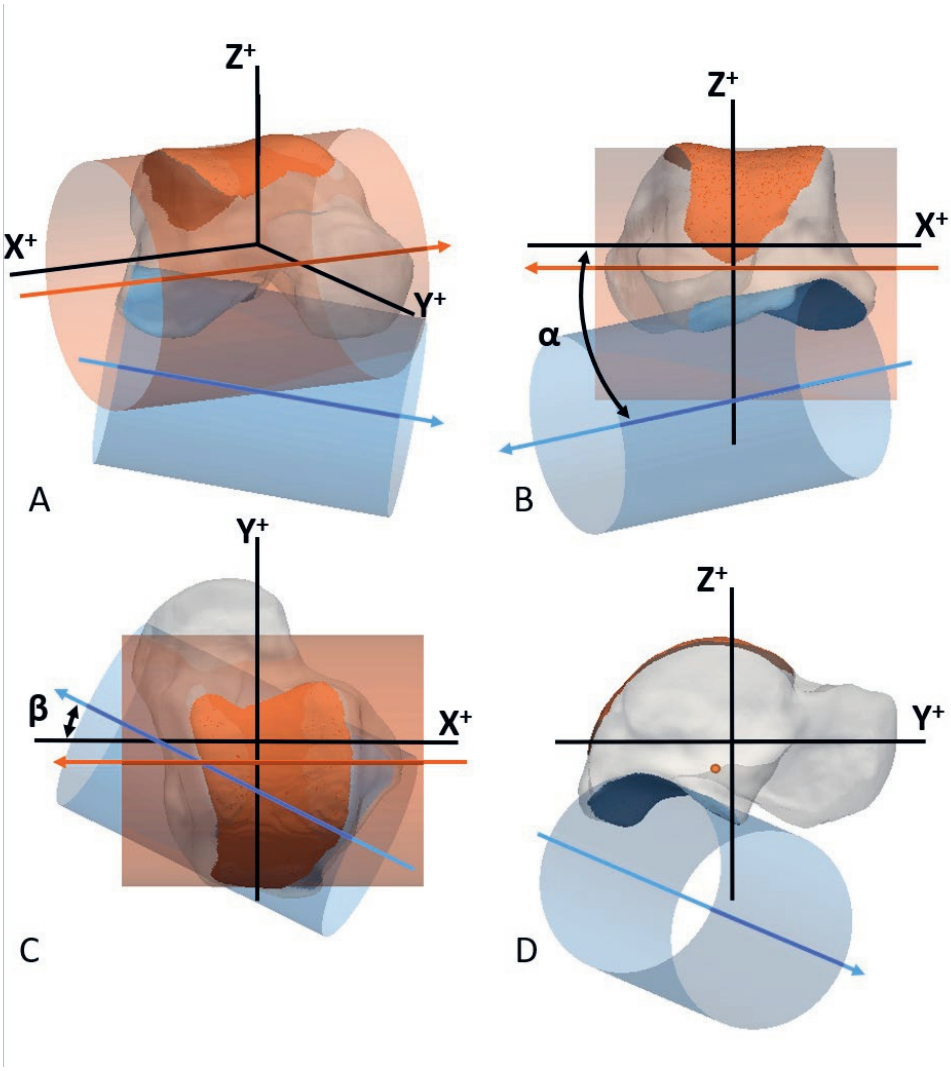

Figure 1. Graphical representation of the talus (transparent), the superior talar facet (orange, TalusSF), and posteroinferior talar facet (blue, TalusIF) in A: anterolateral view; B: posterior view; C: superior view; D: lateral view. The facets were modelled as (segments of) cylinders (transparent in matching colors) by fitting these cylinders to the articulating surfaces. The arrows (in matching color) represent the direction of the axes of the cylinders. The orientation of the TalusIF is represented by the orientation of its cylinder axis in a local coordinate system, and is expressed by an inclination angle (α in figure B) and a deviation angle (β in figure C) (see text for further details). The positive X-axis is directed laterally, the positive Y-axis is directed anteriorly, and the positive Z-axis is directed proximally.

Intra- and inter-observer analysis

The intra-observer reliability in cylinder orientation and radius, introduced by manual selection of the facet surfaces, was evaluated using three randomly chosen feet; one per study cohort. Surface selection was done three times with at least one week in between. Inter-observer reliability was evaluated based on manual selection of the facet surfaces by two observers (RPK and JD; both researchers have several years of experience in segmentation and 3D software) of nine randomly selected hindfeet (three from the CAI group and six from the control group). The two observers were blinded to each other's selections.

Statistical analyses

The orientation angles of TalusIF, the radii of the cylindrical fits, and the root mean square errors were analyzed for normal distribution with the Shapiro–Wilk test. For normally distributed data, outliers were identified as exceeding the value of three times the standard deviation from the mean. For non-normally distributed data, outliers were identified as exceeding the value of 1.5 times the interquartile range from the median. An outlier in one of the orientation angles was removed from further analyses for both angles. An outlier in the root mean square error or radius of a cylinder facet was removed from further analyses for that facet. The differences between the control group and the CAI group were tested with an independent Student t-test in case of normally distributed data and with a Mann-Whitney U test for non-normally distributed data. The Hegdes' g-value for effect size was calculated. The Hedges' g-value was interpreted as small effect (closest to 0.2); medium effect (closest to 0.5); or large effect (closest to 0.8)(24).

The intraclass correlation coefficient (ICC) was calculated as a measure of intra- and inter-observer reliability. The ICC was interpreted as poor (≤ 0.40); moderate (0.40 - 0.75); substantial (0.75 – 0.90); or excellent reliability (>0.90) (25).

The statistical analyses were performed with SPSS (IBM SPSS Statistics for Windows, Version 26.0. Released 2019. IBM Corp. Armonk, NY: IBM Corp). A significance level of 0.05 was used for all tests. Data is presented as mean ± 1 standard deviation (SD) for normally distributed data and as median (interquartile range) for non-normally distributed data.

Results

Facet orientation

The orientation angles were normally distributed. One outlier was identified in the inclination angle in the CAI group, and one outlier was identified in the deviation angle in the control group. The orientation of TalusIF was in an antero-medial-plantar direction. The inclination angle of TalusIF was statistically significantly more plantarly orientated in the CAI group (14.7 ± 3.1 degrees, n=11) compared to the control group (11.2 ± 4.9 degrees, n=39), with a large effect size, t(26) = -2.85, $p = 0.008$, g = 0.76, with a mean difference of 3.5 degrees (Fig. 2). Levene's test indicated unequal variances (F = 4.3, $p = 0.043$), that is, degrees of freedom were adjusted from 48 to 26. The deviation angle of TalusIF was not statistically significantly different between the CAI (29.5 ± 6.3 degrees, n=11) and the control group (31.8 ± 5.7, n=39), t(48) = 1.12, $p = 0.263$.

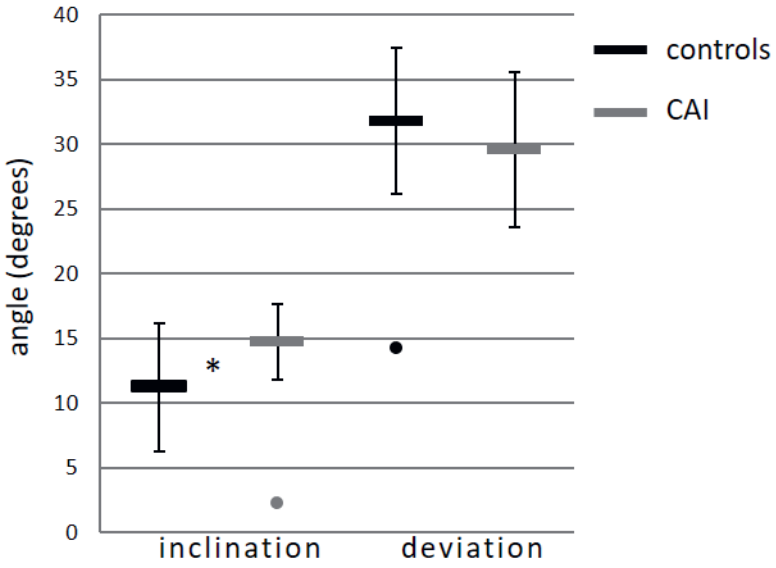

Figure 2. Inclination and deviation angle (mean and standard deviation) of the posteroinferior talar facet (TalusIF) of the control group and the chronic ankle instability group (CAI). The dots indicate outliers (>3 times the standard deviation from the mean value). The asterisk indicates a statistical significant difference between the two groups ($p = 0.008$).

Cylinder radius

The cylinder radii were normally distributed. One outlier was identified for TalusSF in the control group, and one outlier in the CAI group for the root mean square error. The cylinder radii of TalusSF were not statistically significantly different between the CAI (22.2 ± 2.2 mm, n=11) and the control group (21.5 ± 1.8 mm, n=39), t(48) = -1.06, $p = 0.249$ (Fig. 3). In the root mean square error of TalusIF of the CAI group one outlier was identified, and one in the control group. Also, for the cylinder radii of TalusIF, no statistical significant differences were demonstrated between the CAI group (19.2 ± 1.8 mm, n=11) and the control group (20.5 ± 2.9 mm, n=39), t(26)=1.40, $p = 0.084$. For TalusIF, Levene's test indicated unequal variances (F = 4.3, $p = 0.044$). Therefore, degrees of freedom were adjusted from 50 to 26.

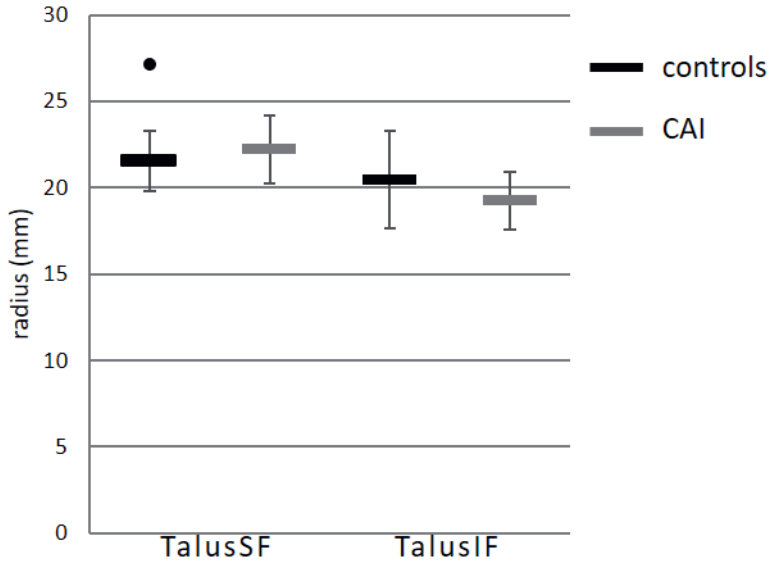

Figure 3. Cylinder radii (mean and standard deviation) of the superior talar facet (TalusSF) and the posteroinferior talar facet (TalusIF). The dot indicates an outliers (>3 times the standard deviation from the mean value).

Root mean square errors fits

The root mean square errors of the cylinder fit were normally distributed, except for TalusIF in the CAI group. After removal of this outlier, the remaining data were normally distributed. The root mean square errors of TalusSF were not statistically significantly different between the CAI (0.45 ± 0.09 mm, n=11) and the control group (0.41 ± 0.09, n=39), t(48) = -1.14, *p = 0.259*. The root mean square errors of TalusIF were not statistically significantly different between the CAI (0.39 ± 0.06 mm, n=11) and the control group (0.43 ± 0.11, n=39), t(48) = 1.22, *p = 0.228*.

Intra-observer and inter-observer analyses

The intra- and inter-observer reliability showed excellent reliability for each of the outcome measurements (Table 2). The differences in the intra-observer measurements were smaller than the inter-observer measurements. The largest differences were found in deviation angle of TalusIF.

Table 2. Intraclass correlations coefficients (ICC) and the 95% confidence interval for the intra-observer analysis and inter-observer measurement. Also, the average ± 1 SD and range (minimal - maximal) of the absolute differences are presented for the intra- and inter-observations.

	Intra-observer (n = 9)			Inter-observer (n = 9)		
Outcome measure	**ICC**	**95% confidence interval**	**Absolute difference**	**ICC**	**95% confidence interval**	**Absolute difference**
Inclination angle TalusIF	0.994	0.944 – 1	0.46 ± 0.39 (0.05-1.28)	0.989	0.953 – 0.998	0.71 ± 0.85 (0.04-2.18)
Deviation angle TalusIF	0.981	0.821 – 1	0.48 ± 0.36 (0.05-1.03)	0.988	0.949 – 0.997	1.27 ± 1.07 (0.24-3.08)
Radius TalusSF	0.969	0.792 – 0.999	0.08 ± 0.05 (0.03-0.17)	0.977	0.828 – 0.990	0.29 ± 0.19 (0.03-0.59)
Radius TalusIF	0.994	0.952 – 1	0.25 ± 0.17 (0.00-0.59)	0.985	0.932 – 0.996	0.49 ± 0.36 (0.06-1.12)

TalusSF: cylinder of superior facet of the talus. TalusIF: cylinder of posteroinferior facet of the talus. Absolute differences angles in degrees, and radius in mm.

Discussion

The present study investigated the orientation and curvature of the superior and posteroinferior talar articulating surfaces of non-symptomatic individuals and of patients with chronic ankle instability. Previous reports have identified a varus hindfoot deformity to be a risk factor in the development of CAI after a first ankle sprain (4–11). Since both the talocrural and subtalar level can be involved in CAI (2), the present study assessed the talar morphology as this bone is the key player between both joint levels.

The most important finding was that the mean inclination angle of the cylinder's axis of the posteroinferior talar facet was statistically significantly more plantarly orientated, by 3.5 degrees, in the CAI group compared to the control group. In a coronal plane this corresponds to a talus with a slight valgus of the posteroinferior facet relative to the talar dome (Fig. 4).

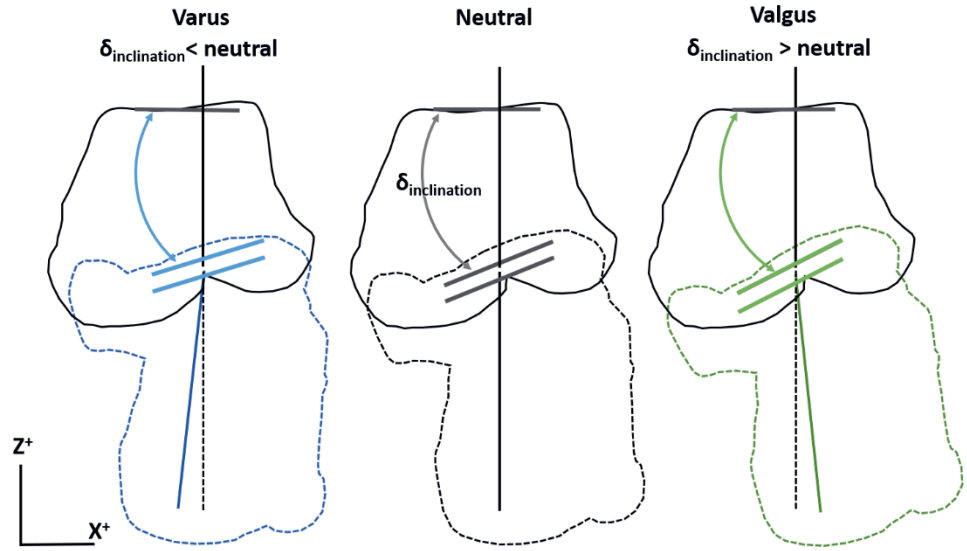

Figure 4. Schematic contour drawing of the talus and calcaneus from a posterior view (same view as in Figure 1B) for three hypothetical inclination angles of the posteroinferior talar facet. In each alignment the orientation of three facets is represented by three short lines: the upper for the superior talar facet, the middle for the posteroinferior talar facet, and the lower for the posterior calcaneal facet. The superior talar orientation is identical between the three alignments. The lower two are parallel and different between the three alignments. The upper and lower vertical lines represent the coronal alignment of the talus and calcaneus, respectively. A larger inclination angle of the posteroinferior talar facet places the calcaneus in a valgus position relative to the talus, and a lower inclination angle places the calcaneus in a varus position.

We expected to find a varus orientation of the subtalar joint in patients with CAI when comparing them to the healthy population. This would have been in accordance with earlier studies who found a correlation between varus malalignment and CAI (4,5,9). In our cohort, however, patients with CAI were found to have a subtalar joint in a slight valgus orientation. These findings are in line with a recent hypothesis from Tümer et al., who found that the calcaneus in patients with CAI creates a higher valgus-directed moment due to particular calcaneal bony shapes present in these patients (12). Patients with CAI may reduce the valgus-directed moment and an unwanted medial shift of the ground reaction force by actively creating a varus-directed moment, that results in a lateral ankle sprain if not timely countered at foot landing. Our results indicate that the posteroinferior talar facet places the calcaneus in valgus position relative to the talus, and this could also be actively compensated by a varus-directed moment (7,13).

The clinical impact of these finding remains uncertain. The literature on CAI in patients with tibia or hindfoot varus alignment shows that they benefit from realignment osteotomies to avoid ligament reconstruction failure caused by the mechanical malalignment (26,27). Corrections of any malalignment, however, should be planned at the level of the center of rotation of angulation (CORA). The offset of the calcaneus in relation to the tibia in ankle malalignment can surgically be corrected with a corrective osteotomy of the distal tibia or the calcaneus and with a corrective subtalar joint fusion. Knowledge of the orientation of the ankle and the subtalar joint in the preoperative planning therefore may improve the surgical outcome. Also, in planning a joint replacement, a sound knowledge of the joint morphology is needed with consideration of the interrelationship of both joint levels (28).

No statistically significant differences were demonstrated between the groups for the radii nor root mean square errors of the cylinder fits. The root mean square error indicates how well the facets fit to a cylinder. These results imply that the morphology of the two facets was comparable between the two study groups. Frigg et al. demonstrated an inverse relationship between the curvature of the talar dome and the stability of the ankle joint (14). This larger curvature alone cannot explain a more instable joint configuration. The coverage of the tibial surface is also important. The most instable joint configuration would be a combination of a small tibial coverage and a large curvature (14). We did not examine the tibial coverage. In both our groups, the average radius of the talar dome was larger compared to the corresponding group of Frigg et al. The most comparable values were found in the CAI group (control group 21.5 ± 1.8 mm and 17.7 ± 1.9 mm, and CAI group 22.2 ± 2.1 mm and 21.2 ± 2.4 mm for our study and Frigg et al. respectively). Our 3D surface fit possibly results in a larger radius than the 2D radiographically determined radius (14). Another explanation is that

in our study groups we had a larger percentage of male subject that resulted in the larger average radius.

The present study focused on the bony morphology of the talus as a possible risk factor for CAI. Caution is required when interpreting the results of this one factor, namely the bony morphology, when in fact CAI is multi-factorial (2). There is an overlap in individuals with and without CAI (Figs. 2 and 3). Subjects that served as controls may in the future acquire CAI. These could be the individuals that also have slightly more valgus in the talus, but that does not have to be the case. Similarly, there were patients in our CAI group who did not have this slight valgus in the talus. Other causes for developing CAI were probably of influence.

It is important to realize that the overall hindfoot alignment could still be varus, but that in our analysis of an isolated talus at the joint levels this could not be demonstrated. The patients could have an overall hindfoot varus alignment when the medial distal tibial angle (MDTA) (29) is more in varus than the subtalar joint is in valgus. However, we did not assess the relationship of the superior facet of the talus with the longitudinal axis of the tibia or other measures for the alignment. Other reasons could come from differences in 3D versus 2D measurements. Previous reports on the orientation of the two joint levels used coronal planes of CT imaging (4,16). However, the posteroinferior talar surface is located more posteriorly than the superior talar surface. Because of this, a coronal plane at for example the center of the superior facet crosses the posteroinferior facet at the anterior edges (16,30). Furthermore, because of the oblique orientation in all anatomical planes of the posterior subtalar joint, the angle of the joint is dependent on the chosen antero-posterior location of the coronal plane (18). These observations of the 3D morphology need further exploration and raise the question whether the 2D analyses are adequate to grasp the complex 3D morphology.

This study has several limitations other than not assessing the hindfoot alignment. The true articulating cartilaginous surfaces cannot be seen in CT images, and as such only the subchondral surfaces were analyzed. Non-homogeneous thickness distribution of the cartilage may shift the cylinder. This could be addressed in a study that uses Magnetic Resonance Imaging. Further, only 12 CAI patients were included. After removal statistical outliers, this was further reduced. Future research could include more patients with CAI.

Up to today, the mechanics of the subtalar joint are not fully elucidated.. Different in vivo, ex vivo, and modelling studies have given more insight into the kinematics of the subtalar joints (28). How our cylinder models reflect in the kinematics of the hindfoot is not clear. The axis of rotation of the subtalar joint does not correspond with what can be predicted from our cylinder model of the posterior subtalar joint (28). The subtalar joints comprise of more than only the posterior articulating surfaces. The whole subtalar

joint is more complex. Our method could be used in determining the 3D orientations of the hindfoot bones, and does not reflect the full complex subtalar joint morphology.

The strength of this present study was that the interrelationship of the superior and posteroinferior talar facets could be determined in 3D without influence of the position of the foot in the CT scanner. The applied method for selecting the articular surface on 3D surface models proved to be very reliable based on the results of the intra- and inter-observer analyses, but was laborious. A (semi-) automatic procedure can make this step more efficient in the future.

The present study provides a next step in identifying morphology of bony structures in the hindfoot being associated with CAI. It is the first study that analyzed the interrelationship of the talocrural and subtalar joints in 3D. Future studies should focus on a method to determine the orientation at each joint level in the chain from the knee to the ground in 3D with a golden standard for a frame of reference, preferably in a weight bearing condition.

In conclusion, it was found that the morphology of the talus itself does not necessarily need to be in "varus" to contribute to CAI. It was demonstrated that CAI patients have a more valgus position of the posteroinferior talar facet that may be a risk factor for CAI by varus compensation. The relationship between the superior and posteroinferior facets of the talus in relation to the lower leg axis in varus and valgus deformities , the overall alignment, needs further research.

References

1. Vuurberg G, Hoorntje A, Wink LM, van der Doelen BFW, van den Bekerom MP, Dekker R, et al. Diagnosis, treatment and prevention of ankle sprains: update of an evidence-based clinical guideline. Br J Sports Med. 2018 Aug;52(15):956.
2. Kobayashi T, Gamada K. Lateral Ankle Sprain and Chronic Ankle Instability: A Critical Review. Vol. 7, Foot & ankle specialist. United States; 2014. p. 298–326.
3. Hertel J. Functional Anatomy, Pathomechanics, and Pathophysiology of Lateral Ankle Instability. J Athl Train. 2002 Dec;37(4):364–75.
4. Van Bergeyk AB, Younger A, Carson B. CT analysis of hindfoot alignment in chronic lateral ankle instability. Foot ankle Int. 2002 Jan;23(1):37–42.
5. Strauss JE, Forsberg JA, Lippert FG 3rd. Chronic lateral ankle instability and associated conditions: a rationale for treatment. Foot ankle Int. 2007 Oct;28(10):1041–4.
6. Bonnel F, Teissier P, Maestro M, Ferre B, Toullec E. Biometry of bone components in the talonavicular joint: a cadaver study. Orthop Traumatol Surg Res. 2011 Oct;97(6 Suppl):S66-73.
7. Sangeorzan A, Sangeorzan B. Subtalar Joint Biomechanics: From Normal to Pathologic. Foot Ankle Clin. 2018 Sep;23(3):341–52.
8. Vuurberg G, Wink LM, Blankevoort L, Haverkamp D, Hemke R, Jens S, et al. A risk assessment model for chronic ankle instability: indications for early surgical treatment? An observational prospective cohort - study protocol. BMC Musculoskelet Disord. 2018 Jul;19(1):225.
9. Lintz F, Bernasconi A, Baschet L, Fernando C, Mehdi N, de Cesar Netto C. Relationship Between Chronic Lateral Ankle Instability and Hindfoot Varus Using Weight-Bearing Cone Beam Computed Tomography. Foot ankle Int. 2019 Oct;40(10):1175–81.
10. Sugimoto K, Samoto N, Takakura Y, Tamai S. Varus tilt of the tibial plafond as a factor in chronic ligament instability of the ankle. Foot ankle Int. 1997 Jul;18(7):402–5.
11. Scranton PEJ, McDermott JE, Rogers J V. The relationship between chronic ankle instability and variations in mortise anatomy and impingement spurs. Foot ankle Int. 2000 Aug;21(8):657–64.
12. Tumer N, Vuurberg G, Blankevoort L, Kerkhoffs GMMJ, Tuijthof GJM, Zadpoor AA. Typical Shape Differences in the Subtalar Joint Bones Between Subjects with Chronic Ankle Instability and Controls. J Orthop Res. 2019 Sep;37(9):1892–902.
13. Hayashi K, Tanaka Y, Kumai T, Sugimoto K, Takakura Y. Correlation of compensatory alignment of the subtalar joint to the progression of primary osteoarthritis of the ankle. Foot ankle Int. 2008 Apr;29(4):400–6.
14. Frigg A, Magerkurth O, Valderrabano V, Ledermann H-P, Hintermann B. The effect of osseous ankle configuration on chronic ankle instability. Br J Sports Med. 2007 Jul;41(7):420–4.
15. Probasco W, Haleem AM, Yu J, Sangeorzan BJ, Deland JT, Ellis SJ. Assessment of coronal plane subtalar joint alignment in peritalar subluxation via weight-bearing multiplanar imaging. Foot ankle Int. 2015 Mar;36(3):302–9.
16. Krähenbühl N, Tschuck M, Bolliger L, Hintermann B, Knupp M. Orientation of the Subtalar Joint: Measurement and Reliability Using Weightbearing CT Scans. Foot ankle Int. 2016 Jan;37(1):109–14.
17. Colin F, Horn Lang T, Zwicky L, Hintermann B, Knupp M. Subtalar joint configuration on

weightbearing CT scan. Foot ankle Int. 2014 Oct;35(10):1057–62.
18. Kleipool RP, Dahmen J, Vuurberg G, Oostra R-J, Blankevoort L, Knupp M, et al. Study on the three-dimensional orientation of the posterior facet of the subtalar joint using simulated weight-bearing CT. J Orthop Res. 2019 Jan;37(1):197–204.
19. Beimers L, Tuijthof GJM, Blankevoort L, Jonges R, Maas M, van Dijk CN. In-vivo range of motion of the subtalar joint using computed tomography. J Biomech. 2008;41(7):1390–7.
20. Kleipool RP, Natenstedt JJ, Streekstra GJ, Dobbe JGG, Gerards RM, Blankevoort L, et al. The Mechanical Functionality of the EXO-L Ankle Brace: Assessment With a 3-Dimensional Computed Tomography Stress Test. Am J Sports Med. 2016 Jan;44(1):171–6.
21. Dobbe JGG, Roo MGA de, Visschers JC, Strackee SD, Streekstra GJ. Evaluation of a Quantitative Method for Carpal Motion Analysis Using Clinical 3-D and 4-D CT Protocols. IEEE Trans Med Imaging. 2019;38(4):1048–57.
22. Colman KL, Dobbe JGG, Stull KE, Ruijter JM, Oostra R-J, van Rijn RR, et al. The geometrical precision of virtual bone models derived from clinical computed tomography data for forensic anthropology. Int J Legal Med. 2017 Jul;131(4):1155–63.
23. Dukes KA. Gram–Schmidt Process. In: Wiley StatsRef: Statistics Reference Online [Internet]. American Cancer Society; 2014. Available from: https://onlinelibrary.wiley.com/doi/abs/10.1002/9781118445112.stat05633
24. Cohen J. Statistical power analysis for the behavioral sciences. 2nd ed. Hillside: Lawrence Erlbaum Associates; 1988.
25. Terwee CB, Bot SDM, de Boer MR, van der Windt DAWM, Knol DL, Dekker J, et al. Quality criteria were proposed for measurement properties of health status questionnaires. J Clin Epidemiol. 2007 Jan;60(1):34–42.
26. Colville MR, Marder RA, Boyle JJ, Zarins B. Strain measurement in lateral ankle ligaments. Am J Sports Med. 1990;18(2):196–200.
27. Tourné Y, Mabit C. Lateral ligament reconstruction procedures for the ankle. Orthop Traumatol Surg Res. 2017 Feb;103(1S):S171–81.
28. Pena Fernandez M, Hoxha D, Chan O, Mordecai S, Blunn GW, Tozzi G, et al. Centre of Rotation of the Human Subtalar Joint Using Weight-Bearing Clinical Computed Tomography. Sci Rep. 2020 Jan;10(1):1035.
29. Stufkens SA, Barg A, Bolliger L, Stucinskas J, Knupp M, Hintermann B. Measurement of the medial distal tibial angle. Foot ankle Int. 2011 Mar;32(3):288–93.
30. Cody EA, Williamson ER, Burket JC, Deland JT, Ellis SJ. Correlation of Talar Anatomy and Subtalar Joint Alignment on Weightbearing Computed Tomography With Radiographic Flatfoot Parameters. Foot ankle Int. 2016 Aug;37(8):874–81.

Chapter 7

Bilateral symmetry of the subtalar joint facets and the relationship between the morphology and osteoarthritic changes

Roeland P. Kleipool
Gwendolyn Vuurberg
Sjoerd A.S. Stufkens
Alie E. van der Merwe
Roelof-Jan Oostra

Clin Anat. 2019 Nov 21.
doi: 10.1002/ca.23525

'stand on your own two feet'
Cambrigde dictionary: to be able to provide all of the things you need for living without help from anyone else

Abstract

There is a paucity in the literature regarding bilateral symmetry between the facets of the subtalar joint. Often surgeons use the contralateral side as a reference when dealing with a fracture or other joint pathology. Moreover, the presence of osteoarthritic (OA) changes in the subtalar joint is suggested to have a relation with its morphology. In this study, we addressed both these issues. Forty pairs of cadaveric tali and calcanei were analyzed by dissection and measurement. Twenty pairs of asymptomatic calcanei were morphologically analyzed by computer tomography imaging. In the cadaveric feet, the length and width of the facets, the number and interfacet connections, the intersection angle, and the presence of OA changes were registered. In the healthy feet, the orientation and curvature of the posterior facet were analyzed based on cylinder fittings. Bilateral symmetry was tested with paired Student's t tests. Significant associations between morphometric parameters and the presence of OA changes were tested with generalized estimating equation logistic regression models. The morphometric data demonstrated a high degree of bilateral symmetry. The types of tali and calcanei between left and right differed in about one-fifth of the individuals. No significant interactions were found between morphological parameters and the presence of OA changes. Only age had a significant association. There was a high degree of symmetry in the subtalar joints facets. No significant associations were found between OA changes and morphological features, whereas other studies did. Further research is needed to explore this relationship in further detail.

Introduction

In most classical anatomy textbooks, the talocalcaneal joint has three distinct articulating facets. However, it has been well documented that inter-individual variation exists in the number, the distance, between angle and connections, and the size of the articulating joint facets (1–8). Despite the known variation only two studies analyzed the degree of bilateral symmetry of the facet joints: one describing the pattern of calcaneal facets (5), and another one describing the surface area and three-dimensional (3D) orientation of the calcaneal facets (9). In general, literature describing the bilateral symmetry of the hindfoot is scarce (10–12). This is remarkable since many surgeons use the contralateral noninjured side as reference for anatomical reduction in case of a fractured bone (13–16). Even less literature is available describing the symmetry of the articulating facets. This is possibly even more important, since the geometry of the articular surfaces primarily determines the kinematics (17). The first objective of the present study was therefore to evaluate and describe the degree of bilateral symmetry present in the pattern and size of articulation facets involved in the talocalcaneal joint.

Although often overlooked in clinical practice, the talocalcaneal joint has also been hypothesized to play a role in multiple ankle pathologies, such as planovalgus and cavovarus deformity, coalitions, chronic ankle instability, and so on (18). The morphology of the joint forms a major component in the joint's stability (19). Bruckner was the first to hypothesize that a "three-facet" configuration contributes to a greater talocalcaneal stability, as the talus is supported by an "osseous tripod" (1). Drayer-Verhagen and Madhavi et al. confirmed this by showing less osteoarthritic (OA) changes associated with the "three-facet" configuration (3,6). Not only the number of facets, but also the angle of the anterior and middle facets in a sagittal plane (intersection angle) has been related to OA changes (3,8). The aforementioned studies only focused on the calcaneus and did not include the talus. A second objective of the present study was therefore to further explore the hypothesis of a relationship between the morphology of the subtalar joint facets and its stability and to evaluate the morphology as a predictive factor for developing OA.

Materials and methods

For the present study two data sets were used. The first data set was acquired for the present study, and the second comes from a previous study (20).

Bilateral symmetry

A convenience sample of a total of 40 pairs (21 male and 19 female) of cadaveric ankles of known age and sex were collected for assessment after a dissection course for first years bachelor medical students (Table 1; mean age at time of death = 79 years ± 13 SD, range 48–104 years). The material originated from the body-donation program of the Amsterdam UMC, location AMC in accordance with Dutch law article 21 of the Burial and Cremation Act (BWBR0005009) and the regulations of the medical ethical committee of the institution. Although ancestry is not recorded for donations, a survey among the donors in The Netherlands showed that up to 98% was of native Dutch origin (21). A tentative assumption can therefore be made that the sample investigated represents a Western-European population.

Table 1. Age distribution (in years) at time of death / at time of scan of all specimen / individuals included in the study, divided into 10 years age intervals.

Age	20 - 29	30 - 39	40 - 49	50 - 59	60 - 69	70 - 79	80 - 89	90 - 99	100 - 109
Cadaveric specimen			1	1	7	11	10	9	1
Living individuals	6	9	2	3					

The hindfoot was isolated from the body by a transverse section through the leg approximately 10 cm proximal from the medial malleolus. Next, the subtalar joint was opened at the lateral side and unfolded to the medial side. Hereto, a deep incision was made from the dorsomedial side of the foot at the level of the talonavicular joint to the inferior tip of the lateral malleolus and from here through the Achilles tendon. The lateral tendons, ligaments, and joint capsules were cut, including the connections in the tarsal sinus and canal. Subsequently, the subtalar joint could be opened with relative ease.

Many classifications for the different patterns of the talar and calcaneal facets are found in the literature. In the present study, the classification of Jung et al. was used (Fig. 1) (7).

- Type A: All three facets are separated.
- Type B: The posterior facet is separated from the middle, but the middle is connected to the anterior facet by a small bridge. At this constriction between the middle and anterior facets is a slope discontinuity or an obvious angle.
- Type C: The posterior facet is separated, but the anterior and middle form one facet. The single facet has a smooth, rounded surface with a slight convexity at the talar head and a slight concavity in the calcaneus.

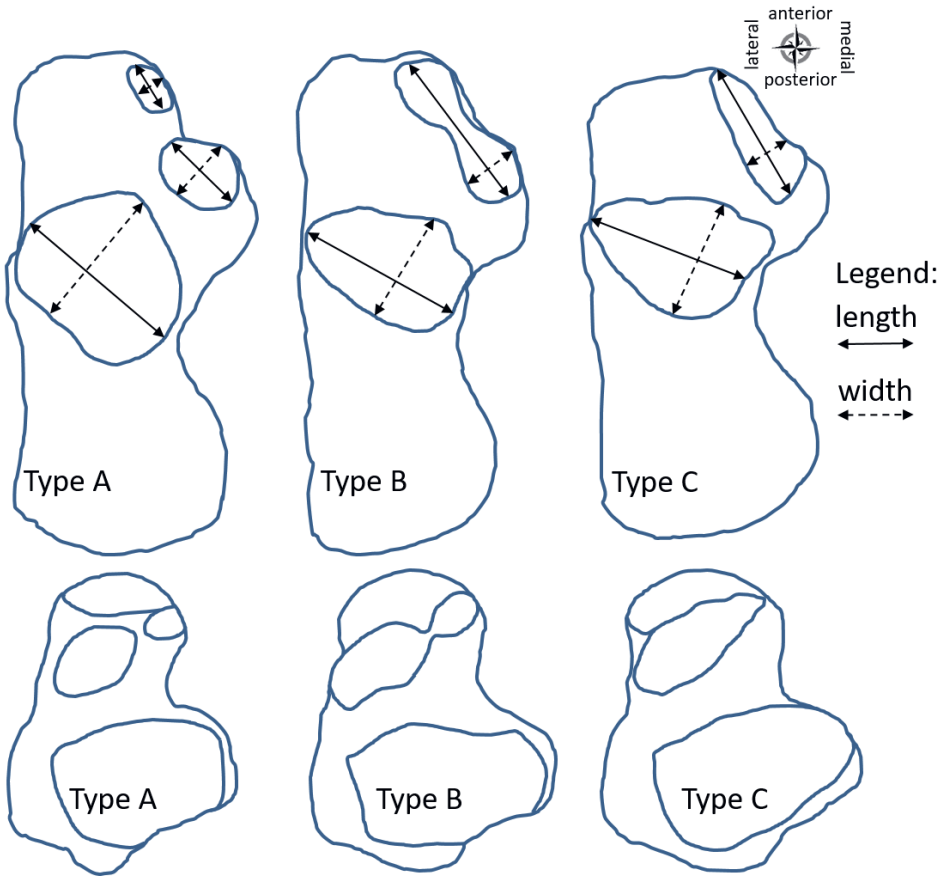

Figure 1. Contour drawings of the different types of calcanei and tali based on the number and connections of the facets. Type A: All three facets are separated. Type B: The posterior facet is separated from the middle, but the middle is connected to the anterior facet by a small bridge. Type C: The posterior facet is separated, but the anterior and middle facets form one facet. Calcaneus drawn from a superior view. Talus drawn from an inferior view. The length and the width of the facets were measured as illustrated with the bidirectional arrows (length: solid line; width: dashed line).

Two other types, a variant where the anterior facet is absent and one where all facets are connected, were not found in this study sample and therefore not included (1,3,22). The classification system described above facilitates comparison of the results of the present study with the results of Drayer-Verhagen and Madhavi et al. (3,6).

Two independent observers assessed the pattern of the calcaneal and talar facets. If the two observers disagreed the observation of Observer 1 was included in further analyses. This was arbitrarily chosen. Also, both observers performed the following

morphometric measurements of the calcaneus with a sliding Vernier caliper, accurate to 0.1 mm. The length of the posterior, middle, and anterior facets was measured in an anterolateral to posteromedial direction along the long axis of the facets. The width was measured perpendicular to this long axis (Fig. 1). In case of a Type B or C the total length of the whole (fused) facet was measured and the width perpendicular to this line at the widest location. The minimal distance between the posterior and middle (in Type A) or fused middle and anterior facets (in Type B or C) was measured in all calcanei, and between the anterior and middle only in Type A calcanei.

Next, the osseous calcanei were isolated by maceration in hot water with common household dish soap for several days. The remaining soft tissue, including the cartilage, was scrubbed off from the calcanei.

The intersection angle between the anterior and middle facets was determined by placing the macerated calcaneus on its medial side on a piece of paper (3,7,8). The medial border of the sustentaculum tali facets contacted the paper, and the planes of the facets were manually orientated perpendicular to the surface of the paper. The contour of the facets was traced with a pencil. Subsequently, the image was digitized by photoscanning the paper and the intersection angle was accordingly measured on the digital image using the angle measurement tool of the imaging software ImageJ (U.S. National Institutes of Health, Bethesda, MD).

As mentioned in the beginning of this section, data from a previous study on living individuals were also included (20) to account for the 3D morphology of the posterior facet compared to measurements taken with a sliding caliper in the cadaveric specimens. In the previous study (approved by the Amsterdam UMC, location AMC Internal Review Board, registration number NL60684.018.17), 20 (10 male and 10 female) left and right healthy and non-symptomatic calcanei were segmented from computer tomography (CT) scans with custom made software (Dobbe et al., 2011; average age at time of scan = 35.9 years ± 11.1 SD, range 23–59 years, Table 1). The surface of the posterior facet was identified and isolated from the acquired surface model of the whole calcaneus. All left calcanei and facets were mirrored to right calcanei and facets for a corresponding orientation. With custom-made routines in Matlab (MATLAB Release 2016a, The MathWorks, Inc., Natick, MA) a cylinder was fitted to the posterior facet using a nonlinear least-squares optimization process with the axis in a predominantly transverse orientation. The orientation of the cylinder's axis was
expressed by two angles in reference to a coordinate system based on the geometric principal axes of the subject's calcaneus (Fig. 2). The inclination angle was defined as the angle between the cylinder's axis and the XY-plane. The deviation angle was defined as the angle between the projection of the cylinder's axis on the XY-plane and the Y-axis, or the sagittal plane. A negative inclination angle corresponds to an inferiorly or

plantarly orientated axis. A negative deviation angle corresponds to a medially orientated axis (Fig. 2). Also the diameter of the cylinder fit was determined as a measure for the curvature of the posterior facet. For further details, see Kleipool et al. (20).

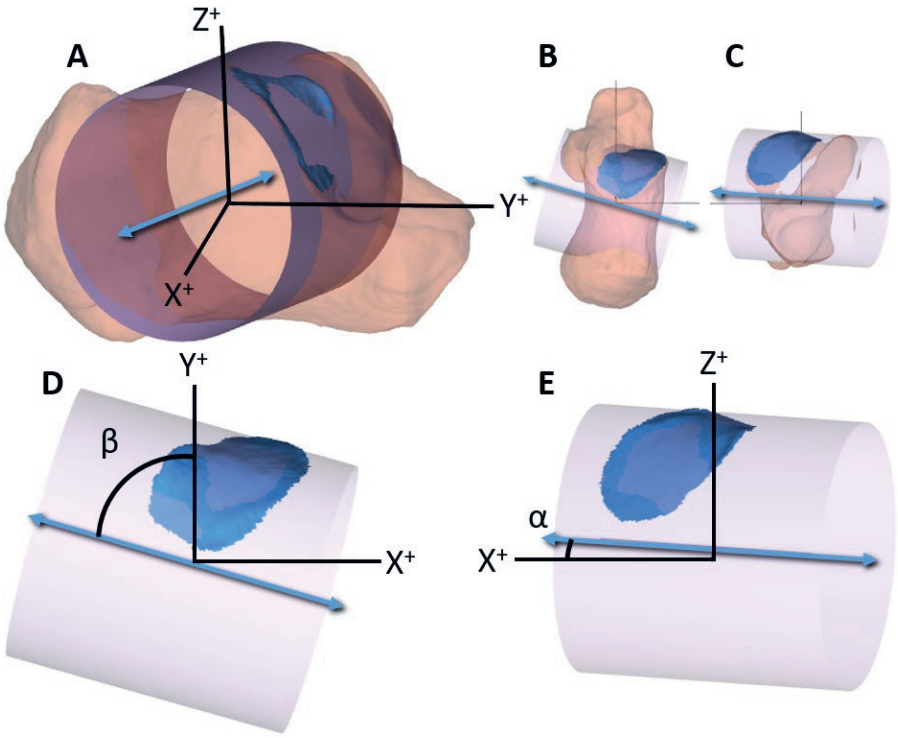

Figure 2. Graphical representation of a surface model of a right calcaneus (brown) and the posterior calcaneal facet of the talocalcaneal joint (in blue). A cylinder was fitted to the posterior facet (pink). The orientation of the cylinder's axis (blue bidirectional arrow) was defined by the inclination angle (alpha) and the deviation angle (beta). a, Anterolateral view; b, superior view; c, anterior view; d, magnification of the same superior view as in b without the calcaneus; and e, magnification of the same anterior view as in c without the calcaneus.

Osteoarthritic changes

After opening the subtalar joint of the cadaveric specimen by dissection of the intact specimen, prior to removal of the soft tissue by maceration, the presence of OA changes was scored on both the talar and the calcaneal facets by one observer (orthopedic researcher). This was performed with the unaided eye. OA changes were scored as absent/present regardless of the severity of the defects. The location of defects was

recorded as posterior, middle, or anterior (also in calcanei B and C) regardless of the facet configuration.

Statistics

The intraclass correlation coefficient (ICC) was calculated as a measure of interobserver reliability. The ICC was interpreted as poor (≤0.40), moderate (0.40–0.75), substantial (0.75–0.90), or excellent reliability (>0.90) (23).

The Stuart–Maxwell tests of marginal homogeneity were used to test for significant left–right differences for the type of bone. Morphometric differences between the left- and right-sided facets were assessed using a paired Student's t test. An analysis of variance (ANOVA) was performed to explore differences between the intersection angle of the three types. A Bonferroni post hoc analysis was performed if the ANOVA indicated a significant difference.

Generalized estimating equation (GEE) logistic regression models were made to identify the factors associated with the presence of OA changes on the calcaneus. A binomial distribution for OA changes was used with subject identifier as repeated effect and an unstructured correlation matrix. In the univariable model, significant interaction was investigated for age (per 5 years), intersection angle, type of calcaneus or talus, matching pattern between talus and calcaneus (on a binary scale; corresponding or noncorresponding type), and dimensions (length and width) of the facets.

Statistical significance was accepted at $p < 0.05$. All analyses were performed using SPSS statistical software (IBM SPSS Statistics for Windows, Version 24.0, Released 2015, IBM Corp., Armonk, NY).

Results

Left–right analyses

Facets pattern. The cadaveric calcanei and tali were classified as Types A, B, or C based on the calcaneal and talar facets pattern of connection and number (Fig. 1). Most of the specimens had the same type between the left and right sides. In total, 77.5% of the calcanei and 80% of the tali had bilateral symmetry in their type (Table 2). The remaining pairs of calcanei (22.5%) and tali (20%) had varying combinations of types between the left and right sides (Table 2). The most frequently observed asymmetry was a combination of Types A and B within individuals. The differences found between the left and right sides in type, for either the calcanei or tali, were, however, statistically nonsignificant.

Table 2. Cross tabulation of types of cadaveric calcanei and tali (type A, B, or C) based on the patterns of the calcaneal and talar facets for the left and right side.

		Right							
	Left	Type A		Type B		Type C		Total left	
Calcaneus	Type A	**22.5%**	**(9)**	5.0%	(2)	-	-	*27.5%*	*(11)*
	Type B	10.0%	(4)	**47.5%**	**(19)**	5.0%	(2)	*62.5%*	*(25)*
	Type C	-	-	-	-	**10.0%**	**(4)**	*10.0%*	*(4)*
Total right		*32.5%*	*(13)*	*52.5%*	*(21)*	*15.0%*	*(6)*	*100%*	*(40)*
Talus	Type A	**57.5%**	**(23)**	7.5%	(3)	-	-	*65.0%*	*(26)*
	Type B	7.5%	(3)	**5.0%**	**(2)**	5.0%	(2)	*17.5%*	*(7)*
	Type C	2.5%	(1)	-	-	**15.0%**	**(6)**	*17.5%*	*(7)*
Total right		*67.5%*	*(27)*	*12/5%*	*(5)*	*20.0%*	*(8)*	*100%*	*(40)*

The diagonal with bold numbers represent the corresponding classifications between the left and right side. Off diagonal numbers represent the non-corresponding classifications. Numbers presented are the percentages of the total with between the brackets the absolute number of specimen.

Metric data calcaneal facets. Both the metric assessment of the calcaneal facets as well as the curvature and orientation of the posterior facet by means of a cylinder fit to the facet's surface were assessed in the analysis of left–right symmetry. All parameters, for both data sets, showed a strong degree of symmetry between the left and right sides (Table 3). No significant differences were found between the left and right sides for all morphometrics of the calcaneal facets, except for the width of the posterior facet ($p = 0.003$, n = 40) (Table 3).

A significant difference was found in the intersection angle of the cadaveric specimens between the three calcanei types (ANOVA, F = 6.83, $p = 0.002$). Bonferroni post hoc analysis showed that intersection angle associated with Type A was significantly smaller (138.8 ± 8.5°) compared to Type C (147.2 ± 6.7°) ($p < 0.001$). A smaller angle corresponds to a steeper slope between the anterior and middle parts.

Table 3. Morphometric data of the left and right calcanei.

	N	Left		Right	
Metric assessment (cadaveric specimen)					
PF Length (in mm) [a]	40	31.7	(3.5)	32.2	(3.6)
PF Width (in mm) [a]	40	22.8*	(2.6)	23.5*	(2.8)
MF Length (in mm) [b]	23	17.6	(2.3)	18.1	(2.5)
MF Width (in mm) [b]	23	11.9	(1.4)	11.7	(1.5)
MF+AF Length (in mm) [c]	10	32.0	(3.0)	31.7	(2.7)
MF+AF Width (in mm) [c]	10	11.9	(1.1)	11.9	(1.6)
AF Length (in mm) [b]	23	11.6	(1.9)	12.1	(2.4)
AF Width (in mm) [b]	23	9.1	(1.4)	8.9	(1.5)
Distance PF-MF (in mm) [a]	40	6.6	(1.5)	6.6	(1.5)
Distance MF-AF (in mm) [b]	23	6.6	(2.1)	6.1	(2.2)
Intersection angle (in degrees) [d]	36	140.3	(8.4)	141.0	(8.5)
Cylinder fit parameters (CT data living individuals)					
Deviation angle (in degrees)[e]	20	-70.1	(5.6)	-68.6	(4.4)
Inclination angle (in degrees)[e]	20	-2.4	(6.9)	-4.1	(7.9)
Diameter (in mm)[e]	20	41.9	(7.4)	42.2	(8.2)

Numbers presented are averages (SD).
Abbreviations: AF, anterior facet; MF, middle facet; PF, posterior facet.
[a]Measured in Type A, B, and C.
[b]Measured in Type A.
[c]Measured in Types B and C.
[d]Measured after maceration of the bone.
[e]Adapted from Kleipool et al. (20)
*$p = 0.003$: significant difference between left and right sides.

Types of coupled tali and calcanei

A large number of coupled cadaveric tali and calcanei, that is, the talus and calcaneus of one side of one individual, had noncorresponding types (Table 4). The frequency of noncorresponding types between the coupled tali and calcanei was as high as 48.8%. Of these noncorresponding combinations within the coupled bones, the Type A calcaneus was most frequently coupled with a Type B talus (36.3%).

These results showed that many combinations are possible between the type of coupled tali and calcanei. The most frequently encountered combinations included calcaneus Type A and talus Type A, and the combination of calcaneus Type A with talus Type B.

Table 4. Cross tabulation of the combinations of types observed in coupled tali and calcanei (the talus and calcaneus of one side of one individual)

	Talus							
Calcaneus	Type A		Type B		Type C		Total calcaneus	
Type A	**28.8%**	**(23)**	37.5%	(30)	-	-	*66.3%*	*(53)*
Type B	1.3%	(1)	**13.8%**	**(11)**	-	-	*15.0%*	*(12)*
Type C	-	-	6.3%	(5)	**12.5%**	**(10)**	*18.8%*	*(15)*
Total Talus	*30.0%*	*(24)*	*57.5%*	*(46)*	*12.5%*	*(10)*	*100%*	*(80)*

The diagonal with bold numbers represent the corresponding classifications between the calcaneus and talus. Off diagonal numbers represent the noncorresponding classifications. Numbers presented are the percentages of the total, and the numbers in parentheses represent the absolute number of specimen.

Osteoarthritic changes

OA changes in the facets were found in 42.5% (n = 34) of the 80 cadaveric calcanei, and in 61.3% (n = 49) of the 80 cadaveric tali in the middle or anterior facet (Table 5). No OA changes were found on the posterior facet. The anterior part, on both the talus and calcaneus, was most frequently affected.

GEE only demonstrated a significant association between the presence of OA changes and age for the calcaneus (OR = 1.38 per 5 years, $p = 0.019$, 95% confidence interval 1.1–3.2). No significant associations were demonstrated between the intersection angle, type of calcaneus, length or width of each facet, or corresponding types of coupled tali and calcanei and OA changes.

Table 5. Osteoarthritic changes found in the 80 calcanei and tali, specified per location, and per type for both calcanei and tali.

	Calcaneus				Talus			
	MF		AF		MF		AF	
A	1.9%	(1)	43.4%	(23)	-	-	66.7%	(16)
B	16.7%	(2)	58.3%	(7)	2.2%	(1)	54.4%	(25)
C	-	-	20.0%	(3)	-	-	80.0%	(8)
Total	3.8%	(3)	41.3%	(33)	1.3%	(1)	61.3%	(49)

Numbers presented are the percentages of the total with between the brackets the absolute number of specimen. Abbreviations: AF = anterior facet, MF = middle facet. Number of calcaneus type A = 53; type B = 12; type C = 15. Number of talus type A = 24, type B = 46, and type C = 10.

Interobserver analyses

Types of bone. Both observers individually classified the cadaveric calcanei and tali as Types A, B, or C based on the calcaneal and talar facets pattern of connection and number (Table 6, Fig. 1). There was complete agreement between both observers in the classification of Type A calcanei. Between the other types of calcanei (Types B and C) and all types of tali (Types A–C), there were also noncorresponding classifications. These noncorresponding classifications of the patterns of the calcaneus were of Types B and C (5%, n = 4). For the 19 tali, these were of Types A and B (18.8%, n = 15), and of Types B and C (5%, n = 4), thus a total of 23.8% (n = 19).

As there were discrepancies between the observed patterns between observers, which make it difficult to present the results, the classification of Observer 1 (Table 6, most right column) was used for analyses and reports as presented earlier.

Table 6. Cross tabulation of the type (A, B, or C) of the cadaveric calcaneus and talus based on the patterns of calcaneal or talar facets classified by both observers

		Observer 2							
Observer 1		Type A		Type B		Type C		Total Observer 1	
Calcaneus	Type A	**66.3%**	**(53)**	-	-	-	-	66.3%	(53)
	Type B	-	-	**15.0%**	**(12)**	-	-	15.0%	(12)
	Type C	-	-	5.0%	(4)	**13.8%**	**(11)**	18.8%	(15)
Total Observer 2		66.3%	(53)	20.0%	(16)	13.8%	(11)	100%	(80)
Talus	Type A	**13.8%**	**(11)**	16.3%	(13)	-	-	66.3%	(24)
	Type B	2.5%	(2)	**53.3%**	**(41)**	3.8%	(3)	15.0%	(46)
	Type C	-	-	1.3%	(1)	**11.3%**	**(9)**	18.8%	(10)
Total Observer 2		66.3%	(13)	68.8%	(55)	15.0%	(12)	100%	(80)

The diagonal with bold numbers represent the corresponding classifications between the two observers. Off diagonal numbers represent the noncorresponding classifications. Numbers presented are the percentages of the total, and the numbers in parentheses represent the absolute number of specimen.

Metric data calcaneal facets. The metric assessment of the cadaveric calcaneal facets included the width and length of the posterior, middle, and anterior facets, and the shortest distances between the facets. The ICCs between the two observers for these measurements of the calcaneus ranged from substantial to excellent (ICC 0.792–0.986) (Table 7) (23).

For the analysis of the morphometric data, the mean distance of both measurements of the two observers was used.

Table 7. Intraclass correlations coefficients (ICC) and the 95% confidence interval between the two observers for measurements on the cadaveric calcaneal facets.

Measurement		ICC	95% confidence interval
Length PF	(n=80)	.965	(.940 - .978)
Width PF	(n=80)	.958	(.932 - .974)
Length MF	(n=80)	.986	(.979 - .991)
Width MF	(n=80)	.885	(.820 - .926)
Length AF	(n=53)	.910	(.833 - .950)
Width AF	(n=53)	.792	(.642 - .880)
Minimal Distance PF-MF	(n=80)	.867	(.792 - .914)
Minimal Distance MF-PF	(n=53)	.940	(.896 - .965)

Abbreviations: AF, anterior facet; MF, middle facet; PF, posterior facet.

Discussion

This study assessed the bilateral symmetry of the subtalar articular joint facets and sought to find a (significant) relationship between the morphology and OA changes.

Bilateral symmetry

Overall, the results demonstrated that the articular facets in pattern, length, and width, and for the posterior facet also in orientation and curvature, are highly symmetrical. However, about one-fifth of the individuals had a left–right asymmetry in the type of bone and a significant difference was found for the width of the posterior facet between left and right. Unfortunately, we do not have information about the laterality preference of the subjects to correlate these results. In a previous study, with a very high number of archeological calcanei, a frequency of left–right asymmetry in type of 10% was reported (5). No literature is available for the symmetry of the type of talus.

The high degree of symmetry is in line with earlier studies that have demonstrated a high degree of symmetry in the lower extremity (24). Specifically for the hindfoot, a strong degree of symmetry was demonstrated for the whole talus (11), the calcaneus (9) and tibia, fibula, talus, and calcaneus (12). A clear cause for the asymmetry in type of the left and right tali or calcanei presented here and in Ragab et al. is not at hand for now (5). Bunning and Barnett for the calcaneus and Rehman for the talus concluded that the patterns are probably genetically determined and are not developmental responses to walking habits, physique of a person, or duration of weight bearing in postnatal life (22,25). Rehman's results show that in the late fetal period already left–right differences are present in tali (25). The asymmetry could be a variation of the symmetrical nature of the embryologic body plan (26) and thus genetically driven, but possibly small environmental in utero differences, such as oligohydramnios or breech presentation, earlier in development might have caused the asymmetry. Be that as it may, this occurrence of asymmetry has to be taken into account by surgeons that use the contralateral noninjured side as a reference.

Osteoarthritic changes and morphology

In the second part of this study, several morphological parameters were investigated to assess a possible relationship with the presence of OA changes. The congruency and stability of the joint are important determining factors in developing OA (27). The first parameter that was investigated was the type of calcaneus as Bruckner hypothesized that a three-facet configuration (Type A) is more stable than a two-facet configuration (Type B or C) (1). This was confirmed by two subsequent studies that reported a

significant higher frequency of OA changes in specimen with two facets (Type B or C) compared to specimens with three facets (Type A) (3,6). However, the reported frequencies of specimens with OA changes between these two studies and the present study differ greatly (Table 8).

Table 8. Frequencies of osteoarthritic changes as observed per type of calcaneus in two other studies and in the present study.

	Three facets (type A)		Two facets (types B and C)	
Drayer-Verhagen (1993)	35.3%	(n = 18/51)	65.4%	(n = 68/104)
Madhavi et al. (2008)	9.3%	(n = 4/43)	24.4%	(n= 39/160)
Present study	45.3%	(n=24/53)	37.0%	(n=10/27)

Even though the two other studies had incomparable frequencies, they still had the same conclusion. The present study could not demonstrate this relationship. A difference in the methodology by which OA changes were scored may, in part, explain the different reported frequencies between these three studies. The present study assessed the joints of wet preserved specimens with intact cartilage, whereas the other two studies used macerated and archeological bones without cartilage. The presence of OA in these latter two studies was thus based on secondary features associated with OA. In the present study, the cartilage itself was examined, thus enabling the identification of changes associated with the early onset of OA, a phase during which the associated changes examined in the previous studies has not yet developed.

A second parameter was the intersection angle which has also been linked to the stability of the subtalar joint and thus to OA changes (3,6). A smaller angle means a steeper slope between the middle and anterior part and potentially contributes to a higher stability. The present study found a significant difference between the intersection angle in Types A and C calcanei. The previous reports on the intersection angle by Drayer-Verhagen and Madhavi et al. did not discriminate between Types B and C and pooled these types into one category (two-facet configuration) (3,6). Their averages differed significantly between Type A and B/C. In the present study, Type B was not significantly different from the other two types and the average angle was in between Types A and C. This can be addressed in future studies with a higher number of specimens. But also for this parameter, no significant interaction could be demonstrated.

A third parameter that was tested for an association with OA changes was whether the types corresponded in one coupled talus and calcaneus. No previous studies reported on the corresponding type of coupled calcaneal and talar facets in a European population. Corresponding or noncorresponding types could indicate a more or less

congruent joint, respectively. Noncongruent joints are prone to develop OA (27). No significant association could be demonstrated. The most frequently affected part of the calcaneus and talus was the anterior part. Interestingly, no OA changes were observed in the posterior facet, which is in agreement with Madhavi et al. (6).

Of the other parameters (such as lengths and widths of the facets) that were evaluated in a possible relationship with OA changes only age showed to be a significant factor. This was expected since aging and OA changes are highly correlated (28).

Interobserver analyses

The interobserver analyses showed discrepancies between the observed types. Both observers agreed on all Type A calcanei. Types B and C are on a gliding scale. Jung et al. introduced a method to quantify the constriction, or the "degree of separation" as they called it, between the anterior and middle facets in Type B or C (7). This elegant method could not be used in our study as it was problematic to accurately identify the borders of the facets on the photographs of the wet specimen with intact periarticular soft tissue. The edges needed to be manually detected. The interobserver analysis of the metric data showed a substantial to excellent correlation. No metric analyses were performed for the tali. The boundaries of the middle and/or anterior facets could not be measured accurately. This is also reflected in the high number of noncorresponding classifications between both observers for the types of the tali. Considering our relative high frequency of discrepancies, we advise to include this analysis in future studies and to take into account some deviation from the presented distributions in current literature that did not present an interobserver analysis.

Strengths, limitations, and recommendations

The strength of the present study was that we assessed paired hindfeet with intact cartilage, whereas most other studies used macerated or archeological specimens. We thereby could examine the cartilage itself and not only the subchondral surface when assessing for OA changes. It also allowed to look at the types within a coupled talus and calcaneus. Furthermore, we had a CT data set of healthy subjects for analyses. A limitation was the low number of cadaveric specimen and their high age. Another limitation was the measurement by sliding calipers of the facets. The posterior facet has a pronounced curvature. To deal with this, we used data from a previous study that did account for this 3D morphology. This limitation was also the case for the fused middle and anterior facets that in some specimen had a concave curvature. A similar approach with a geometrical shape fit as with the cylinder for the posterior facet might be applied to these facets, based on 3D laser scans or CT scanning. Furthermore, demographically

differences that exist in the distribution of the types might also be present in the relationship between OA changes and morphology or left–right symmetry (2). Future studies can address these issues.

Conclusions

Orthopedic and trauma surgeons can use this information to plan an operation using the contralateral noninjured foot in, for example, anatomical reduction or the size and shape of an implant. Continued research will potentially demonstrate an unambiguous relationship between the morphology and the stability or the risks for developing OA, since previous studies did find a significant relationship, but the present study did not (3,6).

In conclusion, the present study demonstrated a strong degree of bilateral symmetry in the morphology of the talocalcaneal joint facets. OA changes are frequently found, primarily at the anterior aspect of both calcanei and tali. However, only age had a significant interaction with the presence of OA changes. Other characteristics need further exploration.

References

1. Bruckner J. Variations in the human subtalar joint. J Orthop Sports Phys Ther. 1987;8(10):489–94.
2. Forriol Campos F, Gomez Pellico L. Talar articular facets (facies articulares talares) in human calcanei. Acta Anat (Basel). 1989;134(2):124–7.
3. Drayer-Verhagen F. Arthritis of the subtalar joint associated with sustentaculum tali facet configuration. J Anat. 1993 Dec;183 (Pt 3:631–4.
4. Barbaix E, Van Roy P, Clarys JP. Variations of anatomical elements contributing to subtalar joint stability: intrinsic risk factors for post-traumatic lateral instability of the ankle? Ergonomics. 2000 Oct;43(10):1718–25.
5. Ragab AA, Stewart SL, Cooperman DR. Implications of subtalar joint anatomic variation in calcaneal lengthening osteotomy. J Pediatr Orthop. 2003;23(1):79–83.
6. Madhavi C, Madhuri V, George VM, Antonisamy B. South Indian calcaneal talar facet configurations and osteoarthritic changes. Clin Anat. 2008 Sep;21(6):581–6.
7. Jung M-H, Choi BY, Lee JY, Han CS, Lee JS, Yang YC, et al. Types of subtalar joint facets. Surg Radiol Anat. 2015 Aug;37(6):629–38.
8. Agarwal S, Garg S, Vasudeva N. Subtalar Joint Instability and Calcaneal Spurs Associated with the Configuration of the Articular Facets of Adult Human Calcaneum in Indian Population. J Clin Diagn Res. 2016 Sep;10(9):AC05–9.
9. Stephan D, Panzer S, Gottlinger M, Augat P. Analysis of the intra-individual differences of the joint surfaces of the calcaneus. Comput Methods Biomech Biomed Engin. 2014 Nov;17(15):1635–41.
10. Shultz SJ, Nguyen A-D. Bilateral asymmetries in clinical measures of lower-extremity anatomic characteristics. Clin J Sport Med Off J Can Acad Sport Med. 2007 Sep;17(5):357–61.
11. Islam K, Dobbe A, Komeili A, Duke K, El-Rich M, Dhillon S, et al. Symmetry analysis of talus bone: A Geometric morphometric approach. Bone Joint Res. 2014;3(5):139–45.
12. Tumer N, Arbabi V, Gielis WP, de Jong PA, Weinans H, Tuijthof GJM, et al. Three-dimensional analysis of shape variations and symmetry of the fibula, tibia, calcaneus and talus. J Anat. 2019 Jan;234(1):132–44.
13. Pierre MA, Zurakowski D, Nazarian A, Hauser-Kara DA, Snyder BD. Assessment of the bilateral asymmetry of human femurs based on physical, densitometric, and structural rigidity characteristics. J Biomech. 2010 Aug;43(11):2228–36.
14. Dobbe JGG, Pre KJ du, Kloen P, Blankevoort L, Streekstra GJ. Computer-assisted and patient-specific 3-D planning and evaluation of a single-cut rotational osteotomy for complex long-bone deformities. Med Biol Eng Comput. 2011 Dec;49(12):1363–70.
15. Young EY, Gebhart J, Cooperman D, Ahn NU. Are the left and right proximal femurs symmetric? Clin Orthop Relat Res. 2013 May;471(5):1593–601.
16. Ten Berg PWL, Dobbe JGG, van Wolfswinkel G, Strackee SD, Streekstra GJ. Validation of the contralateral side as reference for selecting radial head implant sizes. Surg Radiol Anat. 2016 Sep;38(7):801–7.
17. Kleipool RP, Blankevoort L. The relation between geometry and function of the ankle joint complex: a biomechanical review. Knee Surg Sports Traumatol Arthrosc. 2010 May;18(5):618–27.

18. Aynardi M, Pedowitz DI, Raikin SM. Subtalar instability. Foot Ankle Clin. 2015 Jun;20(2):243–52.
19. Stormont DM, Morrey BF, An KN, Cass JR. Stability of the loaded ankle. Relation between articular restraint and primary and secondary static restraints. Am J Sports Med. 1985;13(5):295–300.
20. Kleipool RP, Dahmen J, Vuurberg G, Oostra R-J, Blankevoort L, Knupp M, et al. Study on the three-dimensional orientation of the posterior facet of the subtalar joint using simulated weight-bearing CT. J Orthop Res. 2019 Jan;37(1):197–204.
21. Bolt S, Venbrux E, Eisinga R, Kuks JBM, Veening JG, Gerrits PO. Motivation for body donation to science: more than an altruistic act. Ann Anat. 2010 Apr;192(2):70–4.
22. Bunning PS, Barnett CH. A Comparison of adult and foetal talocalcaneal articulations. J Anat. 1965 Jan;99:71–6.
23. Terwee CB, Bot SDM, de Boer MR, van der Windt DAWM, Knol DL, Dekker J, et al. Quality criteria were proposed for measurement properties of health status questionnaires. J Clin Epidemiol. 2007 Jan;60(1):34–42.
24. Latimer HB, Lowrance EW. Bilateral asymmetry in weight and in length of human bones. Anat Rec. 1965 Jun;152(2):217–24.
25. Rehman FU. Study of human fetal calcaneal articular facets. Int J Dev Res. 2014;4:1362–5.
26. Deng H, Xia H, Deng S. Genetic basis of human left-right asymmetry disorders. Expert Rev Mol Med. 2015 Jan;16:e19.
27. Henak CR, Anderson AE, Weiss JA. Subject-specific analysis of joint contact mechanics: application to the study of osteoarthritis and surgical planning. J Biomech Eng. 2013 Feb;135(2):21003.
28. Loeser RF. Aging processes and the development of osteoarthritis. Curr Opin Rheumatol. 2013 Jan;25(1):108–13.

Chapter 8

General discussion and future perspectives

'have your feet on the ground'

Cambridge dictionary: to be practical and able to take care of yourself

This thesis focused on the clinical and functional anatomy of the hindfoot. For many morphological characteristics it is unknown what the range of variations is in non-symptomatic and healthy feet. Also, the functional implications of these variations are mostly unknown. What is considered to be within the normal range of variation might very well include variations that form a predisposing factor for certain pathology, such as osteoarthritis or chronic ankle instability. With different methods the morphology of the bones and joints, and the function of the hindfoot were quantitatively and qualitatively analysed. With these analyses, whether by new quantitative methods and in 3D, or based on plain observation with the unaided eye, new insights were found that add to the literature on the variations in hindfoot morphology and functioning of the hindfoot. This information will help to adequately optimize the prevention and treatment of pathology of the hindfoot and adjacent regions.

In **Part 1**, the focus was on the mechanics of the hindfoot region to understand the joint force determining factors, the role of the geometry and ligaments of the joints in the kinematics and joint stability, and to provide new data on the kinematics of the hindfoot and the variations herein. **Chapter 2** explains, by a simple biomechanical analysis, what the force determining factors are that work on the ankle joint. It showed that the balance of moment arms of the muscles and their tendons around the ankle joint together with the ground reaction force determine the magnitude of the joint force. The joint forces can be as high as four times the body weight in a static situation, and are even larger in dynamic situations. These high forces explain, in part, the high incidence of injuries of the hindfoot. This simple biomechanical analysis is limited for several reasons. First, it does not provide information on the force distribution over the whole contact area of the ankle joint. In the talocrural joint not only the superior talar surface transmits the force of the tibia and fibula, but also its medial and lateral surfaces (1). The largest force transfer is between the superior surface of the talus and distal inferior surface of the tibia. For example, a small lateral shift of the talus of 1 mm can already decrease the contact area up to 42% (2). This will cause an increase of the load over the remaining contact area, resulting in higher local pressure and increased risk of

wear of cartilage. Therefore, not only the total joint force is important, but also the area of contact surface and the distribution of the force over this area. Second, the other limitation is that the forces in this biomechanical analysis cannot be measured in vivo, but only in vitro, or can be calculated in biomechanical models. Since the muscle activity is one of the determining factors, muscle coordination has to be monitored live. Inefficient co-contraction will generate a larger force than predicted in models. Therefore, the biomechanical analysis of Chapter 2 cannot be applied in active individuals and is only theoretical. The literature concerning the load distribution of the subtalar joints is scarce (3), and this could be addressed in future studies for example to help design subtalar joint prostheses.

The assessment of the range of motions found in the literature and presented in Chapter 2 showed that only a small portion of the potential range of motion is used during normal walking or even in running. This information is useful for the design for prosthetics. Total ankle replacement is applied when other less rigorous options fail (4), such as debridement in case of osteoarthritis (5). Return to a normal physiological mobility is part of the patients' satisfaction (6), but is not per se required for all patients, especially not for those who are not active in sports and do not require a full range of motion for a satisfactory function.

Chapter 2 further describes several aspects of the interaction between shape and function. The joints of the ankle joint complex are very congruent, which determines their stability almost entirely when the joint is compressed (7,8). Variation of the joints morphology also causes variations in the degree of stability provided by the joint's morphology (9,10). Chapter 7 explores this relationship for the subtalar joints, and in Chapters 5 and 6 the orientation of the articulating surfaces of the hindfoot are investigated for the role in the hindfoot alignment.

Chapter 3 presents the change in the dimensions of the tarsal sinus and canal in multiple foot positions. The dimensions were expressed along the medial to lateral direction by the diameter of spheres fitted in the bony boundaries. No previous literature described the dimensions in more than one position and in healthy non-symptomatic adults. In general, this chapter contributes to a reference of the variation in the dimensions of the tarsal sinus and canal in healthy and non-symptomatic feet. For procedures such as arthroereisis this study can help the clinician choose an implant (11), for arthroscopy of the subtalar joints to maneuver in this tight space these results provide useful information (12), and for the sinus tarsi syndrome the insight of the changes in dimensions between different foot positions will help to find the cause of the pain experienced by the patients (13,14).

The change in dimensions between different foot positions demonstrated that there was a region where the dimensions hardly change. This region seemed to act as a pivot

point for motion between the talus and calcaneus. Foot positions with an inversion component showed an increase in the dimensions the lateral side, and a decrease at the medial side. Foot positions with an eversion component demonstrated the opposite effects.

Langelaan, in 1983, described the helical axis of the subtalar joint and tried to correlate the determined helical axes to the location of the ligaments (15). More recent studies, using (weight bearing) CT imaging also calculated the rotation axis (16,17). Together with detailed information of the position and shape of the ligaments, such as derived from magnetic resonance (MR) imaging, a more precise and 3D comparison between the ligaments, the rotation axis, and the region with a fairly constant dimension could be made that add to the understanding of the relationship between the (variations of the) morphology and the functioning of the subtalar joints.

A drawback of the use of CT is that only the subchondral surfaces were analysed. The space is bordered by the osseous channel made up by the sulcus of the calcaneus and talus, and contains blood vessels, nerves, fat, and ligaments (13,18–23). The sulcus is located between the posterior and middle articulating surfaces of the talocalcaneal joints. At the boundaries of these surfaces the articular cartilage might reduce the dimensions of the space, especially in foot positions where the two opposing surfaces are displaced to one another and the edge of a surface protrude in the tarsal sinus or canal.

The functional evaluation of the Exo-L® ankle brace (EXO-L BV, Delft, The Netherlands) in **Chapter 4** was performed in a laboratory setting. Ankles braces are generally applied by athletes to prevent the occurrence and recurrence of ankle sprains (24). The effect of ankle braces has been investigated in many different studies using a variety of methods. These include in vitro and in vivo studies with the specimen or subject's leg fixated to an external frame and the foot placed under load with and without the brace (e.g. (25–29)). Others used a dropping platform to simulate a sudden inversion (30–32) or let the participants land on a force plate with measurements of the kinematics (33,34). Ankle braces have proved to be effective in preventing a recurrence of ankle sprains (24). Ankles braces can however give discomfort and there are reports that demonstrate a decline in sporting performance (35–38). The Exo-L® ankle brace comprises of a custom-fit shell that envelops the posterior aspect of the distal leg at the level of the malleoli. From a clamp at the lateral side of this shell a cord runs to a sling attached to the lateral side of the sporting shoe. The cord acts as an exoskeletal ligament, hence the name of the product. The brace was designed to prevent lateral ankle sprains, without an impairment of the athlete's performance, especially the limitation of other motions than the common motion for a lateral sprain, namely inversion or combined plantar flexion and inversion (39).

In this controlled environment a first exploration of the functionality of this unconventional brace design could be evaluated objectively, safely, and accurately. In this laboratory setting the claimed functionality could be assessed more easily than in daily practice, but whether the results can be applied to sport settings remains to be investigated. The focus was to investigate the change in ranges of motion of the hindfoot in patients with chronic ankle instability without and with the application of the brace. The results demonstrated that the motion of combined plantarflexion and inversion was statistically significantly reduced by the Exo-L® brace. Although the average motion of plantarflexion to dorsiflexion decreased with the appliance of the Exo-L® brace, this was not statistically significant. The results confirmed the claimed functionality. The restriction in motion in this loaded setting cannot simply be extrapolated to a full impact landing. However, the restriction in motion with the feet off ground could already provide a more beneficial joint position to prevent an ankle sprain (40).

Part 2 (Chapters 5-7), together with Chapter 3, of the thesis addressed the variation of several morphological aspects of the hindfoot. In **Chapter 5** a descriptive study is presented on the posterior calcaneal facet. The orientation of this facet has been investigated in hindfoot malalignment (41–46), but the 3D morphology and orientation has not been taken into account in these studies. The shape of this facet has been described and simplified as a (segment of a) cylinder (10,47). This was used in this study as a starting point to analyze both the morphology and orientation of this facet. The other geometrical shape was a plane, which proved to be an oversimplification that does not fit well to the curved surface of the posterior facet.

The results of the orientation of the planes and cylinders fitted to the subchondral articulating surface were presented in two different coordinate systems. As can be appreciated from Chapter 5, evidently the choice of the reference coordinate system has an influence on the values of the orientation angles.

This study also presented the difference between a 2D and 3D determination of the orientation of the posterior calcaneal facet in a coronal plane. The 2D analysis of the orientation by others was conducted at three different antero-posterior locations in coronal planes (44,48). At corresponding locations the fitted cylinders were virtually cut and at the intersection of the cylinder with the facet the orientation was determined. At each location the orientation differed. With (interactive) illustrations the oblique orientation of the cylinder in the coordinate system clearly demonstrated the reason for a different orientation at each location.

This study demonstrated that a cylinder approach can be used to quantify the 3D morphology and orientation of the posterior calcaneus facet, irrespectively of a chosen

plane for analysis. The results provide a reference for healthy and non-symptomatic individuals that serves future investigation on the influence of the subtalar joint on the evolution of ankle joint arthritis in valgus and varus hindfoot deformities.

Chapter 6 presents a study of the orientation of the superior and postero-inferior talar facets, and posterior calcaneal facets. This study builds on the findings and methodology of the study presented in Chapter 5. The inferior talar facet is the counterpart of the posterior calcaneal facet in the congruent posterior subtalar joint. As such, the cylinder fit to the posterior calcaneal facet presented in Chapter 5 could also be applied to the inferior talar facet. Others have already simplified and analyzed the superior talar facet, or talar dome, as a part of a cylinder with good results for the fitting accuracy (e.g. (49)). Two control groups with healthy and asymptomatic hindfeet were compared to a group of patients with chronic ankle instability (CAI). CAI commonly results from an ankle sprain. In up to 30–40% of patients an initial ankle sprain progresses to CAI (50,51). A risk of CAI is damage to the ankle joint and osteoarthritis on the long term (52). Identifying characteristics that contribute to the progress of CAI after an initial ankle sprain will help to determine the choice of treatment, for example surgery. The results of the study in Chapter 6 demonstrated that the CAI had a statistically significant larger interrelationship inclination angle between the superior and inferior talar facet. In a coronal view this corresponds to a valgus position of the inferior talar facet relative to the superior talar facet. This result was somewhat surprising since most literature describe varus alignment of the hindfoot associated to CAI (53–55). The current literature does not use 3D analyses nor does it analyze the talar morphology. Also, it analyzed the whole hindfoot alignment without a discrimination to each level in the mechanical chain of the hindfoot. The overall hindfoot alignment was not assessed of the included patients and healthy volunteers. The study therefor demonstrated at least that the talar morphology is a risk factor in CAI and does not have to contribute to a varus hindfoot deformity.

In **Chapter 7** the presented study addressed the question to what extend the talocalcaneal facets are bilaterally symmetric. Bilateral symmetry is assumed in many clinical (and research) settings, where the contralateral joint is used as the reference during diagnosis and treatment of joint pathologies. This bilateral symmetry was not evaluated yet. One important result that has to be taken into account in future studies was that the two observers disagreed on the classification in several specimen. As with Shahabpour et al. (56) this was especially between configurations where the middle and anterior facets are joined with a broad or narrow cartilaginous bridge. The introduced method of Jung et al. (57) where the constriction between these facets was quantified could be optimized for specimen with intact soft tissue. Such methods where the variation of facet configuration is matched to a quantified observation might contribute

to less non-corresponding classifications by multiple observers. The results demonstrated that the degree of bilateral symmetry is large but not 100%. Individuals also demonstrated an asymmetry in for example the facet configuration.

The other research question in the study presented in Chapter 7 tested the hypothesis that the shape and congruency of the talocalcaneal joints are related to the presence of osteoarthritic changes (58). This hypothesis was based on previous findings (59,60). The results presented in Chapter 7 did not demonstrated a statistically significant relationship between the morphological parameters and osteoarthritic changes where the other studies did. The different techniques between this study and others (59–61) might explain the difference in results. Both these and the study presented in Chapter 7 used post-mortem material, but the previous studies used dried bones whereas the study in Chapter 7 examined cadaveric specimen with cartilage and inspected the status of the cartilage itself and not osteoarthritic related changes in the bones such as osteophytes. Whether the calcaneus and talus had a corresponding facet configuration had no influence on the presence of osteoarthritic changes. The shape of the contacting facets could still match and the joint could still have a high congruency.

A major limitations in previous studies, including the study presented in Chapter 7, is that the talonavicular joint is not included in the analysis. This joint contributes to what is also known as the acetabulum pedis, a highly congruent joint in the anterior part of the talocalcaneonavicular joint. The congruency is partly attributed to the plantar calcaneonavicular ligament (part of the spring ligament complex (62)), a fibrocartilaginous band, that supports the inferior aspect of the talar head. As described in the introduction of this thesis, the talocalcaneal and talocalcaneonavicalar joints do not move independently, comparable to a door with two hinges. Therefore, the stability of this complex is also determined by the talonavicular joint. The positioning of the talar head has an influence on the contact area in the talocalcaneal joints (63). The degree of the navicular bone coverage of the talar head (64), the curvature of the talar head and concave proximal articulating surface of the navicular bone are variable (65). This variation could be of influence to the total stability of this complex.

Future perspectives

In this thesis CT scanning was the primary imaging modality. One limitation is that soft tissue, such as ligaments and cartilage are not depicted in CT images. CT is currently the preferred imaging modality for depicting the bones, either cortical or trabecular. However, recent results have been reported for the use of synthetic CT based on MR for the imaging of bone (66). MR can image soft tissue, such as ligaments and cartilage,

thus depicting the soft tissue in relationship to the bony boundaries. This would be beneficial in, for example, the determination of the dimensions of the tarsal sinus and canal. Here, the cartilage might reduce the dimensions in certain foot positions as discussed above.

Future research can include patients with for example sinus tarsi syndrome (67) or patients with cavovarus, or pes planus. The causes for sinus tarsi syndrome, which is mainly characterized by pain at the lateral aspect of the sinus, vary in the literature from impingement to undue stretching of tissue. Other reported causes are tear of and scarring on the interosseous ligament, synovial hyperplasia and deposits of hemosiderin, post-traumatic fibrotic changes in surrounding veins, and nociception and proprioception disorders (13,14,68). Whether these patients indeed have different dimensions or changes in dimensions between different foot positions could be explored with the introduced methodology, ideally with information of the soft tissue such as ligaments and cartilage by MR imaging. MR could also elucidate on relations between bony variations and ligament variations, for example in location of ligament insertions, or architecture of fascicles. MR has already been used in vivo to discriminate between the different subtalar joint configurations as presented in Chapter 7 (56). Subsequently, this was used to explore the relationship between the joint configuration and the quality of the subtalar cartilage (61). Future research could combine these morphological characteristics to elucidate the relationship between stability and shape.

Another drawback and limitation of CT is the ionizing radiation. MR is without ionizing radiation, which is particularly favorable in the pediatric population. Continuing efforts are made to reduce the dosage with CT imaging. For example, Schallig et al. (69) recently demonstrated that the radiation dosage in the CT scanning protocol for multiple foot positions, comparable to the study presented in Chapter 4, can be reduced to 50 milliampere-seconds (mAs) with no significant differences in the precision in detecting bone orientation compared to the often clinically used 150 mAs. This same 150 mAs high dose scan was used for segmentation of the bones in the study presented in Chapter 4. Scans with 25 mAs were used for the different foot positions. This is already lower than the reported 50 mAs and seems to be the lower limit. Therefore, the radiation dosage is truly a limiting factor for save evaluation of other orthoses by means of this CT protocol.

During the preparation of this thesis at the Amsterdam UMC, location AMC, this institute did not have a full weight bearing CT scanner. Therefore, for the addressed research questions of the study presented in Chapter 5 (and others outside this thesis), a custom-made device was constructed to simulate weight bearing in a supine position compatible with a conventional CT scanner. This device to simulate weight bearing was not unique (e.g. (41–43,70). The drawbacks that are mentioned in literature compared

to full weight bearing with a horizontally tilted gantry are that the load is passively applied and thus the muscles are not active, and that the load is only at a percentage (e.g. a fifth, third or half) of the body weight (71), although full weight bearing devices have been used in previous studies (72,73). Our loading device that was constructed for the study in Chapter 5 did require active muscle force to keep the lower extremity in a 'standing position'. Also, the load could be adjusted to over 100% body weight. It therefor overcomes these drawbacks. Another mentioned drawback is that the device and scan protocol is cumbersome (71). This was not overcome with our device. An advance with our device above some of the full weight bearing scanners is that our device also accommodates scanning of one or both legs at different percentages of the body weight. The literature clearly demonstrate that the orientation of the bones change between a non-loaded condition and a weight bearing condition (e.g. (74)). However, it remains unclear if a simulated weight bearing results in differences in bone positions and load compared to full weight bearing. This can be explored in future research. If no significant differences occur, the design can be optimized to make it less cumbersome and also to make it compatible with MR.

The advantages of weight bearing imaging in ankle and foot imaging have been advocated by a large group of clinicians and researchers, partly joined in the International Weight Bearing CT Society. One of the tasks that this group stands for is to standardize the methodology of the measurement methods. This connects well with the suggestions made in Chapters 5 and 6. As discussed in Chapters 5 and 6 for future research, and subsequently for clinical practice, a standardized coordinate system needs to be defined. This issue is already addressed in previous studies (e.g. (75–79)), and continuing efforts are made to standardize measurements of joint orientation and alignment in normal supine CT scanning or in full weight bearing CT scanning. This can be seen in for example the Foot and Ankle Offset measurement. This is a measure for the lever arm between the ground reaction force in the foot and the center of the ankle joint. As elucidated in Chapter 2 the size of the lever arm is one of the determining factors for the muscle forces and the joint reaction force. The larger this lever arm is, the larger the counteracting muscle forces have to be. Originally, this measurement was introduced as a 2D measurement (80), but is presently in a validation process for approval in diagnosis as an integrated tool in CubeVue Software in 3D (CurveBeam LLC, Warrington, PA) (81,82).

A scan of the whole lower extremity provides useful information of the whole limb axis in the assessment of lower limb alignment. This is also not possible in the full weight bearing scanners, but could be included with our custom made simulated weight bearing device. If the radiation dose is a limiting factor, the scans could be reduced to segments of the lower extremity. For the limb axis one can suffice with the regions of hip, knee,

and hindfoot. The metaphysis of the bones between this regions might potentially be left out of the scan. Additionally, a force plate could be integrated in the protocol to acquire the location of the ground reaction force in relation to the foot and limb axis. These are thoughts to be explored in future research.

Although in Chapter 6 a patient group with chronic ankle instability was included, this analysis is not yet accessible for clinical routine. The use of geometrical shapes such as the cylinders in Chapters 5 and 6 are investigational only and intended to be used for research. One hurdle in the workflow is segmentation. In Chapters 3 to 7 in the thesis one of the steps in data acquisition was the segmentation of the bones in the CT images. This is also in many other studies part of the workflow. Segmentation is a time consuming process. Advances are being made with automated segmentation of bony structures in CT imaging (83). Bones with a thick cortex, such as the tibia, are more easily segmented than bones that only have a thin cortex. The talus and calcaneus both have a thin cortex and the segmentation was therefore more laborious and time consuming. For research purposes often cadaveric specimens are used, but segmentation in embalmed cadaveric feet of old individuals, especially females, is even more difficult, because of the lower bone density. The expectation is that the advances in automated segmentation and 3D modelling will become more accessible and will result in time reduction and increased accuracy.

The above described and other ongoing advances in medical imaging and computational power will result in more powerful and realistic 3D computer models, such as that of Imhauser et al. (84). These models are powerful tools to investigate the effects of variations of the morphology on function. In such models it is possible to vary for example the shape of the bones and joints, the insertion locations of the ligaments, or the characteristics of the ligaments (such as force-length relationships). With these models the influence of variations in the input parameters on the functioning of the hindfoot can be studied. One challenge is to gather data for such a model. Before variations can be applied to the input parameters, it must be ascertained that the baseline input represents a normally functioning hindfoot. This requires a detailed input of the morphology, but also of the dynamic properties of the ligaments, cartilage, and other structures that contribute to the force balance. Even though this is challenging, the information from such models can truly elucidate the interaction between shape and function.

In conclusion, this thesis provides information about the range of inter- and/or intra-individual variation. These, mainly preclinical, data can serve as a framework to improve the identification and understanding of hindfoot pathologies. This thesis contributes to

the ongoing search to find characteristics that are related to the development of chronic ankle instability and osteoarthritis, and by no means can be considered as the end point and has opened many doors for future research.

References

1. van Dijk CN, Reilingh ML, Zengerink M, van Bergen CJA. Osteochondral defects in the ankle: why painful? Knee Surg Sports Traumatol Arthrosc. 2010 May;18(5):570–80.
2. Ramsey PL, Hamilton W. Changes in tibiotalar area of contact caused by lateral talar shift. J Bone Joint Surg Am. 1976 Apr;58(3):356–7.
3. Procter P, Paul JP. Ankle joint biomechanics. J Biomech. 1982;15(9):627–34.
4. Gougoulias N, Khanna A, Maffulli N. How successful are current ankle replacements?: a systematic review of the literature. Clin Orthop Relat Res. 2010 Jan;468(1):199–208.
5. Osti L, Del Buono A, Maffulli N. Arthroscopic debridement of the ankle for mild to moderate osteoarthritis: a midterm follow-up study in former professional soccer players. J Orthop Surg Res. 2016 Mar;11:37.
6. Casaroli G, Villa T, Bianchi A, Caboni E, Malerba F, Galbusera F, et al. In vivo kinematics of fixed-bearing total ankle arthroplasty. Foot Ankle Surg. 2019 Apr;
7. Stindel E, Udupa JK, Hirsch BE, Odhner D. An in vivo analysis of the motion of the peritalar joint complex based on MR imaging. IEEE Trans Biomed Eng. 2001 Feb;48(2):236–47.
8. Watanabe K, Crevoisier XM, Kitaoka HB, Zhao KD, Berglund LJ, Kaufman KR, et al. Analysis of joint laxity after total ankle arthroplasty: cadaver study. Clin Biomech (Bristol, Avon). 2009 Oct;24(8):655–60.
9. Barnett CH, Napier JR. The axis of rotation at the ankle joint in man; its influence upon the form of the talus and the mobility of the fibula. J Anat. 1952 Jan;86(1):1–9.
10. Inman VT. The joints of the ankle. Baltimore: Williams and Wilkins;
11. Bali N, Theivendran K, Prem H. Computed tomography review of tarsal canal anatomy with reference to the fitting of sinus tarsi implants in the tarsal canal. J Foot Ankle Surg. 2013;52(6):714–6.
12. Lui TH, Tong SC. Subtalar arthroscopy: When, why and how. World J Orthop. 2015 Jan;6(1):56–61.
13. Lektrakul N, Chung CB, Ym L, Theodorou DJ, Yu J, Haghighi P, et al. Tarsal sinus: arthrographic, MR imaging, MR arthrographic, and pathologic findings in cadavers and retrospective study data in patients with sinus tarsi syndrome. Radiology. 2001 Jun;219(3):802–10.
14. Taillard W, Meyer JM, Garcia J, Blanc Y. The sinus tarsi syndrome. Int Orthop. 1981;5(2):117–30.
15. van Langelaan E. Relative talotibial movements and relative tarsal movements. Acta Orthop Scand. 1983;54:135–265.
16. Beimers L, Tuijthof GJM, Blankevoort L, Jonges R, Maas M, van Dijk CN. In-vivo range of motion of the subtalar joint using computed tomography. J Biomech. 2008;41(7):1390–7.
17. Pena Fernandez M, Hoxha D, Chan O, Mordecai S, Blunn GW, Tozzi G, et al. Centre of Rotation of the Human Subtalar Joint Using Weight-Bearing Clinical Computed Tomography. Sci Rep. 2020 Jan;10(1):1035.
18. Smith JW. The ligamentous structures in the canalis and sinus tarsi. J Anat. 1958 Oct;92(4):616–20.
19. Schmidt HM. [Form and attachment of the human sinus tarsi and canalis tarsi ligaments]. Acta Anat (Basel). 1978;102(2):184–94.

20. Schwarzenbach B, Dora C, Lang A, Kissling RO. Blood vessels of the sinus tarsi and the sinus tarsi syndrome. Clin Anat. 1997;10(3):173–82.
21. Rab M, Ebmer J, Dellon AL. Innervation of the sinus tarsi and implications for treating anterolateral ankle pain. Ann Plast Surg. 2001 Nov;47(5):500–4.
22. Jotoku T, Kinoshita M, Okuda R, Abe M. Anatomy of ligamentous structures in the tarsal sinus and canal. Foot ankle Int. 2006 Jul;27(7):533–8.
23. Li S-Y, Hou Z-D, Zhang P, Li H-L, Ding Z-H, Liu Y-J. Ligament structures in the tarsal sinus and canal. Foot ankle Int. 2013 Dec;34(12):1729–36.
24. Dizon JMR, Reyes JJB. A systematic review on the effectiveness of external ankle supports in the prevention of inversion ankle sprains among elite and recreational players. J Sci Med Sport. 2010 May;13(3):309–17.
25. Tohyama H, Yasuda K, Beynnon BD, Renstrom PA. Stabilizing effects of ankle bracing under a combination of inversion and axial compression loading. Knee Surg Sports Traumatol Arthrosc. 2006 Apr;14(4):373–8.
26. Choisne J, Hoch MC, Bawab S, Alexander I, Ringleb SI. The effects of a semi-rigid ankle brace on a simulated isolated subtalar joint instability. J Orthop Res. 2013 Dec;31(12):1869–75.
27. Kamiya T, Kura H, Suzuki D, Uchiyama E, Fujimiya M, Yamashita T. Mechanical stability of the subtalar joint after lateral ligament sectioning and ankle brace application: a biomechanical experimental study. Am J Sports Med. 2009 Dec;37(12):2451–8.
28. Eils E, Demming C, Kollmeier G, Thorwesten L, Volker K, Rosenbaum D. Comprehensive testing of 10 different ankle braces. Evaluation of passive and rapidly induced stability in subjects with chronic ankle instability. Clin Biomech (Bristol, Avon). 2002 Aug;17(7):526–35.
29. Siegler S, Liu W, Sennett B, Nobilini RJ, Dunbar D. The three-dimensional passive support characteristics of ankle braces. J Orthop Sports Phys Ther. 1997 Dec;26(6):299–309.
30. Zhang S, Wortley M, Chen Q, Freedman J. Efficacy of an ankle brace with a subtalar locking system in inversion control in dynamic movements. J Orthop Sports Phys Ther. 2009 Dec;39(12):875–83.
31. Tang YM, Wu ZH, Liao WH, Chan KM. A study of semi-rigid support on ankle supination sprain kinematics. Scand J Med Sci Sports. 2010 Dec;20(6):822–6.
32. Nishikawa T, Kurosaka M, Mizuno K, Grabiner M. Protection and performance effects of ankle bracing. Int Orthop. 2000;24(5):285–8.
33. Ubell ML, Boylan JP, Ashton-Miller JA, Wojtys EM. The effect of ankle braces on the prevention of dynamic forced ankle inversion. Am J Sports Med. 2003;31(6):935–40.
34. Lee WCC, Kobayashi T, Choy BTS, Leung AKL. Comparison of custom-moulded ankle orthosis with hinged joints and off-the-shelf ankle braces in preventing ankle sprain in lateral cutting movements. Prosthet Orthot Int. 2012 Jun;36(2):190–5.
35. Beriau MR, Cox WB, Manning J. Effects of ankle braces upon agility course performance in high school athletes. J Athl Train. 1994 Sep;29(3):224–30.
36. Rosenbaum D, Kamps N, Bosch K, Thorwesten L, Volker K, Eils E. The influence of external ankle braces on subjective and objective parameters of performance in a sports-related agility course. Knee Surg Sports Traumatol Arthrosc. 2005 Jul;13(5):419–25.

37. Lardenoye S, Theunissen E, Cleffken B, Brink PR, de Bie RA, Poeze M. The effect of taping versus semi-rigid bracing on patient outcome and satisfaction in ankle sprains: a prospective, randomized controlled trial. BMC Musculoskelet Disord. 2012 May;13:81.
38. Papadopoulos ES, Nikolopoulos CS, Athanasopoulos S. The effect of different skin-ankle brace application pressures with and without shoes on single-limb balance, electromyographic activation onset and peroneal reaction time of lower limb muscles. Foot (Edinb). 2008 Dec;18(4):228–36.
39. Kerkhoffs GMMJ, Van Dijk CN. Acute lateral ankle ligament ruptures in the athlete: the role of surgery. Foot Ankle Clin. 2013 Jun;18(2):215–8.
40. Eils E, Rosenbaum D. The main function of ankle braces is to control the joint position before landing. Foot ankle Int. 2003 Mar;24(3):263–8.
41. Burssens A, Peeters J, Buedts K, Victor J, Vandeputte G. Measuring hindfoot alignment in weight bearing CT: A novel clinical relevant measurement method. Foot Ankle Surg. 2016 Dec;22(4):233–8.
42. Burssens A, Van Herzele E, Leenders T, Clockaerts S, Buedts K, Vandeputte G, et al. Weightbearing CT in normal hindfoot alignment - Presence of a constitutional valgus? Foot Ankle Surg. 2018 Jun;24(3):213–8.
43. Cody EA, Williamson ER, Burket JC, Deland JT, Ellis SJ. Correlation of Talar Anatomy and Subtalar Joint Alignment on Weightbearing Computed Tomography With Radiographic Flatfoot Parameters. Foot ankle Int. 2016 Aug;37(8):874–81.
44. Colin F, Horn Lang T, Zwicky L, Hintermann B, Knupp M. Subtalar joint configuration on weightbearing CT scan. Foot ankle Int. 2014 Oct;35(10):1057–62.
45. Kim J-B, Yi Y, Kim J-Y, Cho J-H, Kwon M-S, Choi S-H, et al. Weight-bearing computed tomography findings in varus ankle osteoarthritis: abnormal internal rotation of the talus in the axial plane. Skeletal Radiol. 2017 Aug;46(8):1071–80.
46. Probasco W, Haleem AM, Yu J, Sangeorzan BJ, Deland JT, Ellis SJ. Assessment of coronal plane subtalar joint alignment in peritalar subluxation via weight-bearing multiplanar imaging. Foot ankle Int. 2015 Mar;36(3):302–9.
47. Kapandji IA. The Physiology of the Joints: Lower Limb, Volume 2. Churchill: Livingstone; 1987.
48. Krähenbühl N, Tschuck M, Bolliger L, Hintermann B, Knupp M. Orientation of the Subtalar Joint: Measurement and Reliability Using Weightbearing CT Scans. Foot ankle Int. 2016 Jan;37(1):109–14.
49. Huang J, Liu H, Wang D, Griffith JF, Shi L. Talar dome detection and its geometric approximation in CT: Sphere, cylinder or bi-truncated cone? Comput Med Imaging Graph. 2017 Apr;57:62–6.
50. Pijnenburg AC, Van Dijk CN, Bossuyt PM, Marti RK. Treatment of ruptures of the lateral ankle ligaments: a meta-analysis. J Bone Joint Surg Am. 2000 Jun;82(6):761–73.
51. van Rijn RM, van Os AG, Bernsen RMD, Luijsterburg PA, Koes BW, Bierma-Zeinstra SMA. What is the clinical course of acute ankle sprains? A systematic literature review. Am J Med. 2008 Apr;121(4):324-331.e6.
52. Struijs PA, Kerkhoffs GM. Ankle sprain. BMJ Clin Evid. 2010 May;2010.
53. Van Bergeyk AB, Younger A, Carson B. CT analysis of hindfoot alignment in chronic lateral ankle instability. Foot ankle Int. 2002 Jan;23(1):37–42.
54. Strauss JE, Forsberg JA, Lippert FG 3rd. Chronic lateral ankle instability and associated conditions: a rationale for treatment. Foot ankle Int. 2007 Oct;28(10):1041–4.

55. Lintz F, Bernasconi A, Baschet L, Fernando C, Mehdi N, de Cesar Netto C. Relationship Between Chronic Lateral Ankle Instability and Hindfoot Varus Using Weight-Bearing Cone Beam Computed Tomography. Foot ankle Int. 2019 Oct;40(10):1175–81.
56. Shahabpour M, Deville A, Van Roy P, Vaes P, De Mey J, De Maeseneer M. Magnetic resonance imaging of anatomical variants of the subtalar joint. Surg Radiol Anat. 2011 Sep;33(7):623–30.
57. Jung M-H, Choi BY, Lee JY, Han CS, Lee JS, Yang YC, et al. Types of subtalar joint facets. Surg Radiol Anat. 2015 Aug;37(6):629–38.
58. Henak CR, Anderson AE, Weiss JA. Subject-specific analysis of joint contact mechanics: application to the study of osteoarthritis and surgical planning. J Biomech Eng. 2013 Feb;135(2):21003.
59. Bruckner J. Variations in the human subtalar joint. J Orthop Sports Phys Ther. 1987;8(10):489–94.
60. Drayer-Verhagen F. Arthritis of the subtalar joint associated with sustentaculum tali facet configuration. J Anat. 1993 Dec;183 (Pt 3:631–4.
61. Van Ginckel A, De Mits S, Bennell KL, Bryant AL, Witvrouw EE. T2* mapping of subtalar cartilage: Precision and association between anatomical variants and cartilage composition. J Orthop Res. 2016 Nov;34(11):1969–76.
62. Taniguchi A, Tanaka Y, Takakura Y, Kadono K, Maeda M, Yamamoto H. Anatomy of the spring ligament. J Bone Joint Surg Am. 2003 Nov;85(11):2174–8.
63. Sangeorzan BJ, Wagner UA, Harrington RM, Tencer AF. Contact characteristics of the subtalar joint: the effect of talar neck misalignment. J Orthop Res. 1992 Jul;10(4):544–51.
64. Louie PK, Sangeorzan BJ, Fassbind MJ, Ledoux WR. Talonavicular joint coverage and bone morphology between different foot types. J Orthop Res. 2014 Jul;32(7):958–66.
65. Bonnel F, Teissier P, Maestro M, Ferre B, Toullec E. Biometry of bone components in the talonavicular joint: a cadaver study. Orthop Traumatol Surg Res. 2011 Oct;97(6 Suppl):S66-73.
66. Zijlstra F, M.D. KW, Florkow MC, M.D. RJBS, Weinans HH, M.D. BCH van der W, et al. CT synthesis from MR images for orthopedic applications in the lower arm using a conditional generative adversarial network. In: ProcSPIE [Internet]. 2019. Available from: https://doi.org/10.1117/12.2512857
67. O'Connor D. Sinus tarsi syndrome: A clinical entity. J Bone Jt Surg. 1958;40:720–6.
68. Lee K-B, Bai L-B, Park J-G, Song E-K, Lee J-J. Efficacy of MRI versus arthroscopy for evaluation of sinus tarsi syndrome. Foot ankle Int. 2008 Nov;29(11):1111–6.
69. Schallig W, van den Noort JC, Kleipool RP, Dobbe JGG, van der Krogt MM, Harlaar J, et al. Precision of determining bone pose and marker position in the foot and lower leg from computed tomography scans: How low can we go in radiation dose? Med Eng Phys. 2019;69:147–52.
70. Richter M, Lintz F, de Cesar Netto C, Barg A, Burssens A. Results of more than 11,000 scans with weightbearing CT - Impact on costs, radiation exposure, and procedure time. Foot Ankle Surg. 2019 Jun;
71. Barg A, Bailey T, Richter M, de Cesar Netto C, Lintz F, Burssens A, et al. Weightbearing Computed Tomography of the Foot and Ankle: Emerging Technology Topical Review. Foot ankle Int. 2018 Mar;39(3):376–86.

72. Kido M, Ikoma K, Imai K, Maki M, Takatori R, Tokunaga D, et al. Load response of the tarsal bones in patients with flatfoot deformity: in vivo 3D study. Foot ankle Int. 2011 Nov;32(11):1017–22.
73. Kido M, Ikoma K, Imai K, Tokunaga D, Inoue N, Kubo T. Load response of the medial longitudinal arch in patients with flatfoot deformity: in vivo 3D study. Clin Biomech (Bristol, Avon). 2013 Jun;28(5):568–73.
74. Hirschmann A, Pfirrmann CWA, Klammer G, Espinosa N, Buck FM. Upright cone CT of the hindfoot: comparison of the non-weight-bearing with the upright weight-bearing position. Eur Radiol. 2014 Mar;24(3):553–8.
75. Ikoma K, Noguchi M, Nagasawa K, Maki M, Kido M, Hara Y, et al. A new radiographic view of the hindfoot. J Foot Ankle Res. 2013 Dec;6(1):48.
76. Barg A, Harris MD, Henninger HB, Amendola RL, Saltzman CL, Hintermann B, et al. Medial distal tibial angle: comparison between weightbearing mortise view and hindfoot alignment view. Foot ankle Int. 2012 Aug;33(8):655–61.
77. Buck FM, Hoffmann A, Mamisch-Saupe N, Espinosa N, Resnick D, Hodler J. Hindfoot alignment measurements: rotation-stability of measurement techniques on hindfoot alignment view and long axial view radiographs. AJR Am J Roentgenol. 2011 Sep;197(3):578–82.
78. Liu H, Sugamoto K, Itohara T, Tomita T, Hashimoto J, Yoshikawa H. In vivo three-dimensional skeletal alignment analysis of the hindfoot valgus deformity in patients with rheumatoid arthritis. J Orthop Res. 2007 Mar;25(3):330–9.
79. Williamson ERC, Chan JY, Burket JC, Deland JT, Ellis SJ. New radiographic parameter assessing hindfoot alignment in stage II adult-acquired flatfoot deformity. Foot ankle Int. 2015 Apr;36(4):417–23.
80. Lintz F, Barton T, Millet M, Harries WJ, Hepple S, Winson IG. Ground Reaction Force Calcaneal Offset: A new measurement of hindfoot alignment. Foot ankle Surg Off J Eur Soc Foot Ankle Surg. 2012 Mar;18(1):9–14.
81. Lintz F, Welck M, Bernasconi A, Thornton J, Cullen NP, Singh D, et al. 3D Biometrics for Hindfoot Alignment Using Weightbearing CT. Foot ankle Int. 2017 Jun;38(6):684–9.
82. Zhang JZ, Lintz F, Bernasconi A, Zhang S. 3D Biometrics for Hindfoot Alignment Using Weightbearing Computed Tomography. Foot ankle Int. 2019 Jun;40(6):720–6.
83. Lenchik L, Heacock L, Weaver AA, Boutin RD, Cook TS, Itri J, et al. Automated Segmentation of Tissues Using CT and MRI: A Systematic Review. Acad Radiol. 2019 Dec;26(12):1695–706.
84. Imhauser CW, Siegler S, Udupa JK, Toy JR. Subject-specific models of the hindfoot reveal a relationship between morphology and passive mechanical properties. J Biomech. 2008;41(6):1341–9.

Chapter 9

English and Dutch Summary

'from head to toe'
Cambridge dictionary: completely covering your body

English summary

All body parts demonstrate a certain range of inter- and intra-individual anatomical variations. Some variations may affect the chance of developing pathologies. This thesis focuses on the frequently injured hindfoot, the posterior part of the foot. The studies described in this thesis contribute to identifying these variations. This information will help to adequately optimize the prevention and treatment of problems of the hindfoot and adjacent regions.

In **Part 1** the mechanics of the hindfoot are evaluated in a narrative review, the dimensions of the tarsal sinus and canal are investigated by kinematic measurements, and the functionality of a new kind of ankle brace is evaluated by a 3D stress test with computed tomography (CT). The narrative review presented in **Chapter 2** begins with a simple biomechanical analysis that demonstrates that the magnitude of the joint force in the talocrural joint is determined by the balance between muscle forces and the ground reaction force, and their moment arms relative to the joint. The magnitude of the joint force can be as high as four times the body weight in a standing position on one leg. Next, a quantitative overview is given of the maximum ranges of motion of the talocrural and subtalar joints and compared these to the ranges of motion during normal walking and running, which require only a small portion of the maximum or potential ranges. Finally, the joint morphology can attribute up to 100% of the stability when the joint is compressed. The ligaments are considered to be slack or only slightly taut within the functional range of motion. In general, ligament restraint will increase towards the limits of the maximal range of motion. They will restrain excursions within the maximal range of motion and contribute collectively with the joint´s morphology, to the passive stability of the joints. One issue that is not easily resolved is the determination of the zero-slack length of the ligaments. This is the length at which a ligament becomes tensioned. For modelling functional analysis, this parameter is important input.

Chapter 3 introduces a new method to determine the dimensions of the tarsal sinus and canal. This space lies between the talus and calcaneus, and changes between

different foot positions. The size of this space in adults, for multiple foot positions, is not documented in the literature, but can be helpful in, for example, arthroscopy or diagnosis of tarsal sinus syndrome. A dataset of 20 healthy individuals with non-symptomatic hindfeet is analysed. With a 3D stress test their foot was pulled in 8 different positions and scanned. The talus and calcaneus were segmented from the 3D-CT image and modelled as 3D polygon models. In the computer model of the bones, along the medial-lateral directed axis of the space at 20 equidistant locations, small spheres are placed. Each sphere is virtually inflated to a maximum size within the bony boundaries of the tarsal sinus and canal, with the restriction that the centre of the sphere could only move in a plane perpendicular to the axis of the space. Generally, the results show that the diameter of the spheres in the tarsal sinus and canal on the lateral side is larger than on the medial side. Foot positions with an inversion component show an increase in the radius of the fitted spheres at the lateral side, and a decrease at the medial side. Foot positions with an eversion component demonstrate the opposite. The region just medial from the middle, where the diameter of the spheres is about 3 mm, hardly shows any change in diameter of the spheres between different foot positions which makes this region to act as a pivot point for motion between the talus and calcaneus. The pattern of changes in dimensions between different foot positions is intra-individually reproducible but there are relevant inter-individual differences.

In **Chapter 4** a study evaluates the functionality of a new kind of ankle brace. This brace, the Exo-L®, is designed to restrict only the motion of most common ankle sprains. i.e. inversion or a combination of inversion and plantarflexion without restraining other motions. 12 patients with chronic ankle instability had their hindfoot scanned with CT with a custom made device to pull the foot in different foot positions. This study used an adapted protocol of a previous study of which the data are used in the study presented in chapter 3. In this study each foot position was scanned without and with the brace. The results demonstrate that the use of the ankle brace significantly restricts the rotation between the foot position of combined eversion and dorsiflexion to combined inversion and plantar flexion in both the talocrural (from a mean of 49.2 to 40.0 degrees, mean decrease of 9.2° (18.7%), $p = .004$) and subtalar joints (from a mean of 24.4 to 15.6 degrees, mean decrease of 8.8° (36.1%), $p < .001$). No statistically significant differences are found in both joints in the rotation between the foot positions of dorsiflexion to plantar flexion. The results of this exploratory study, with an objective and accurate method that allowed a discrimination between the talocrural and subtalar joints, are in agreement with the functionality claimed by the manufacturer.

In **Part 2** the variations in the anatomy of the hindfoot is further investigated by a model approach of the posterior subtalar articulating facet of the calcaneus in healthy subjects, and of the interrelationship of the superior and posteroinferior talar facets in healthy

subjects and in patients with chronic ankle instability. Furthermore, the extent of bilateral symmetry and variations of the subtalar joint facets is analysed. In **Chapter 5** geometrical models are used to quantitatively describe the 3D morphology of the articulating surface on the calcaneus of the posterior subtalar joint, since the literature is limited to 2D analyses. Insight of the orientation is needed since the orientation of the subtalar joint contributes to the overall alignment of the hindfoot, that has an influence on the evolution of ankle joint osteoarthritis. A plane and cylinder are fitted to the subchondral surface of 3D polygonal calcaneal models of 20 healthy and non-symptomatic individuals. These participants had both their feet, ankles, and legs scanned in a CT scanner with a custom made device to simulate weight bearing. The accuracy of the fit of the plane and cylinder is expressed as the root mean square error. The 3D orientation of the normal of the plane and of the axis of the cylinder is expressed with an inclination and deviation angle. The plane fit has high root mean square errors and thus does not fit well to the curved surface and only roughly provides information of the orientation. The cylinder fit is more accurate and proves to be a good geometrical model to represent the articulating surface. The mean diameter of the fitted cylinder is 42.0 ± 7.7 mm and the root mean square error is 0.5 ± 0.1 mm. The cylinder's axis directs from supero-postero-laterally to infero-antero-medially (inclination angle -2.4 ± 6.9 (left) and -4.1 ± 7.9 (right) degrees, and deviation angle -70.1 ± 5.6 (left) and -68.6 ± 4.4 (right) degrees). The cylinder is further used to determine the subtalar vertical angle. This angle is used in the literature as a measure for the orientation of this facet, and is measured in coronal planes. In this study the angle is determined based on the cylinder model at the intersection with the facet, and is 97.1 ± 7.2 (left) and 95.8 ± 6.6 (right) degrees at the middle coronal plane. These values were similar to values reported in the literature. The difference in the subtalar vertical angle in different anteroposterior coronal planes is explained by the oblique orientation of the cylinder. In conclusion, this study demonstrates that a cylinder can be used to quantify the 3D morphology and orientation of the posterior calcaneus facet, irrespectively of a chosen plane for analysis. The results provide a reference for healthy and non-symptomatic individuals that serves future investigation on the influence of the subtalar joint on the evolution of ankle joint osteoarthritis in valgus and varus hindfoot deformities.

Chapter 6 presents an exploratory study that investigates whether the orientation of the talar articulating surfaces is associated with chronic ankle instability that may develop after a first-time ankle sprain. The rationale behind this is that the alignment of the hindfoot is one of the identified risk factors for chronic ankle instability and the orientation of the talar facets is a major determining factor in the overall alignment of the hindfoot. The method to model a curved articulating surface with a cylinder as developed in Chapter 5 is also used here to describe the morphology and orientation of

the superior and posteroinferior talar facets. The orientation is compared between healthy controls, from the studies presented in chapters 3 and 5, and the patients with chronic ankle instability from the study presented in chapter 4. A cylinder is fitted to the subchondral superior and posteroinferior articulating surfaces of 3D models of the talus. The axis of the cylinder represents the facet orientation, which is expressed by an inclination and deviation angle in an anatomic coordinate system based on the cylinder of the superior talar facet and the geometric principal axes of the subject's talus. The results demonstrate that the inclination angle of the posteroinferior talar facet is significantly more plantarly orientated, by 3.5 degrees, in the chronic instability group (14.7 ± 3.1 degrees) compared to the control group (11.2 ± 4.9 degrees) ($p < 0.05$). In the coronal plane this corresponds to a slight valgus orientation of the posteroinferior talar facet relative to the talar dome. This demonstrates that the talar morphology can be associated with chronic ankle instability, but not necessarily contributes to a varus hindfoot deformity. Further research, with a larger number of patients with chronic ankle instability and an inclusion of the orientation of adjacent facets, is required for a more conclusive statement of the role of the talar morphology in developing chronic ankle instability.

In **Chapter 7** the bilateral symmetry of the subtalar joint facets is assessed. Bilateral symmetry is assumed in many clinical and research settings, where the contralateral joint is used as normal reference during diagnosis and treatment of joint pathologies. This bilateral symmetry is not evaluated yet. To examine the degree of symmetry, 40 pairs of cadaveric subtalar joints were dissected and opened. The following morphometric data are acquired: length and width of the facets, distance between the facets of the specimen with intact cartilage and the intersection angle, i.e. the angle between middle and anterior part in a sagittal plane. Also, the orientation and curvature of the posterior facet are included in the analysis of symmetry. This is based on the cylinders fitted to the posterior calcaneal facet from the study presented in Chapter 5. Three different patterns of the presence of and connections between the posterior, middle and anterior subtalar facets are identified and classified in the specimens. The morphometric analyses demonstrate no statistically significant differences between left and right for all measurements, except for the width of the posterior calcaneal facet that is on average larger on the right side (22.8 ± 2.6 (left) and 23.5 ± 2.8 (right) mm). In total, 77.5% of the calcanei and 80% of the tali have bilateral symmetry of the facet pattern. The remaining pairs of calcanei (22.5%) and tali (20%) have varying combinations of facet patterns between the left and right sides. The most frequent left-right corresponding calcaneal pattern is that of a separate posterior facet and a connected anterior and middle facet with a constriction between these two parts (47.5 %). For the talar facets the most frequent pattern is with three separated facets

(57.5%). The second research question addressed in this study is whether the facet configuration or the morphometric parameters are related to osteoarthritic changes observed in the intact specimen after exposure of the facets by dissection. No significant relationships can be found between osteoarthritic changes and the morphology. Only age is a determining factor for the presence of osteoarthritic changes.

In **Chapter 8** all previous chapters are discussed. The content of this thesis has contributed to new insights of the variations in the morphology and kinematics of the hindfoot and has introduced new methods to determine the 3D morphology quantitatively. Also the limitations of the presented studies are discussed and alternatives are addressed. Among the limitation is the use of CT, which in contrast to MR does not depict soft tissue and comes with ionizing radiation. Other issues that need further optimization is a standard for determining the alignment of the foot and ankle, and to include the adjacent joints of the hindfoot in subsequent studies evaluating variations and abnormalities.

'van top tot teen'
Van Dale woordenboek: van boven tot onder, helemaal

Nederlandse samenvatting

Alle lichaamsdelen vertonen een zekere mate van inter- en intra-individuele variaties. Sommige van deze variaties kunnen een invloed hebben op het verkrijgen van pathologie. Dit proefschrift richt zich op de vaak aangedane achtervoet. De achtervoet is het posterieure deel van de voet. De studies die beschreven zijn in dit proefschrift dragen bij aan het identificeren van dergelijke variaties. Deze informatie zal helpen bij het adequaat optimaliseren van preventie en behandeling van pathologie van de achtervoet en aangrenzende regio's.

In **Deel 1** wordt in een beschrijvende literatuurstudie de mechanica van de achtervoet besproken, worden de dimensies van de canalis en sinus tarsi onderzocht met metingen van de kinematica en wordt de functionaliteit van een nieuw type enkelbrace geëvalueerd met een 3D stress test en computertomografie (CT). Het beschrijvende review in **Hoofdstuk 2** begint met een eenvoudige biomechanische analyse die laat zien dat de grootte van de kracht op het talocrurale gewricht afhankelijk is van de balans tussen spierkracht en de grondreactiekracht, en hun momentarmen ten opzichte van het gewricht. De grootte van de kracht op het talocrurale gewricht is tot wel vier maal het lichaamsgewicht bij het staan op een been. Vervolgens wordt er een kwantitatief overzicht gegeven van de maximale bewegingsuitslagen en hoe deze zich verhouden tot de bewegingsuitslagen bij lopen en rennen. Deze laatsten beslaan slechts een klein deel van de maximale bewegingsuitslagen. Tot slot, de gewrichtsmorfologie draagt tot 100% bij aan de stabiliteit van de gewrichten bij compressie. In het algemeen zal een ligament meer weerstand bieden tegen de beweging naarmate die de grens van de maximale bewegingsuitslag nadert. Ze zullen de beweging tegengaan aan de grenzen van de maximale bewegingsuitslagen en samen met de gewrichtsmorfologie zorgen zij voor de

passieve stabiliteit van het gewricht. Een probleem dat niet eenvoudig op te lossen is, is de bepaling van de lengte waarbij het ligament op spanning komt. Voor functionele analysen met analytische modellen is dit een belangrijke inputparameter.

Hoofdstuk 3 introduceert een nieuwe methode om de dimensies te bepalen van de canalis en sinus tarsi. Deze ruimte ligt tussen de talus en calcaneus. De geometrie van deze ruimte verandert bij verschillende voetstanden. Deze dimensies zijn niet gedocumenteerd in de literatuur. Deze informatie is nuttig bij bijvoorbeeld artroscopie en bij de diagnose van het sinus tarsi syndroom. Een dataset van een eerdere studie met 20 gezonde personen met niet-symptomatische achtervoeten die waren gescand met CT wordt geanalyseerd. Die dataset is verkregen met een 3D CT stress-test waarbij de voet in 8 verschillende standen werd getrokken en gescand in elke positie. De talus en de calcaneus werden gesegmenteerd in de 3D-CT beelden en gemodelleerd als 3D polygoon modellen. In de computermodellen wordt vervolgens in deze studie op een gedefinieerde as van de canalis en sinus tarsi 20 kleine bollen geplaatst op gelijke afstand van elkaar. Elke bol wordt virtueel opgeblazen tot een maximum binnen de benige grenzen met de restrictie dat het centrum van de bol alleen kan bewegen in een vlak haaks op de gedefinieerde as van de ruimte. Algemeen gezien zijn de dimensies aan de laterale zijde groter dan aan de mediale zijde. Voetstanden met een inversiecomponent laten een toename van de radii van de bollen zien aan de laterale zijde en een afname aan de mediale zijde. Voetstanden met een eversiecomponent laat een tegenovergesteld patroon zien. In de regio net mediaal van het midden, waar de radii ongeveer 3 mm zijn, verandert de radii van de bollen nauwelijks tussen de verschillende voetstanden. Deze regio vertoont gelijkenissen met een draaipunt van de talus en calcaneus ten opzichte van elkaar. Het patroon van dimensies en de veranderingen in dimensies tussen de verschillende voetstanden is reproduceerbaar tussen de personen, maar er zijn ook relevante interindividuele verschillen.

In **Hoofdstuk 4** wordt een evaluatie van de functionaliteit van een nieuw type enkelbrace gepresenteerd. Deze brace is ontworpen om alleen de beweging van de meest voorkomende verzwikking tegen te gaan, te weten een inversie of een combinatie van plantairflexie met inversie, zonder andere bewegingen te belemmeren. Van 12 patiënten met chronische enkelinstabiliteit wordt hun achtervoet gescand met CT met een aangepast protocol van de studie beschreven in hoofdstuk 3. Met deze CT stress-test wordt elke voetstand zonder en mét enkelbrace gescand. De resultaten laten een statistisch significante reductie zien met brace ten opzichte van zonder brace in de rotatie tussen de standen van gecombineerde eversie en dorsaalflexie naar gecombineerde inversie en plantairflexie in zowel het talocrurale (van een gemiddelde van 49,2° naar 40.0°, met een gemiddelde afname van 9,2° (18,7%), $p = 0,004$) als de subtalaire gewrichten (van een gemiddelde van 24.4° naar 15.6°, met een gemiddelde

afname van 8,8° (36,1%), $p < 0,001$). Er zijn geen statistisch significante verschillen gevonden in de rotaties tussen de voetpositie van dorsaalflexie naar plantairflexie. In deze eerste verkennende studie met een objectieve en accurate methode, die een onderscheid kan maken tussen de talocrurale en subtalaire gewrichten, is de door de fabrikant beweerde functionaliteit bevestigd.

In **Deel 2** worden variaties in de anatomie van de achtervoet verder onderzocht met een modelbenadering van het posterieure subtalaire gewrichtsoppervlak van de calcaneus in gezonde personen en wordt de onderlinge relatie bepaald tussen het superieure en het posteroinferieure talaire gewrichtsoppervlak bij gezonde personen en bij patiënten met chronische enkelinstabiliteit. Verder wordt de mate van bilaterale symmetrie en de variaties van de subtalaire gewrichten geanalyseerd. In **Hoofdstuk 5** zijn geometrische modellen gebruikt om een kwantitatieve beschrijving te geven van de morfologie en oriëntatie van het gewrichtsoppervlak van het calcaneale deel van het posterieure subtalaire gewricht. In 3D worden een vlak en een cilinder met de kleinste-kwadratenmethode gepast op het subchondrale oppervlak van 3D polygoonmodellen van de calcaneus van 20 gezonde en niet-symptomatische personen. De nauwkeurigheid van het passen van het geometrische model met de punten van het oppervlak wordt uitgedrukt met de gemiddelde kwadratische afwijking. De 3D oriëntatie van de normaal van het vlak en de as van de cilinder wordt uitgedrukt met een inclinatie- en deviatiehoek. Het vlak blijkt niet goed te passen op het gekromde oppervlak en geeft alleen een grove indicatie van de oriëntatie. De cilinder heeft een hogere nauwkeurigheid en vormt een goede representatie van het oppervlak. De gemiddelde diameter van de cilinder is 42,0 ± 7,7 mm en de gemiddelde kwadratische afwijking is 0,5 ± 0,1 mm. De oriëntatie van de as van de cilinder loopt van supero-postero-lateraal naar infero-antero-mediaal (inclinatie hoek -2,4 ± 6,9 (links) en -4,1 ± 7,9 (rechts) graden, deviatie hoek -70,1 ± 5,6 (links) en -68,6 ± 4,4 (rechts) graden). De cilinder wordt verder gebruikt om de subtalaire verticale hoek te bepalen. Deze hoek wordt in de literatuur gebruikt als maat voor de oriëntatie van dit gewrichtsoppervlak en wordt gemeten in coronale vlakken. In deze studie wordt deze hoek bepaald op basis van waar het cilindermodel het gewrichtsoppervlak snijdt. De hoek is 97,1 ± 7,2 (links) en 95,8 ± 6,6 (rechts) graden bij een coronaal vlak door het midden van het gewrichtsoppervlak en laat vergelijkbare waarden zien als gerapporteerd in de literatuur. De verschillen in deze hoek tussen verschillende anteroposterieure coronaal vlakken kan verklaard worden door de schuine stand van de cilinder. Concluderend laat deze studie zien dat een cilinder gebruikt kan worden om de 3D morfologie en oriëntatie van het posterieure calcaneale gewrichtsoppervlak te kwantificeren en dat dit ongeacht het gekozen vlak geanalyseerd kan worden. De resultaten dienen als referentie voor

gezonde en niet-symptomatische personen. Deze referentie maakt toekomstige onderzoeken mogelijk naar de invloed van de subtalaire gewrichten op de ontwikkeling van enkelartrose bij valgus- en varusdeformiteit van de achtervoet.

In **Hoofdstuk 6** wordt in een verkennende studie onderzocht of de oriëntatie van de talaire gewrichtsvlakken geassocieerd is met chronische enkelinstabiliteit. Het idee hierachter is dat een varus-achtervoetuitlijning een risicofactor is voor chronische enkelinstabiliteit en de oriëntatie van de talaire gewrichtsvlakken een bepalende rol hebben voor de totale achtervoetuitlijning. De methode om een gekromd gewrichtsoppervlak te modelleren als een cilinder, zoals in hoofdstuk 5, wordt ook hier gebruikt om de oriëntatie te beschrijven van de superieure en postero-inferieure talaire gewrichtsvlakken. De oriëntatie wordt vergeleken tussen een controlegroep met gezonde en niet-symptomatische proefpersonen (van hoofdstuk 3 en 5) en een groep patiënten met chronische enkelinstabiliteit (van hoofdstuk 4). Cilinders worden gepast op de subchondrale gewrichtsoppervlakken van 3D modellen van de talus. De as van de cilinder representeert de oriëntatie van het gewrichtsoppervlak, en wordt uitgedrukt met een inclinatie- en deviatiehoek in een anatomisch coördinatenstelsel dat gebaseerd is op de cilinder door het superieure gewrichtsoppervlak en de geometrische zwaarteassen van de talus van elk individu. De resultaten laten een statistisch significant meer plantair gerichte as van het postero-inferieure gewrichtsoppervlak zien bij de groep patiënten met chronische enkelinstabiliteit (14,7 ± 3,1 graden) ten opzichte van de controle groep (11,2 ± 4,9 graden) ($p < 0,05$). In een coronaal aanzicht komt dit overeen met een matige valgusstand van het postero-inferieure gewrichtsoppervlak ten opzicht van het superieure. Dit toont aan dat de morfologie van de talus geassocieerd kan zijn aan chronische enkelinstabilteit, maar niet niet per se bij hoeft te dragen aan een varusuitlijning van de achtervoet. Nader onderzoek, met een groter aantal patiënten met chronische enkelinstabiliteit en een analyse van aangrenzende gewrichtsvlakken, zijn nodig om een meer eenduidige uitspraak te doen over de rol van de morfologie van de talus bij de ontwikkeling van chronische enkelinstabiliteit.

In **Hoofdstuk 7** wordt de bilaterale symmetrie van de gewrichtsoppervlakken van de subtalaire gewrichten bestudeerd. In de kliniek en in het onderzoek wordt er vaak uitgegaan van bilaterale symmetrie, waar de contralaterale zijde als referentie wordt gebruikt voor diagnose en behandeling. Echter, deze bilaterale symmetrie is niet eerder geëvalueerd voor deze gewrichtsvlakken. Om de mate van symmetrie te bepalen werden 40 paar subtalaire gewrichten van stoffelijk overschotten opgemeten. De lengte, breedte en afstand tussen de verschillende gewrichtsoppervlakken worden gemeten bij de preparaten met intact kraakbeen, alsook de kruisingshoek, i.e. de hoek tussen het middelste en anterieure deel in een sagittaal vlak. De oriëntatie en kromming van de gewrichtsvlakten zoals bepaald in de studie gepresenteerd in hoofdstuk 5 worden

ook geïncludeerd in de analyse van bilaterale symmetrie. Drie verschillende patronen van de aanwezigheid van en verbindingen tussen de posterieure, middelste en anterieure gewrichtsvlakken worden geïdentificeerd en geclassificeerd. De morfometrische analyse toont geen statistisch significante verschillen aan tussen links en rechts, behalve voor de breedte van het posterieure gewrichtsfacet van de calcaneus dat gemiddeld rechts breder is (22,8 ± 2,6 (links) en 23,5 ± 2,8 (rechts) mm). In totaal heeft 77,5% van de calcanei en 80% van de tali bilaterale symmetrie van de facetpatronen. De resterende paren calcanei (22,5%) en tali (20%) hebben verschillende combinaties van facetpatronen tussen de linker en rechter zijde. Het meest voorkomende corresponderende facetpatroon tussen links en rechts is voor de calcaneus die met een separaat posterieur facet en een verbonden anterieur en middelste facet met een versmalling tussen de twee delen (47,5%). Voor de talaire facetten is dit het patroon met drie separate facetten (57,5%). Een tweede onderzoeksvraag is of er kenmerken zijn die gerelateerd zijn aan de aanwezigheid van kraakbeenslijtage of -beschadiging. Slijtage of beschadiging wordt geobserveerd in de intacte preparaten na het openen van de gewrichten. Er worden geen statistisch significante relaties gevonden tussen de morfometrische gegevens of de verschillende aangetoonde patronen en de aanwezigheid van kraakbeenslijtage of -beschadiging. Alleen leeftijd blijkt een bepalende factor te zijn voor slijtage of beschadiging.

In **Hoofdstuk 8** worden alle voorgaande hoofdstukken besproken. De inhoud van dit proefschrift draagt bij aan nieuwe inzichten in de variatie in de morfologie en kinematica van de achtervoet en introduceert nieuwe methoden om in 3D de morfologie kwantitatief vast te leggen. Echter, er worden in hoofdstuk 8 ook beperkingen van de verrichte studies genoemd en welke alternatieven er zijn om deze beperkingen op te lossen. Een van de beperkingen is het gebruik van CT. Weke delen worden daarmee slecht in beeld gebracht en CT gaat gepaard met ioniserende straling. Het alternatief is magnetische resonantie (MR) beeldvorming. Andere kwesties die verdere optimalisatie behoeven zijn een standaardmethode voor de bepaling van de uitlijning van de voet en enkel en het includeren van de aangrenzende gewrichten van de achtervoet bij de analyse van afwijkingen.

Appendices

I. List of co-authors and affiliations

II. PhD Portfolio

III. Dankwoord

IV. About the author

I. List of co-authors and affiliations

Blankevoort, Leendert, PhD
Department of Orthopaedic Surgery, Amsterdam UMC, University of Amsterdam, Amsterdam Movement Sciences, Amsterdam, The Netherlands

Dahmen, Jari, Msc, MD
Department of Orthopaedic Surgery, Amsterdam UMC, University of Amsterdam, Amsterdam Movement Sciences, Amsterdam, The Netherlands

Dobbe, Johannes G.G., PhD
Department of Biomedical Engineering and Physics, Amsterdam UMC, University of Amsterdam, Amsterdam Movement Sciences, Amsterdam, The Netherlands

Gerards, Rogier M., Msc, MD
Department of Orthopaedic Surgery, Amsterdam UMC, University of Amsterdam, Amsterdam Movement Sciences, Amsterdam, The Netherlands

Kerkhoffs, Gino M.M.J., PhD, MD
Department of Orthopaedic Surgery, Amsterdam UMC, University of Amsterdam, Amsterdam Movement Sciences, Amsterdam, The Netherlands

Knupp, Markus, PhD, MD
Mein Fusszentrum, Basel, University of Basel, Switserland

Merwe, Alie E. van der, PhD
Department of Medical Biology, Amsterdam UMC, University of Amsterdam, Amsterdam Movement Sciences, Amsterdam, The Netherlands

Natenstedt, Jerry J., Msc.
Department of Biomechanical Engineering, Faculty of Mechanical, Materials and Maritime Engineering, Delft University of Technology, Delft, the Netherlands

Oostra, Roelof-Jan, PhD
Department of Medical Biology, Amsterdam UMC, University of Amsterdam, Amsterdam Movement Sciences, Amsterdam, The Netherlands

Ruijter, Jan M., PhD
Department of Medical Biology, Amsterdam UMC, University of Amsterdam, Amsterdam Movement Sciences, Amsterdam, The Netherlands

Streekstra, Geert J., PhD
Department of Biomedical Engineering and Physics, Amsterdam UMC, University of Amsterdam, Amsterdam Movement Sciences, Amsterdam, The Netherlands

Tuijthof, Gabriëlle J.M., PhD
Department of Faculty of Health, Medicine and Life Sciences, Maastricht University

Vuurberg, Gwendolyn, PhD, MD
Department of Orthopaedic Surgery, Amsterdam UMC, University of Amsterdam, Amsterdam Movement Sciences, Amsterdam, The Netherlands

Stufkens, Sjoerd A.S., PhD, MD
Department of Orthopaedic Surgery, Amsterdam UMC, University of Amsterdam, Amsterdam Movement Sciences, Amsterdam, The Netherlands

II. PhD Portfolio

Oral presentations

Kleipool RP. Functional anatomy of the hindfoot with quantitative medical imaging. 181st annual meeting Nederlandse Anatomen Verening (NAV), 2019, Lunteren, The Netherlands

Kleipool RP. Blankevoort L. Functional Anatomy of the Ankle Joint Complex. 14th Congress of the European Society of Sports Traumatology, Knee Surgery and Arthroscopy (ESSKA), 2010, Oslo, Norway.

Kleipool RP. Anatomy of the ankle. 6th MR Symposium of the International Society for Magnetic Resonance in Medicine (ISMRM), 2013, Amsterdam, The Netherlands.

Poster presentations

The Mechanical Functionality of the EXO-L Ankle Brace. Assessment With a 3-Dimensional Computed Tomography Stress Test. 7th Annual MOVE research meeting, 2016, Amsterdam, The Netherlands.

The Mechanical Functionality of the EXO-L Ankle Brace. Assessment With a 3-Dimensional Computed Tomography Stress Test. 178st annual meeting Nederlandse Anatomen Vereniging (NAV), 2016, Lunteren, The Netherlands.

Projects supervised

The hamstring muscle complex. van der Made AD, Wieldraaijer T, Kerkhoffs GM, Kleipool RP. Student internship project 2009-2013

Study behavior of first year biomedical, psychobiology, and biology students. van der Wateren IM, Kleipool RP. Student internship project 2009/2010

Features of the popliteal lymph nodes seen on musculoskeletal MRI in a Western population. Musters GD, Kleipool RP, Bipat S, Maas M. Student internship project 2008/2009

Peer reviewed

Fat is consistently present within the compartments of the plantar muscular space of the foot – a cadaveric study, Clinical Anatomy, 2021

Intrinsic and Extrinsic Risk Factors for Lateral Ankle Sprain: A Literature Review, Archives of Sports Medicine, 2019

Sex- and Age-Related Morphological Variations in the Talar Articular Surfaces of the Calcaneus, Clinical Anatomy, 2019

Radiological and goniometric assessment of the maximal dorsiflexion position of the ankle in healthy persons, JSM Foot & Ankle, 2019

Effects of prophylactic ankle and knee braces on leg stiffness during hopping, Open Access Journal of Sports Medicine, 2017

Effect of Semi-Rigid and Soft Ankle Braces on Static and Dynamic Postural Stability in Young Male Adults, Journal of Sports Science and Medicine, 2015

Comparison of Kinematics Descriptors for Multi-segment Foot and Ankle Complex, Medical & Biological Engineering & Computing, 2010

(Inter)national conference visitor

Amsterdam Movement Sciences (AMS)	2017, 2018, 2019
MOVE research institute meeting	2016
European Society of Sports Traumatology, Knee Surgery & Arthroscopy (ESSKA)	2010
Nederlandse Anatomen Vereniging	2009, 2013, 2016, 2019

Publications (this thesis, first author)

Kleipool RP, Dahmen J, Vuurberg G, Blankevoort L, Dobbe JG, Streekstra GJ, Stufkens SAS, Knupp M. Difference in orientation of the talar articular facets between healthy ankle joints and ankle joints with chronic instability.
J Orthop Res. 2021 Apr 29. doi: 10.1002/jor.25068

Kleipool RP, Vuurberg G, Stufkens SAS, van der Merwe AE, Oostra RJ.
Bilateral symmetry of the subtalar joint facets and the relationship between the morphology and osteoarthritic changes.
Clin Anat. 2019 Nov 21. doi: 10.1002/ca.23525.

Kleipool RP, Dahmen J, Vuurberg G, Oostra RJ, Blankevoort L, Knupp M, Stufkens SAS. Study on the three-dimensional orientation of the posterior facet of the subtalar joint using simulated weight-bearing CT.
J Orthop Res. 2019 Jan;37(1):197-204. doi: 10.1002/jor.2416

Kleipool RP, Blankevoort L, Ruijter JM, Kerkhoffs GMMJ, Oostra RJ.
The dimensions of the tarsal sinus and canal in different foot positions and its clinical implications.
Clin Anat. 2017 Nov;30(8):1049-1057. doi: 10.1002/ca.22908

Kleipool RP, Natenstedt JJ, Streekstra GJ, Dobbe JG, Gerards RM, Blankevoort L, Tuijthof GJ.
The mechanical functionality of the EXO-L ankle brace: Assessment with a 3-dimensional computed tomography stress test.
Am J Sports Med. 2016 Jan;44(1):171-6. doi: 10.1177/036354651561187

Kleipool RP, Blankevoort L.
The relation between geometry and function of the ankle joint complex: a biomechanical review.
Knee Surg Sports Traumatol Arthrosc. 2010 May;18(5):618-27. doi: 10.1007/s00167-010-1088-2

Publications (other)

Schallig W, Streekstra GJ, Hulshof CM, Kleipool RP, Dobbe JGG, Maas M, Harlaar J, van der Krogt MM, van den Noort JC.
The influence of soft tissue artifacts on multi-segment foot kinematics.
J Biomech. 2021 Mar 6;120:110359. doi: 10.1016/j.jbiomech.2021.110359.

Minnaard J, Kleipool RP, Baars W, Dankelman J, Stufkens S, Horeman T.
A new bone-cutting approach for minimally invasive surgery.
Med Eng Phys. 2021 Jan;87:56-62. doi: 10.1016/j.medengphy.2020.11.011.

Donders JCE, Prins J, Kloen P, Streekstra GJ, Cole PA, Kleipool RP, Dobbe JGG.
Three-dimensional topography of scapular nutrient foramina.
Surg Radiol Anat. 2020 Feb 28. doi: 10.1007/s00276-020-02441-7.

Chekrouni N, Kleipool RP, de Bakker BS.
The impact of using three-dimensional digital models of human embryos in the biomedical curriculum.
Ann Anat. 2020 Jan;227:151430. doi: 10.1016/j.aanat.2019.151430

Vuurberg G, Dahmen J, Dobbe JGG, Kleipool RP, Stufkens SAS, Maas M, Kerkhoffs GMMJ, van Dijk CN, Streekstra GJ.
The effect of foot rotation on measuring ankle alignment using simulated radiographs: a safe zone for pre-operative planning.
Clin Radiol. 2019 Nov;74(11):897.e1-897.e7. doi: 10.1016/j.crad.2019.07.012

Schallig W, van den Noort JC, Kleipool RP, Dobbe JGG, van der Krogt MM, Harlaar J, Maas M, Streekstra GJ.
Precision of determining bone pose and marker position in the foot and lower leg from computed tomography scans: How low can we go in radiation dose?
Med Eng Phys. 2019 Jul;69:147-152. doi: 10.1016/j.medengphy.2019.05.004

Wellenberg RHH, Donders JCE, Kloen P, Beenen LFM, Kleipool RP, Maas M, Streekstra GJ.
Exploring metal artifact reduction using dual-energy CT with pre-metal and post-metal implant cadaver comparison: are implant specific protocols needed?
Skeletal Radiol. 2018 Jun;47(6):839-845. doi: 10.1007/s00256-017-2750-2

van der Made AD, Wieldraaijer T, Kerkhoffs GM, Kleipool RP, Engebretsen L, van Dijk CN, Golanó P.
The hamstring muscle complex.
Knee Surg Sports Traumatol Arthrosc. 2015 Jul;23(7):2115-22. doi: 10.1007/s00167-013-2744-0

van Sterkenburg MN, Kerkhoffs GM, Kleipool RP, Niek van Dijk C.
The plantaris tendon and a potential role in mid-portion Achilles tendinopathy: an observational anatomical study.
J Anat. 2011 Mar;218(3):336-41. doi: 10.1111/j.1469-7580.2011.01335.x

Musters GD, Kleipool RP, Bipat S, Maas M.
Features of the popliteal lymph nodes seen on musculoskeletal MRI in a Western population.
Skeletal Radiol. 2011 Aug;40(8):1041-5. doi: 10.1007/s00256-010-1093-z

Book chapter:
van den Hoff MJB, Kleipool RP, Vermeij-Keers C. Clinical anatomy and embryology (Klinische anatomie en embryologie). Chapter 2: General Embryology (Algemene Embryologie). Reeds Business Education, ten Donkelaar HJ & Oostra RJ (2014)

III. Dankwoord

Een dankwoord schrijf je op het eind. In 'eindelijk' zit ook het woord 'eind'. Beide woorden zijn van toepassing. Men durfde mij bijna niet meer te vragen naar de status van mijn proefschrift. Het was een werk van lange adem, maar *eindelijk* is het *eind* bereikt. Het schrijven van dit proefschrift doe ik naast het geven en organiseren van onderwijs en ik mag mij ook nog gelukkig prijzen met een gezinsleven. Mijn dank gaat in eerste instantie uit naar alle mensen die geduld en begrip hebben getoond dat ik mij niet vol op het ene of het andere kon storten, dat het een soms langere tijd stil lag of wat minder aandacht kreeg en naar diegenen die mij gesteund hebben bij het combineren van deze werelden. Mijn lieve vriendin **Fenna** verdient in dit verhaal de eerste vermelding. Het is niet heel gebruikelijk in een dankwoord met het thuisfront te beginnen, maar zonder haar was het combineren van al deze mooie (en soms lastige) facetten niet mogelijk. Lieve Fenna, jouw steun en liefde zijn onmisbaar geweest. Ik hou van je.

Mijn carrière als docent en onderzoeker startte op de afdeling Anatomie & Embryologie. Ik werd met open armen ontvangen op de afdeling en kon daar als docent groeien. Met Antoon Moorman als hoofd van de afdeling was er veel mogelijk. Gelukkig wist hij ook een ingang te vinden voor mijn ambities om onderzoek te doen. **Antoon**, ik ben je nog altijd zeer dankbaar voor de kansen die je mij hebt gegeven. Nadat jij de samenwerking met de afdeling Orthopedie had geïnitieerd, kwam ik al snel samen te werken met Leendert Blankevoort. **Leendert**, jij hebt mij vanaf het eerste uur als onderzoeker binnen de muren van het AMC intensief begeleid. Ik waardeer de tijd die je nam om kennis met mij te delen, de manuscripten te verbeteren, kritische noten te plaatsen en te stimuleren van elk werk een degelijk werk te maken. Jouw visie over onderzoek bedrijven heb je meermaals door laten schemeren en de kern van die boodschap draag ik voor altijd mee. Ik ben blij dat jij het ius promovendi voor mijn promotie hebt gekregen en ik voel mij bevoorrecht dat jij die rol op je neemt. Mijn andere begeleider werd Roelof-Jan Oostra. **Roelof-Jan**, ik had jaren terug niet gedacht dat degene met wie ik menig 'broodje alles' zou verorberen na weer een avondje 'Eppen', mijn promotor zou worden. Die rol vervulde je op eigen wijze; losjes en liet me zelf ontdekken. Bedankt voor je begeleiding in mijn promotietraject.

Veel van mijn onderzoek voltrok zich buiten de afdeling Anatomie & Embryologie en stond meestal los van de andere bezigheden van de afdeling. Desalniettemin zou ik het onderzoek niet gedaan kunnen hebben zonder mijn anatomie collega's. Het hele technische team, in veranderlijke samenstelling door de vele jaren heen: **Cindy Cleypool**, **Rijk Gihaux**, **Eric Lichtenberg**, **Mara Clerkx**, **Nachet Islam** (veel te kort onder ons geweest), **Inge Dijkman**, **Jermo Hanemaaijer** en **Semmie van den Berg**, dank voor al het werk dat jullie verzet hebben. Jullie inspanningen maken het mogelijk dat vele onderzoekers, waaronder ik, hun werk kunnen doen. Jullie hebben heel wat enkels voorbij zien komen voor mijn onderzoek en hebben om mijn verschillende (omslachtige) meetopstellingen heen moeten werken die altijd weer ergens in de weg stonden. Docentcollega's van de afdeling, **Kees de Jong**, **Christian Wallner**, **Lida van der Merwe**,

Roelof-Jan Oostra, **Petra Habets**, **Bernadette de Bakker**, **Karl Jacobs**, **Maurice van der Hoff**, dank voor jullie betrokkenheid, geduld en interesse. Maar ook zeker mijn dank voor de ruimte die jullie gunden voor mijn onderzoek. **Lida**, kamergenoot van de laatste jaren, met veel respect kijk ik naar jouw wetenschappelijke en onderwijs output. Ik ben blij dat we ook nog samen een wetenschappelijk project hebben gedaan en ik hoop dat we nog vele projecten samen kunnen doen. **Jaco Hagoort**, bedankt voor je ondersteuning bij alle complexe 3D beeldverwerking en ICT hulpvragen. Waar zou de afdeling zonder jou zijn? **Jan Ruijter**, bedankt voor het bijstaan bij verschillende statistische vraagstukken. **Eric Reits**, bedankt voor al jouw inzet de laatste jaren als vervangend hoofd van de sectie en hoe je mij hebt bijgestaan in de afronding van mijn proefschrift. Het waren roerige tijden en jouw vastberadenheid en positieve insteek werken inspirerend. En tot slot, mijn dank aan alle studentassistenten met wie ik een ontzettend leuke tijd heb gehad. Met jullie samenwerken, samen een onderwijsblok verzorgen, is altijd een feest en is mij heel veel waard.

Buiten de afdeling heb ik veel samen mogen werken met Geert Streekstra en Iwan Dobbe. Bedankt voor jullie hulp. **Geert**, met jou aan de knoppen hebben we menig avond bij de CT scanner gestaan. Zelfs bij een oververhitte spoel of een vastlopende computer en een wachtkamer vol proefpersonen bleef jij altijd rustig en zorgde dat we verder konden. **Iwan**, jij bent met wat kladpapier erbij in staat het beste antwoord te vinden op lastige vraagstukken. Ik vond het sparren met jou, aan het bureau en met commentaren in de manuscripten, erg waardevol.

Naast Leendert heb ik met veel collega's van de afdeling Orthopedie mogen samenwerken, zowel in het onderwijs als in wetenschappelijke projecten. Stuk voor stuk gedreven collega's vol enthousiasme en ik dank hen allen voor de fijne samenwerking. **Gwen Vuurberg**, jij bent met al je projecten een duizendpoot en je hebt energie voor tien, je bent een aanwinst voor elke afdeling waar je werkt. Bedankt voor de fijne samenwerking. Nog zo een fijne collega is **Jari Dahmen**. Jari, het is zo fijn samenwerken met je. Ik kijk met interesse uit naar jouw toekomstige stappen. **Gabriëlle Tuijthof**, bedankt voor de samenwerking en jouw vertrouwen om samen op te trekken in het onderzoek naar de Exo-L brace. **Sjoerd Stufkens**, ik ben blij dat onze paden gekruist zijn. Bedankt voor je vertrouwen en input. Ik kijk uit naar onze vervolgprojecten.

Leden van de promotiecommissie, **prof. dr. M. Maas**, **prof. dr. ir. J. Harlaar**, **prof. dr. D. Eygendaal**, **dr. ir. G.J. Streekstra**, **prof. dr. G.J. Kleinrensink**, **prof. dr. R.L.A.W. Bleys**, heel hartelijk dank voor de beoordeling van het manuscript. Ik kijk uit naar de openbare discussie.

Het schrijven van dit proefschrift heeft al met al meer dan een decennium geduurd. Met zo'n lange periode en zoveel verschillende mensen die een bijdrage hebben geleverd, kan het zo maar zijn dat ik enkele van deze mensen niet heb genoemd in dit dankwoord. Ik hoop dat deze personen zich ook aangesproken voelen als ik zeg dat ik iedereen die mij geholpen heeft met en tijdens mijn promotietraject wil bedanken.

Tot slot, mijn twee lieve, prachtige, ondeugende, vrolijke en enthousiaste **Joppe en Olle**. Ik heb dit boekje aan jullie opgedragen, want ik heb veel aan jullie gehad om door te

zetten. Eindelijk kan ik jullie dit boekje laten zien waar papa zo lang aan gewerkt heeft. Ik ben benieuwd of jullie het hele boekje ooit zullen lezen en niet alleen dit dankwoord zoals de meeste mensen doen ;-) Ik hou heel veel van jullie en ik kijk uit naar de jaren voor ons.

IV. About the author

Roeland Paulus Kleipool was born on June 4th, 1980 in Alpen aan den Rijn. He moved to Almere around his first birthday and grew up in this young and growing city. Roeland had his primary and pre-university education in Almere. He spent most of his spare time at the field hockey pitch. In 1999 he went to the Vrije Universiteit in Amsterdam to study Physics, but after one year he changed study at the same university. He graduated in 2004 with a Master of Science at the faculty of Human Movement Sciences with a specialisation in functional anatomy. Within his course of study he successfully followed a training for first degree lecturer. In 2006 Roeland started as a junior lecturer in anatomy and embryology at the department of Medical Biology, AmsterdamUMC, location AMC, faculty of Medicine of the University of Amsterdam (formerly department of Anatomy and Embryology). After a period of about five years with full focus on developing courses, and giving lectures and practicals, he started in 2010 on a part time basis with scientific research. In that same year the first paper was published with dr. ir. Leendert Blankevoort, who became supervisor together with prof. dr. Roelof-Jan Oostra, of his PhD trajectory. In the subsequent years Roeland participated in research projects of colleagues and of his own, mainly in the field of the human musculoskeletal system.

Since 2010 Roeland lives in the east of Utrecht with his life partner Fenna. In February 2013 they became parents of a boy, named Joppe. About two years later, in February 2015, a second son, named Olle, came into their live. Roeland loves carpentry and cycling on road or cross country. As a family they love going camping and have drinks with friends.